Diversity Techniques in Free-Space Optical Communications

by

Sahar Molla Aghajanzadeh

A thesis
presented to the University of Waterloo
in fulfillment of the
thesis requirement for the degree of
Doctor of Philosophy
in
Electrical and Computer Engineering

Waterloo, Ontario, Canada, 2011

I hereby declare that I am the sole author of this thesis. This is a true copy of the thesis, including any required final revisions, as accepted by my examiners.

I understand that my thesis may be made electronically available to the public.

Abstract

Free-space optical (FSO) communication offers significant technical and operational advantages such as higher bandwidth capacity, robustness to electromagnetic interference, a high degree of spatial confinement (bringing virtually unlimited reuse and inherent security), low power requirements, and unregulated spectrum. FSO communication can be deployed as an efficient solution for a wide range of applications such as last-mile access, fiber back-up, back-haul for wireless cellular networks, and disaster recovery among others.

Although FSO system have many appealing features, they have rather disappointing performance for long links due to the degrading effects of atmospheric turbulence-induced fading. In this dissertation, we investigate different diversity techniques to boost the performance of FSO systems in the presence of the atmospheric turbulence-induced fading.

In Chapter 3, we investigate receive diversity in coherent FSO systems considering both turbulence-induced amplitude and phase fluctuations under weak turbulence regime. To mitigate the wavefront phase distortion effect, modal compensation is deployed at the receiver. Under the assumption of Rician channel that models the combined effects of the atmospheric fading and modal compensation, we derive outage probability and diversity-multiplexing tradeoff of such systems. Our results show that, at high signal to noise ratio (SNR) regime, the diversity gain as great as the number of receiving apertures is achieved. Moreover, it is found that the modal compensation provides finite-SNR diversity advantages in coherent receivers.

In Chapter 4, we investigate multi-hop transmission (serial relaying) as a form of diversity technique to combat atmospheric fading in coherent FSO systems. Utilizing the same channel model as in Chapter 3 and considering decode-and-forward relaying strategy, we quantify the outage probability and the finite-SNR diversity-multiplexing tradeoff of this relaying scheme. Exploiting the fact that fading variance is distance-dependent in the atmospheric channel, our results demonstrate that the multi-hop transmission takes advantage of the resulting shorter hops and yields significant performance improvements in the presence of fading.

In Chapter 5, we study hybrid-ARQ protocols in coherent FSO communications over Gamma-Gamma atmospheric fading channels. We investigate and compare the perfor-

mance of three hybrid-ARQ protocols in terms of the outage probability and throughput. Furthermore, we characterize the outage performance at high-SNR regime by diversity and coding gains. Our results provide insight into the performance mechanisms of different hybrid-ARQ protocols in coherent FSO systems and demonstrate that hybrid-ARQ significantly improves the outage performance of a coherent FSO system particularly in strong turbulence regime.

In Chapter 6, we investigate parallel relaying in an intensity modulation/direct detection (IM/DD) FSO system. Assuming Gamma-Gamma fading model, we analyze both decode-and-forward and amplify-and-forward modes of cooperation. Focusing on high SNR regime, we investigate the outage probability and characterize it by the diversity and coding gains. The diversity-multiplexing tradeoff expression of each cooperation mode is also derived. Our performance analysis reveals that large energy savings can be achieved through the use of parallel relaying in FSO systems.

Acknowledgements

I would never have been able to finish my PhD degree without the help and support from many individuals who deserve sincere recognition.

I owe my foremost gratitude to my supervisor, Professor Murat Uysal, for providing tremendous guidance and encouragement throughout the course of my PhD studies. This work would not have been possible without his consistent support. I have learnt many valuable lessons from him not restricted to the research work. I also would like to thank my other supervisor, Professor Mohamed Oussama Damen, for his guidance and support.

I sincerely wish to thank the members of my dissertation committee, Professors Steve Hranilovic, Amir Hamed Majedi, Patrick Mitran, and Shoja'eddin Chenouri for taking the time to carefully read my thesis and providing me with insightful questions and constructive suggestions.

I would like to lovingly thank my dear husband, Mehdi Torbatian, for all his love, patience, and support. This work could not have been accomplished without his encouragement and guidance.

I wish to express my deepest thanks to my family back home, especially to my dear parents, who have instilled in me the desire to learn. I could not get to this stage without their endless love, inspiration, and support. I also would like to thank all my wonderful friends with whom I have shared many happy moments of my life.

To my beloved husband,

Mehdi

and

to my dear parents,

Simin and Mohammad Ebrahim

Table of Contents

List of Tables

List of Figures

List of Abbreviations

ACK	Acknowledgement
AF	Amplify-and-Forward
ALO	At Least Once
ARQ	Automatic Retransmission reQuest
AWGN	Additive White Gaussian Noise
cdf	Cumulative Distribution Function
DF	Decode-and-Forward
DMT	Diversity-Multiplexing Tradeoff
DT	Direct Transmission
FSO	Free-Space Optical
H-ARQ	Hybrid-ARQ
IF	Intermediate Frequency
IM/DD	Intensity Modulation/Direct Detection
INR	Incremental Redundancy
LO	Local Oscillator
MIMO	Multiple-Input Multiple-Output
NACK	Negative Acknowledgement
PAM	Pulse Amplitude Modulation
pdf	Probability Density Function
RF	Radio Frequency
RTD	Repetition Time Diversity
SIMO	Single-Input Multiple-Output
SISO	Single-Input Single-Output
SNR	Signal to Noise Ratio

Notation

$\Re$	Photodetector reponsivity
q	Electron's charge
λ	Wavelength
η	Quantum efficiency of photodetector
$\mathbf{r}$	Position vector
$\hbar$	Planck's constant
$\ell(\cdot)$	Path loss
$\mathcal{L}$	Normalized path loss
σ	Power attenuation coefficient
j	$\sqrt{-1}$
$E[\cdot]$	Expectation operator
ν_c	Optical carrier frequency
ν_{IF}	Intermediate frequency
ν_L	Frequency of local oscillator
α	Effective number of large-scale eddies in Gamma-Gamma channel model
β	Effective number of small-scale eddies in Gamma-Gamma channel model
x follows $\Gamma\Gamma(\alpha, \beta, \mu)$ distribution	x follows Gamma-Gamma distribution with mean μ and channel parameters α and β
y follows $\Gamma\Gamma^2(\alpha, \beta, \mu)$ distribution	$y = x^2$ and x follows $\Gamma\Gamma(\alpha, \beta, \mu)$ distribution
$\mathcal{D}$	Receive aperture diameter in the single receiver system
Z	Path length
χ	Turbulence-induced log-amplitude fluctuation

φ	Turbulence-induced phase variation
J	Number of Zernike compensated modes
A_{TX}	Transmit aperture area
A_{RX}	Receive aperture area in the single receiver system
$\mathcal{R}$	Data transmission rate
h	Atmospheric fading power coefficient
r_0	Fried parameter
ρ_0	Generalized Fried parameter
σ_χ^2	Fading log-amplitude variance
σ_φ^2	Residual phase variance after phase compensation
$\mathfrak{K}$	Rician channel parameter
$\mathfrak{I}_s$	Average intensity of received optical field
B_s	Signal carrier bandwidth
$\mathbb{C}_n^2$	Refractive-index structure constant
σ_R^2	Rytov variance
κ	Wave number
$\mathbb{I}_n(\cdot)$	Modified Bessel function of the fist kind of order n
$\mathbb{K}_\nu(\cdot)$	Modified Bessel function of the second kind of order ν
$G_{p,q}^{m,n}(\cdot)$	Meijer G-function
$Q_n(\cdot,\cdot)$	Generalized Marcum Q-function of order n
$\Gamma(\cdot)$	Gamma function
$\mathrm{B}(\cdot,\cdot)$	Beta function
$\lvert x\rvert$	Absolute value of x
$\triangleq$	Equality by definition
$\approx$	Approximate equality
$f(x) \sim g(x)$ as $x \to x_0$	$\lim_{x\to x_0} f(x)/g(x) = 1$
$f(x) = o(g(x))$ as $x \to x_0$	$\lim_{x\to x_0} f(x)/g(x) = 0$
$f(x) \doteq x^a$	$\lim_{x\to\infty} \log f(x)/\log x = a$

Chapter 1

Introduction

1.1 Free-Space Optical Communications

In optical communication systems, information is transferred by using a carrier frequency selected from the optical frequency region, the highest portion of the electromagnetic spectrum. Since using higher carrier frequencies increases the available transmission bandwidth of a system, optical communication has the capability of transmitting data at the rates as high as terabits per second.

Figure 1.1 depicts the block diagram of a generic optical communication system [1]. The source generates information bits which are modulated onto an optical carrier. The resulting optical field then propagates through an optical channel such as optical fiber or turbulent atmosphere. At the receiver, the field is optically collected and converted into an electrical signal via a photodetector. The transmitted information is then inferred from the detected electrical signal. Based on the operating channel, optical communications can be categorized into two main classes: fiber optical communications and free-space optical (FSO) communications. The latter which is also known as "wireless optical" is the focus of this dissertation.

Free-space optical communication refers to terrestrial line-of-sight optical transmission through the atmosphere [2]. It offers significant technical and operational advantages such as higher bandwidth capacity, robustness to electromagnetic interference, a high degree of

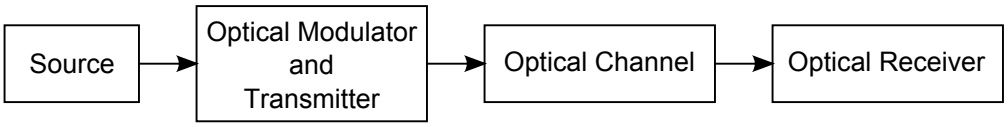

Figure 1.1: Block diagram of an optical communication system.

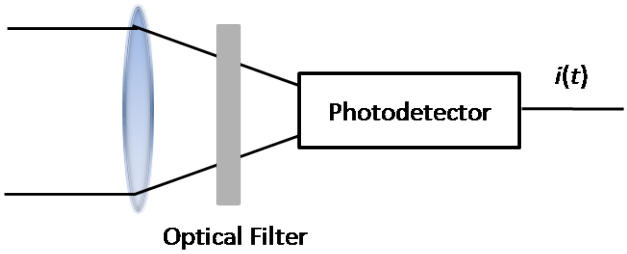

Figure 1.2: Direct detection receiver.

spatial confinement (bringing virtually unlimited reuse and inherent security), low power requirements and unregulated spectrum. FSO communication can be deployed as an efficient solution for a wide range of applications such as last-mile access, fiber back-up, back-haul for wireless cellular networks, and disaster recovery among others [3].

FSO systems can be categorized as either non-coherent (direct detection) or coherent systems based on the employed detection type [1]. In the direct detection (See Figure 1.2), the photodetector directly detects the instantaneous power of the collected field. This detection type is cost-effective and easy to implement. However, it can only be employed for intensity-modulated signals in which the information is contained in the power variation of the transmitted field. In contrast to intensity modulation/direct detection (IM/DD) systems, coherent receivers (See Figure 1.3) first mix the incoming optical field with a strong local oscillator (LO) field. The combined field is then photodetected. The frequency difference between the received field and the LO field can be set either to zero (homodyne detection) or to a desired radio frequency carrier (heterodyne detection).

The implementation of coherent receivers is more difficult since the LO field should be spatially and temporally coherent with the received field. However, the advantageous properties of coherent FSO systems have recently motivated many researchers to direct their attention to such systems. Coherent systems, by virtue of mixing the received signal

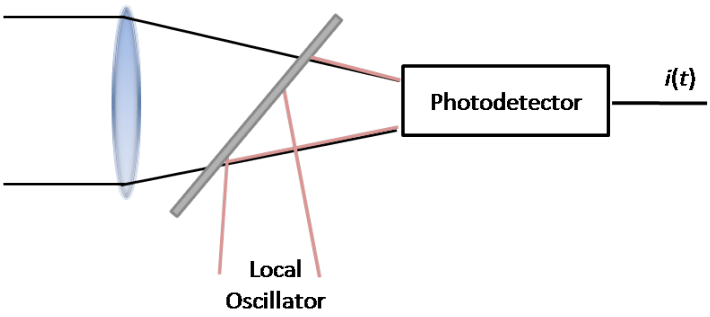

Figure 1.3: Coherent detection receiver.

with the strong LO field, have much better spatial selectivity compared to their non-coherent counterpart. The spatial selectivity property is particularly useful for applications where background noise, multiple access (or intentional) interference, and atmospheric turbulence are performance-limiting factors rather than fundamental quantum effects which are usually only encountered in vacuum channels. In multiple access scenarios, where there are multiple users willing to communicate with a central terminal, coherent systems can increase interference suppression by tens of decibel [4]. In addition, with heterodyne detection, information can be recovered from the amplitude, phase or polarization of the received field, which can considerably increase the spectral efficiency.

1.2 Diversity Techniques in FSO Communications

A major performance degrading factor in FSO systems, particularly for long ranges, is turbulence-induced fading [5]. A typical fade can last milliseconds and considering that FSO systems operate at the rate of several gigabits per second, a single fade can result in the loss of a large number of consecutive bits. This has motivated many researchers to investigate temporal and spatial diversity techniques such as channel coding, [6, 7], advanced sequence detection techniques [8, 9], and spatial diversity [10–17]. Among those, spatial diversity is particularly attractive with its lower complexity. Spatial diversity involves the use of multiple transmit and/or receive apertures and has been well investigated in wireless radio frequency (RF) communications. Spatial diversity can be easily implemented in FSO systems since the optical wavefront coherence length in the atmosphere is of the

order of centimeters. Therefore, multiple transmitters or receivers only need to be placed centimeters apart to experience independent fading channels. Besides its role as a fading-mitigation tool, multiple-aperture structure reduces the potential for temporary blockage of the laser beam by obstructions e.g., birds.

Although spatial diversity has been investigated in detail for IM/DD systems, see e.g., [11–13, 16, 17] and the references therein, the current literature on coherent FSO systems with spatial diversity is sparse [10, 14, 15]. Haas et al. have addressed the concept of transmit diversity in [10] and proposed space-time channel codes (inspired from RF wireless communication literature) through the minimization of pair wise error probability. In [14] and [15], Lee and Chan have studied receive diversity in coherent FSO systems through the derivation of outage probability. The main focus of their work is the spatial selectivity of coherent receivers which mitigates the effect of background light.

An alternative method to exploit spatial diversity advantages is cooperative diversity, also known as user cooperation, which has been originally introduced for RF wireless systems [18–20]. In RF wireless communications, a cooperative diversity system takes advantage of the broadcasting nature of RF transmission in which the signal transmitted by a source node is overheard by other than destination nodes. The source node along with those nodes which overhear and are willing to share their resources (these nodes are defined as relays) create a virtual antenna array. Such a cooperative scheme is able to extract spatial diversity advantages in a distributed manner.

Cooperative diversity has been also investigated in the context of FSO communications [21–26]. Particularly, in [24], two different configurations of cooperative diversity are considered, namely *parallel* and *serial* relaying. In parallel relaying, the source deploys multiple transmitters with each of them pointing out in the direction of a corresponding relay node. This induces an artificial broadcasting which is normally not possible with a single transmitter in FSO communication due to the line-of-sight nature. The outage analysis of parallel FSO relaying presented in [24] has been obtained for log-normal turbulence model which is limited to weak turbulence conditions. This analysis has been extended to Gamma-Gamma fading channels in [26] for decode-and-forward (DF) relaying strategy. Both of these works have assumed that there is no line-of-sight link between the source and the destination.

On the other hand, serial relaying is a multi-hop transmission scheme where the signal transmitted by the source node (equipped with a single transmitter) propagates through a number of intermediate relay nodes until the destination node. It should be emphasized that serial relaying is typically used in wireless RF communication to broaden the signal coverage for limited-power transmitters and does not offer increase in spatial diversity order. However, unlike the RF channel, the fading variance of FSO channel is distance-dependent. Smartly exploiting this fact, it has been demonstrated in [24] and [27] that impressive performance improvements can be obtained against the degrading effects of turbulence fading in FSO systems through increase in spatial diversity order. It should be also noted that all previous works [21–26] on cooperative FSO communications assume IM/DD systems.

Besides different physical layer techniques, automatic retransmission request (ARQ) can be also applied to FSO systems for further performance improvement. ARQ is a packet-oriented feedback-based data transmission technique which is implemented at the data link layer [28]. With the help of ARQ, the receiver reports back the decoding status to the transmitter. If the received signal is successfully decoded, an acknowledgement (ACK) is fed back to the transmitter and it moves on to the next information message in the transmission queue. On the other hand, in the case of failure, the receiver feeds back a negative acknowledgement (NACK) and the transmitter retransmits the same message. The process continues this way until either the transmitter receives an ACK or the maximum number of ARQ rounds[1] per message is reached. If the latter case happens, an error is declared. In this case, the message may be kept in the transmission buffer for a later attempt or simply discarded. Besides stand-alone ARQ protocols, several types of hybrid-ARQ (H-ARQ) protocols (i.e., protocols which combine channel coding with ARQ) have been proposed in the context of RF communication, see e.g. [28–30], and the references therein.

Recently, the concept of H-ARQ has been extended to FSO communications [31–33]. In [31], an incremental redundancy H-ARQ protocol has been studied for FSO systems through simulations using a low-density-parity-check code family with a particular focus on practical implementation aspects. In [32], the packet error rate performance of chase

[1]The successive transmission of the same massage in an ARQ protocol is referred as "round".

combining H-ARQ protocol over log-normal atmospheric fading channels has been analyzed. In [33], an ARQ protocol based on Round Robin algorithm and random network coding has been proposed for FSO systems. The currently available sparse literature on ARQ in FSO systems has mainly considered IM/DD systems.

1.3 Summary of the Dissertation and Main Contributions

In Chapter 2, we present a brief introduction to FSO communications over atmospheric channels. In Chapter 3, we investigate receive diversity in coherent FSO systems considering the effects of both atmospheric turbulence-induced amplitude fluctuations and phase aberrations. Our analysis differs from earlier work [10, 14, 15] in the sense that we take into account the effect of turbulence-induced phase distortion. Phase compensation techniques [34] can be deployed in coherent receivers to mitigate the phase distortion effects. Our analysis builds on a recently introduced statistical model [35] that characterizes the combined effects of the log-normal turbulence-induced fading and phase compensation. Because of the slowly varying nature of fading in optical channels, we consider outage probability as an appropriate performance measure. Our results demonstrate that significant performance gains can be obtained through the deployment of multiple receive apertures and phase compensation in coherent FSO communications. We also investigate the link reliability, as quantified by the diversity gain [36], and the tradeoff between the link reliability and the spectral efficiency, as quantified by the diversity-multiplexing tradeoff (DMT) [37]. We derive a DMT expression for finite SNR regime which provides insight into performance mechanisms of coherent FSO systems under practical operation range. The derived expression is shown to be a function of the number of receive apertures as well as the effective channel parameter which depends on the turbulence-induced fading characteristics and the number of compensated modes. Our results also demonstrate that modal compensation acts as an additional diversity source besides multiple apertures at the receiver side. The main results of this chapter have been reported in [38, 39].

In Chapter 4, we investigate multi-hop transmission as a distributed spatial diversity technique. In contrast to earlier works [21–24] which have assumed IM/DD systems, we

focus on coherent FSO systems. Specifically, we consider a serial relaying configuration in which the relay nodes employ DF relaying strategy and each of them and the receiver are equipped with multiple heterodyne receivers with phase compensation. Taking into account the effects of both amplitude fluctuations and phase aberrations, we derive outage probability and DMT expressions for the system under consideration. Our outage analysis yields impressive power savings for multi-hop relaying even with a single-relay. Our DMT analysis further demonstrates that the multi-hop transmission improves the diversity gain throughout the range of the multiplexing gain at practical SNR values. The main results of this chapter have been published in [40, 41].

In Chapter 5, we present fundamental performance measures on H-ARQ protocols in coherent FSO communications. Specifically, we consider three H-ARQ protocols: 1) At least once (ALO), 2) Repetition time diversity (RTD) with maximum ratio combiner at the receiver, and 3) Incremental redundancy (INR). We analyze the outage performance and throughput of these protocols in the presence of the Gamma-Gamma turbulence channel. Our analysis demonstrates significant performance improvements through the deployment of ARQ protocols particularly in the strong turbulence regime. Our asymptotic outage analysis further shows that all protocols provide the same diversity order given by $MN \min\{\alpha, \beta\}$ where α and β are the Gamma-Gamma channel parameters, N is the number of receive apertures, and M is the maximum number of ARQ rounds. On the other hand, the coding gains achieved by these three protocols are different. While the coding gain of the ALO scheme is independent of M, those of the RTD and INR schemes grow linearly with respect to M in the range of sufficiently large M values. Our throughput analysis further demonstrates that the INR protocol provides considerably more throughput advantages at large values of transmission rate compared to other protocols. The main results of this chapter have been reported in [42, 43].

In Chapter 6, we return our attention to IM/DD systems and investigate parallel relaying in IM/DD FSO communications over Gamma-Gamma fading channels. We assume a single relay and a line-of-sight link between the source and the destination. For relay node, we consider both DF and amplify-and-forward (AF) modes of cooperation. We develop performance characterizations in terms of the outage probability focusing on high-SNR regime. Specifically, we derive the asymptotic outage performance of each cooperation mode and then, based on the derived expression, quantify the diversity and coding gains

at high-SNR regime. Furthermore, we present DMT expressions for direct transmission and underlying cooperation schemes. Our analysis demonstrates that parallel relaying improves the performance of FSO systems by bringing diversity advantages. The diversity gain in the cooperative transmission improves as much as the minimum of the diversities of the source-relay and the rely-destination channels compared to direct transmission. In addition, between the source-relay and the relay-destination channels, the channel that has worse statistical characteristics dominates the outage performance (diversity and coding gains) at high-SNR regime. Furthermore, comparing two protocols, we show that DF and AF cooperation modes always provide the same diversity gain. However, their coding gains can be different depending on the underlying channels' conditions.

Chapter 2

Background

In this chapter, we present a brief overview of the optical communication through the atmosphere. First, the photodetection process is reviewed. This process represents the key operation in the optical receivers. Afterward, the characteristics of atmospheric turbulent channels are summarized and widely used statistical models for these channels are presented.

2.1 Optical Detection Theory

Photodetection is the process of converting information-bearing optical beam into its equivalent electrical signal with the aim of recovering the transmitted information. The photosensitive surface of the photodector responds to the impinging light by releasing free electrons. These released electrons are then affected by an external electric voltage which causes a current flow at the output of the photodector.

The average rate of the electron release is proportional to the incident optical power as [1]

$$n_q(t) = \frac{\eta}{\hbar\nu_c} \int |U(t, \mathbf{r})|^2 W(\mathbf{r}) d\mathbf{r}, \tag{2.1}$$

where $U(t, \mathbf{r})$ is the incident optical field, $\mathbf{r}$ is the position vector on the receive aperture plane, ν_c is the optical carrier frequency in Hertzs, $\hbar$ is the Planck's constant, and η is the quantum efficiency of the photodetector. The quantum efficiency indicates the fraction of

the incident field power which will be actually detected [1]. The function $W(\mathbf{r})$ in (2.1) defines the area of the receive aperture, i.e.,

$$W(\mathbf{r}) = \begin{cases} 1 & \text{if} \quad |\mathbf{r}| \leqslant \mathcal{D}/2 \\ 0 & \text{if} \quad |\mathbf{r}| > \mathcal{D}/2 \end{cases}, \tag{2.2}$$

where $\mathcal{D}$ is the aperture's diameter.

The probability of observing an electron over an extremely short time interval $(t, t+\Delta t)$ is given by

$$\Pr\{\text{one electron in } (t, t+\Delta t)\} \approx n_q(t)\Delta t \tag{2.3}$$

and the probability of not observing an electron is given by

$$\Pr\{\text{zero electron in } (t, t+\Delta t)\} \approx 1 - n_q(t)\Delta t. \tag{2.4}$$

Consequently, the probability of observing two or more electrons in this small time interval is approximately zero. In addition, the number of electrons observed in non-overlapping time intervals is statistically independent. Therefore, the electron count during a certain time interval can be modeled by a Poisson process with the average count rate of $n_q(t)$ [1].

An electron released at a random time instance t_m produces a response function $\Lambda(t - t_m)$ which is determined by the electron's transit behavior. The area under the response function is equal to a single electron charge q. Assuming $t = 0$ as the time origin for the photodetection process, the photodetected output current is the superposition of the individual effects of each electron released during the time interval $(0, t)$. Hence, the output current can be written as [1]

$$i(t) = \sum_{m=0}^{k(0,t)} \Lambda(t - t_m), \tag{2.5}$$

where t_m is the release time of the m^{th} electron and $k(0, t)$ is the electron count process during $(0, t)$. Therefore, $i(t)$ is a sum of a random number of randomly located response functions $\Lambda(t - t_m)$. Such processes are called *shot noise* processes [1].

For an ideal photodetector with $\Lambda(t) = q\delta(t)$, where $\delta(t)$ is the Dirac delta function,

the mean and the auto-covariance of $i(t)$ can be respectively obtained as [1, 44]

$$E\left[i(t)\right] = \frac{\eta q}{\hbar \nu_c} \int \left|U\left(t, \mathbf{r}\right)\right|^2 W(\mathbf{r}) d\mathbf{r}, \tag{2.6}$$

$$\mathrm{cov}\left[i(t), i(t')\right] = \delta(t - t') \frac{\eta q^2}{\hbar \nu_c} \int \left|U\left(t, \mathbf{r}\right)\right|^2 W(\mathbf{r}) d\mathbf{r}, \tag{2.7}$$

where $E[\cdot]$ denotes the expectation operator. Although the mean and the auto-covariance of $i(t)$ can be computed by (2.6) and (2.7), the actual probability distribution function of this shot noise process at any time instance t is generally difficult to determine. However, when the incident field on the photodector surface is strong enough, $i(t)$ can be modeled by a Gaussian random process [1]. In a typical heterodyne receiver, the local oscillator field is much stronger than the received optical field. This condition assures the Gaussian shot noise model in this type of receivers [1]. On the other hand, the presence of strong background light radiation in the practical IM/DD FSO systems justifies this model [5].

2.2 Statistical Characterization of the Atmospheric Turbulent Channel

An optical beam propagating through the atmosphere experiences a number of degradations. Aerosols and molecules trapped by the Earth's gravity and the thermal inhomogeneities in the atmosphere cause absorption and scattering which result in power loss and wavefront distortion of the transmitted optical field. The path loss of the atmospheric channels is given by [44]

$$\ell(Z) = \frac{A_{TX} A_{RX}}{\left(Z\lambda\right)^2} e^{-\sigma Z}, \tag{2.8}$$

where A_{TX} and A_{RX} respectively denote the areas of the transmit and the receive apertures, Z is the path length in meters, λ is the wavelength of the optical field in meters, and σ is the power attenuation coefficient which consists of scattering and absorption components [1,44].

Besides the path loss, the FSO channel is subject to atmospheric turbulence-induced fading. Space-varying and time-varying thermal inhomogeneous structure of the atmosphere induces random refractive-index fluctuations. Atmospheric medium consists of

many thermal pockets with varying temperatures and diameters. The flow of these thermal pockets create eddies of refractive index turbulence. This turbulence causes random amplitude fluctuations (scintillation) and phase variations (aberration) of the optical field propagating through the atmosphere. The size of turbulence eddies normally ranges from a few millimeters to a few meters, denoted as the inner scale l_0 and the outer scale L_0, respectively [2].

Several statistical models, such as log-normal distribution, K distribution, I-K distribution, negative exponential distribution [2,45], and most recently Gamma-Gamma distribution [46] have been proposed for the atmospheric fading channel. Among them, log-normal and Gamma-Gamma models have attracted most attention in the literature respectively for weak turbulence and weak to strong turbulence regimes because of their better fit to experimental measurements.

2.2.1 Log-normal Turbulence Model

A simple statistical model for the atmospheric turbulence-induced fading is based on the Rytov method [45]. According to this method, the atmosphere turbulent medium consists of several thin slabs. As the optical beam propagates through the atmosphere, each slab modulates the field from the previous slab's perturbation by some incremental amount. The perturbation caused by the k^{th} slab is given by $e^{\chi_k + j\varphi_k}$. Therefore, the atmospheric fading can be obtained by the superposition of these perturbations as

$$g = \prod_k e^{\chi_k + j\varphi_k} = \exp\left(\sum_k \chi_k + j\sum_k \varphi_k\right) = \exp\left(\chi + j\varphi\right), \tag{2.9}$$

where the log-amplitude variable, $\chi = \sum_k \chi_k$, and the phase variable, $\varphi = \sum_k \varphi_k$, have normal distributions according to the central limit theorem [45].

Therefore, the atmospheric fading power coefficient, also called *scintillation* in the optical literature, is a log-normal random variable with the probability distribution function (pdf) of

$$f_h(h) = \frac{1}{h\sqrt{8\pi\sigma_\chi^2}} \exp\left(\frac{-\left(\ln(h) - 2\mu_\chi\right)^2}{8\sigma_\chi^2}\right), \tag{2.10}$$

where h denotes the fading power coefficient ($h = |g^2|$), and μ_χ and σ_χ^2 are the mean and the variance of the random variable χ, respectively. For plane wave propagation through a horizontal path, the log-amplitude variance σ_χ^2 is given by [45]

$$\sigma_\chi^2 = 0.307\mathbb{C}_n^2\kappa^{7/6}Z^{11/6}, \tag{2.11}$$

where κ and $\mathbb{C}_n^2$ respectively denote the optical wave-number and the refractive-index structure constant [45].

2.2.2 Gamma-Gamma Turbulence Model

Although log-normal distribution is the most widely used model for the probability density function of the atmospheric fading power coefficient due to its simplicity, this model is only applicable to weak turbulence conditions [45]. As the strength of the turbulence increases and multiple self-interference effects must be considered, log-normal statistics exhibit large deviations compared to experimental data. It has been particularly observed that log-normal pdf underestimates the behavior in the tails as compared with measurement results [47,48]. Since detection and outage probabilities are primarily based on the tails of the pdf, underestimating this region significantly affects the accuracy of the performance analysis.

Due to the limitations of log-normal distribution for moderate and strong turbulence, Gamma-Gamma statistical model has been proposed recently by Al-Habash et al. [46] which provides a good match to experimental measurements for a wide range of turbulence conditions from weak to strong fluctuation regimes. In this model, the irradiance (optical power per unit surface area) of an optical beam propagating through the atmosphere is modeled as a modulation process in which small-scale (diffractive) fluctuations are multiplicatively modulated by large-scale (refractive) fluctuations. Small-scale fluctuations are associated with turbulent eddies smaller than the Fresnel zone or the spatial coherence radius, whichever is smaller. Large-scale fluctuations in the irradiance are generated by turbulent eddies larger than the first Fresnel zone or the scattering disk, whichever is larger. Small-scale and large-scale fluctuations are assumed to be statistically independent and both of them follow Gamma distribution [46].

Consequently, the atmospheric fading power coefficient can be modeled by Gamma-Gamma ($\Gamma\Gamma$) distribution with the probability density function of

$$f_h(h) = \frac{2(\alpha\beta/\mu)^{(\alpha+\beta)/2}}{\Gamma(\alpha)\Gamma(\beta)} h^{(\alpha+\beta)/2-1} \mathbb{K}_{\alpha-\beta}\left(2\sqrt{\alpha\beta h/\mu}\right), \tag{2.12}$$

where $\mathbb{K}_\nu(\cdot)$ denotes the modified Bessel function of the second kind of order ν [49] and $\mu = E[h]$. The positive parameters α and β respectively represent the effective number of large-scale and small-scale eddies in the scattering process. For plane-wave propagation and zero inner scale, α and β are respectively given by [2]

$$\begin{aligned} \alpha &= \left[\exp\left(\frac{0.49\sigma_R^2}{\left(1+1.11\sigma_R^{12/5}\right)^{7/6}}\right) - 1\right]^{-1} \\ \beta &= \left[\exp\left(\frac{0.51\sigma_R^2}{\left(1+0.69\sigma_R^{12/5}\right)^{5/6}}\right) - 1\right]^{-1} \end{aligned} \tag{2.13}$$

where σ_R^2 denotes the Rytov variance

$$\sigma_R^2 = 1.23\mathbb{C}_n^2\kappa^{7/6}Z^{11/6}. \tag{2.14}$$

Rytov variance indicates the strength of the turbulence fluctuations. Weak, moderate, and strong turbulence conditions are characterized by $\sigma_R^2 < 1$, $\sigma_R^2 \approx 1$, and $\sigma_R^2 > 1$, respectively [2]. In the weak turbulence regime, the effective numbers of small-scale and large-scale eddies are large resulting in $\alpha \gg 1$ and $\beta \gg 1$. Note that in this regime, $\sigma_R^2 \approx 4\sigma_\chi^2$, where σ_χ^2 is the log-amplitude variance given in (2.11). As the fluctuations increase and the focusing regime is approached[1], both α and β decrease considerably. With increasing path length or turbulence strength, multiple-scattering process weakens the focusing effect and the irradiance fluctuations slowly begin to decrease and ultimately saturates. Beyond the focusing regime and approaching the saturation regime, β approaches to one, indicating that the effective number of small-scale eddies finally reduces to one. On the other hand, α increases again by increasing turbulence strength and eventually becomes unbounded in the saturation regime. In this regime, the Gamma-Gamma distribution approaches the negative exponential distribution [46].

[1] In this regime, the focusing caused by large-scale eddies achieves its strongest effect.

2.2.3 Rician Channel Model

Atmospheric turbulence also distorts the spatial coherence of a coherent optical beam propagating through the atmosphere. In effect, the coherent wavefront is divided into several smaller regions over which the beam is approximately coherent. The spatial coherence of an optical wavefront is quantified by the *coherence function* which can be obtained at weak turbulence regime by using the Rytov method as [45]

$$\Gamma_C(\mathrm{r}) = \exp\left(-6.88(\mathrm{r}/\mathrm{r}_0)^{5/3}\right), \tag{2.15}$$

where r denotes the separation distance between two points on the wavefront, and r_0 is the Fried parameter [50] which indicates the atmospheric coherence length. For plane wave propagation, r_0 is given by [50]

$$\mathrm{r}_0 = 1.68\big(\mathbb{C}_n^2\kappa^2 Z\big)^{-3/5}. \tag{2.16}$$

r_0 places fundamental limitations on the performance of the coherent receivers. In fact, it has been shown that [50] when the receive aperture diameter $\mathcal{D}$ is less than r_0, the performance of the coherent receivers improves by increasing the receive aperture size. However, when $\mathcal{D}$ goes beyond r_0, the performance of the system is saturated respect to the receive aperture size and cannot be improved by increasing $\mathcal{D}$. It means that the receiver responds only to an effective aperture diameter $\mathcal{D} = \mathrm{r}_0$. Hence, r_0 indicates a saturation length which characterizes the sensitivity of coherent receivers to the coherence properties of the atmospheric turbulent medium.

To mitigate the distortion of the received optical field due to the turbulence, phase compensation techniques can be employed in coherent receivers. Phase compensation can be implemented as either zonal or modal method [34]. In the zonal method, the aperture is divided into an array of independent segments which are controlled individually to compensate the phase distortion. In the modal compensation, the total phase distortion is decomposed into a set of basis functions (modes) such as Zernike polynomials [51] and then a few modes of this expansion are corrected. The commonality of circular apertures and lenses makes Zernike polynomials attractive for modal compensation because they are a set of orthonormal polynomials defined over a unit circle. The residual phase variance after

the compensation of J Zernike terms over an aperture with diameter $\mathcal{D}$ is given by [51]

$$\sigma_{\varphi}^2 = \Delta_J (\mathcal{D}/\mathrm{r}_0)^2, \tag{2.17}$$

where the coefficient Δ_J is determined by the number of compensated modes. The first few values of Δ_J are shown in Table 2.1. For large values of J ($J > 10$), Δ_J can be approximated as $\Delta_J \approx 0.2944 J^{-\sqrt{3}/2}$ [51].

$\Delta_1 = 1.0299$	$\Delta_5 = 0.0880$	$\Delta_9 = 0.0483$	$\Delta_{13} = 0.0328$	$\Delta_{17} = 0.0255$
$\Delta_2 = 0.582$	$\Delta_6 = 0.0648$	$\Delta_{10} = 0.0401$	$\Delta_{14} = 0.0304$	$\Delta_{18} = 0.0244$
$\Delta_3 = 0.134$	$\Delta_7 = 0.0587$	$\Delta_{11} = 0.0377$	$\Delta_{15} = 0.0279$	$\Delta_{19} = 0.0232$
$\Delta_4 = 0.111$	$\Delta_8 = 0.0525$	$\Delta_{12} = 0.0352$	$\Delta_{16} = 0.0267$	$\Delta_{20} = 0.0220$

Table 2.1: Zernike coefficients

In [35], Belmonte and Kahn have developed a statistical model to characterize the *combined effects* of turbulence-induced phase distortion and amplitude fluctuation on the performance of the coherent receivers with modal phase compensation. This model is based on the Rytov method which is valid only for the weak turbulence regime. The parameters of the proposed model depend on the turbulence conditions and the number of compensated modes applied at the receive aperture.

Let $U_{RX}(t, \mathbf{r})$ be the received field at the receive aperture plane perturbed by turbulence after propagation through the atmosphere. $U_{RX}(t, \mathbf{r})$ can be represented as

$$U_{RX}(t, \mathbf{r}) = U_s(t) \exp\left(\chi(\mathbf{r}) + j\varphi(\mathbf{r})\right), \tag{2.18}$$

where $U_s(t)$ is the turbulence-free received field, and $\chi(\mathbf{r})$ and $\varphi(\mathbf{r})$ respectively represent the log-amplitude and the phase variations caused by the atmospheric turbulence.

The information carrying current at the output of the photodetector can be obtained as [1, 35]

$$\begin{aligned} x(t) &= 2\Re \,\mathrm{Re}\left\{ \int U_{RX}(t, \mathbf{r}) U_L^*(t) W(\mathbf{r}) d\mathbf{r} \right\} \\ &= 2\Re A_{RX} \,\mathrm{Re}\left\{ \xi U_s(t) U_L^*(t) \right\}, \end{aligned} \tag{2.19}$$

where $\Re = q\eta/(\hbar\nu_c)$ is the photodetector responsivity [45], $U_L(t)$ is the local oscillator field, $A_{RX} = \pi\mathcal{D}^2/4$ is the receive aperture area, and ξ is the effective fading coefficient after heterodyning which is given by

$$\begin{aligned}\xi &= \frac{1}{A_{RX}} \int \exp\left(\chi(\mathbf{r}) + j\varphi(\mathbf{r})\right) W(\mathbf{r}) d\mathbf{r} \\ &= \underbrace{\frac{1}{A_{RX}} \int \exp\left(\chi(\mathbf{r})\right) \cos\varphi(\mathbf{r}) W(\mathbf{r}) d\mathbf{r}}_{\xi_r} + j \underbrace{\frac{1}{A_{RX}} \int \exp\left(\chi(\mathbf{r})\right) \sin\varphi(\mathbf{r}) W(\mathbf{r}) d\mathbf{r}}_{\xi_i},\end{aligned} \tag{2.20}$$

where ξ_r and ξ_i respectively represent the integrals of the real and the imaginary parts of the turbulence effect over the receive aperture. These continuous integrals can be expressed as finite sums over $\mathcal{G}$ statistically independent cells (the area within which the received wavefront is approximately coherent) existing in the aperture, i.e.,

$$\xi_r \approx \frac{1}{\mathcal{G}} \sum_{k=1}^{\mathcal{G}} \exp\chi_k \cos\varphi_k, \tag{2.21}$$

$$\xi_i \approx \frac{1}{\mathcal{G}} \sum_{k=1}^{\mathcal{G}} \exp\chi_k \sin\varphi_k, \tag{2.22}$$

where χ_k and φ_k are the log-amplitude and the phase of the k^{th} cell, respectively. The number of independent coherent cells in the aperture is given by[2] [35]

$$\mathcal{G} = \left\{1.09(\rho_0/\mathcal{D})^2 \Gamma\left[1.2, 1.08(\mathcal{D}/\rho_0)^{5/3}\right]\right\}^{-1}, \tag{2.23}$$

where $\Gamma(\cdot,\cdot)$ denotes the lower incomplete Gamma function, and ρ_0 is the generalized Fried parameter which corresponds to partially compensated wavefronts. The generalized Fried parameter after the compensation of J Zernike terms is given by [52]

$$\rho_0 \approx (3.44/\Delta_J)^{3/5} 0.286 J^{-0.362} \mathrm{r}_0. \tag{2.24}$$

Under the assumption that $\mathcal{G}$ is large enough, ξ_r and ξ_i approach jointly normal distribution with probability density function of [53]

$$f_{\xi_r,\xi_i}(\xi_r,\xi_i) = \frac{1}{2\pi\sigma_r\sigma_i} \exp\left(-\frac{(\xi_r-\mu_r)^2}{2\sigma_r^2}\right) \exp\left(-\frac{(\xi_i-\mu_i)^2}{2\sigma_i^2}\right), \tag{2.25}$$

[2]Note that r_0 in Equation (22) of [35] should be replaced by ρ_0.

where μ_r, σ_r^2, μ_i, and σ_i^2 respectively denote the mean of ξ_r, the variance of ξ_r, the mean of ξ_i, and the variance of ξ_i which can be obtained as [35]

$$\mu_r = \mathrm{e}^{-(\sigma_\chi^2+\sigma_\varphi^2)/2}, \tag{2.26}$$

$$\sigma_r^2 = (1/2\mathcal{G})\left(1+\mathrm{e}^{-2\sigma_\varphi^2}-2\mathrm{e}^{-\sigma_\chi^2-\sigma_\varphi^2}\right), \tag{2.27}$$

$$\mu_i = 0, \tag{2.28}$$

$$\sigma_i^2 = (1/2\mathcal{G})(1-\mathrm{e}^{-2\sigma_\varphi^2}). \tag{2.29}$$

In (2.26)-(2.29), σ_χ^2 and σ_φ^2 are the log-amplitude variance and the residual phase variance after modal compensation given by (2.11) and (2.17), respectively.

Consequently, the fading amplitude, $a = |\xi|$, approximately follows Ricean distribution with the following pdf [35]

$$f_a(a) = \frac{2a\,(1+\mathfrak{K})}{\overline{a^2}} \exp\left(-\mathfrak{K} - \frac{(1+\mathfrak{K})\,a^2}{\overline{a^2}}\right) \mathbb{I}_0\left(2a\sqrt{\frac{\mathfrak{K}(1+\mathfrak{K})}{\overline{a^2}}}\right), \tag{2.30}$$

where $\mathbb{I}_0(\cdot)$ denotes the zero-ordered modified Bessel function of the first kind [49] and $\overline{a^2} = \sigma_r^2+\sigma_i^2+\mu_r^2$. The parameter $\mathfrak{K}$ is the ratio of the strength of the coherent component to the incoherent one in the detected field and is given by

$$\mathfrak{K} = \left[\frac{\overline{a^2}}{\sqrt{\mu_r^4+2\mu_r^2(\sigma_i^2-\sigma_r^2)-(\sigma_i^2-\sigma_r^2)^2}} - 1\right]^{-1}. \tag{2.31}$$

Chapter 3

Coherent FSO Communications with Multiple Receivers

In this chapter, we investigate the performance of a coherent FSO communication system with multiple heterodyne receivers. Our analysis builds on the Rician channel model which characterizes the combined effects of turbulence-induced phase distortions and amplitude fluctuations on coherent receivers. We derive closed-form expressions for the outage probability, diversity-multiplexing tradeoff, and diversity gain both for finite and asymptotically high SNR values.

3.1 System Description

Figure 3.1 illustrates the block diagram of a coherent FSO system with N heterodyne receivers. Receive apertures are separated by more than a coherence length to ensure the independence of the fading channels. All receive apertures are assumed to be located within the transmitter field-of-view. To compensate the phase distortion due to the turbulence, modal compensation [34] is deployed in each receive aperture.

The received field at the aperture plane of the k^{th} $(1 \leqslant k \leqslant N)$ receiver is given by

$$U_{r_k}(t, \mathbf{r}) = u_s(t) e^{j(2\pi\nu_c t + \theta_s(t))} \mathrm{e}^{[\chi_k(\mathbf{r}) + j\varphi_k(\mathbf{r})]}, \tag{3.1}$$

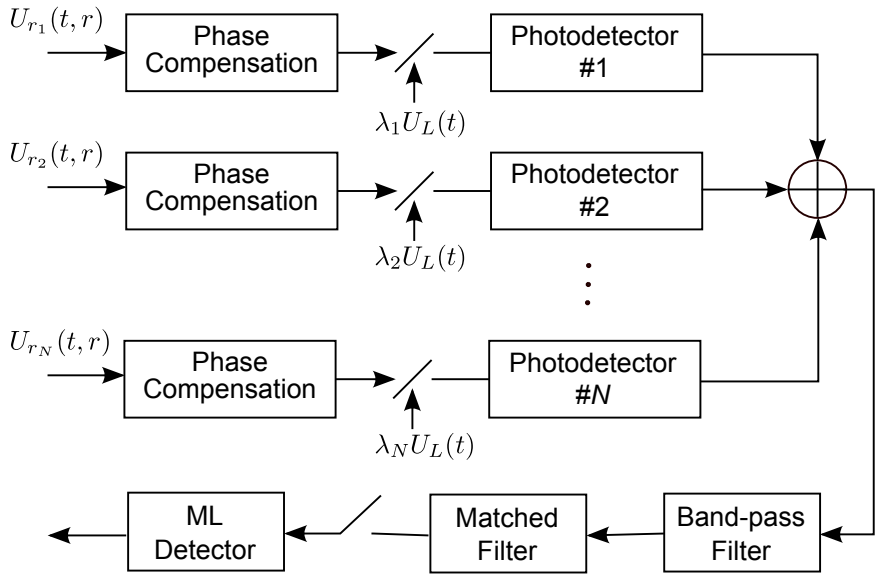

Figure 3.1: Block diagram of a coherent FSO system with multiple heterodyne receivers.

where $u_s(t)e^{j\theta_s(t)}$ is the complex envelope of the modulation signal. $\chi_k(\mathbf{r})$ and $\varphi_k(\mathbf{r})$ represent the turbulence-induced log-normal amplitude fluctuations and Gaussian phase variations of the k^{th} channel, respectively.

Let $U_L(t) = A_L \mathrm{e}^{j(2\pi\nu_L t+\theta_L)}$ be the LO field in the single receiver scenario with amplitude A_L, frequency ν_L, and phase θ_L. The LO field of the k^{th} receiver is multiplied by a proper weighting factor λ_k, $1 \leqslant k \leqslant N$, i.e., $U_{L_k}(t) = \lambda_k U_L(t)$ under the constraint of $\sum_{k=1}^{N} |\lambda_k|^2 = 1$. This constraint ensures that the total LO power in the multi-receiver scenario is equivalent to the LO power in the single receiver case. The summation of the received optical field and the LO field in each diversity branch passes into a photodetector. The total output current of the system is the summation of the output currents of N photodetectors. After the combination of diversity branches' outputs, a band-pass filter is employed to extract the intermediate frequency (IF) component of the total output current.

The noise term at each photodetector output is dominated by the local oscillator shot noise and can be modeled as AWGN [1]. Hence, the IF component of the k^{th} photodetec-

tor's output current can be presented as

$$\begin{aligned} y_k(t) &= x_k(t) + n_k(t) \\ &= 2\Re \operatorname{Re}\left\{ \int U_{r_k}(t,\mathbf{r}) U^*_{L_k}(t) W_k(\mathbf{r}) d\mathbf{r} \right\} + n_k(t) \\ &= \frac{\pi}{2}\Re \mathcal{D}_k^2 u_s(t) A_L \operatorname{Re}\left\{ e^{j(2\pi\nu_{IF}t + \theta_s(t) - \theta_L)} \xi_k \lambda_k^* \right\} + n_k(t), \end{aligned} \tag{3.2}$$

where $n_k(t)$ is the Gaussian noise term and $x_k(t)$ is the information carrying part in which $\nu_{IF} = \nu_c - \nu_L$ denotes the intermediate frequency, $W_k(\mathbf{r})$ defines the area of the k^{th} receive aperture with diameter $\mathcal{D}_k$, and ξ_k represents the effective fading coefficient (after phase compensating and heterodyning) of the k^{th} diversity branch. As discussed in Section 2.2.3, ξ_k can be modeled by a complex Gaussian random variable and its amplitude, $a_k = |\xi_k|$ follows Rician distribution. We assume that ξ_ks are independent identically distributed (i.i.d). The noise term $n_k(t)$ has zero mean and its power spectral density can be calculated by using (2.7) as

$$\begin{aligned} \mathcal{N}_{0,k} &= q\Re \int |U_{L_k}(t)|^2 W_k(\mathbf{r}) d\mathbf{r} \\ &= q\Re \frac{\pi}{4} \mathcal{D}_k^2 |\lambda_k|^2 A_L^2. \end{aligned} \tag{3.3}$$

For the sake of fair comparison in terms of the received signal power, the aperture area of each receiver in the multiple receiver system is assumed to be $1/N$ times the aperture area of a single receiver system, i.e., $\mathcal{D}_k = \mathcal{D}/\sqrt{N}$, $1 \leqslant k \leqslant N$, where $\mathcal{D}$ denotes the receive aperture diameter in the benchmark single receiver system ($N = 1$). Consequently, using (3.2), the IF component of the total output current can be presented as

$$y_T(t) = \sum_{k=1}^{N} y_k(t) = \underbrace{\sum_{k=1}^{N} x_k(t)}_{x_T(t)} + \underbrace{\sum_{k=1}^{N} n_k(t)}_{n_T(t)}, \tag{3.4}$$

where $x_T(t)$ is given by

$$x_T(t) = \frac{\pi \mathcal{D}^2}{2N}\Re A_L u_s(t) \operatorname{Re}\left\{ e^{j(2\pi\nu_{IF}t + \theta_s(t) - \theta_L)} \sum_{k=1}^{N} \xi_k \lambda_k^* \right\}, \tag{3.5}$$

and the power of $n_T(t)$ in the signal carrier bandwidth B_s can be calculated by using (3.3) as

$$P_{n_T} = \frac{\pi}{2} q B_s \Re \frac{\mathcal{D}^2}{N} A_L^2. \tag{3.6}$$

Therefore, the output instantaneous SNR of the system after heterodyning and combining diversity branches can be obtained as

$$\gamma = \frac{P_{x_T}}{P_{n_T}} = \frac{\pi}{4}\mathcal{D}^2 \frac{\Re\mathfrak{I}_s}{qNB_s}\left|\sum_{k=1}^{N}\xi_k\lambda_k^*\right|^2, \tag{3.7}$$

where P_{x_T} is the output signal power and $\mathfrak{I}_s = \overline{|u_s(t)|^2}$ denotes the time average irradiance of the optical signal in Watts per square meters ($\mathrm{W/m^2}$). By using Cauchy-Schwartz inequality [54], the values of λ_ks which maximize SNR can be found as

$$\lambda_{k,opt} = \frac{\xi_k}{\sqrt{\sum_{i=1}^{N}|\xi_i|^2}}. \tag{3.8}$$

Consequently, the corresponding SNR at the maximal ratio combiner output is given by

$$\gamma = \frac{\rho}{N}\sum_{k=1}^{N} a_k^2, \tag{3.9}$$

where $\rho = \pi\Re\mathfrak{I}_s\mathcal{D}^2/(4qB_s)$ is the SNR in the absence of turbulence.

3.2 Diversity and Multiplexing Gains

In this section, we first provide some basic definitions of diversity and multiplexing gains, then present the related derivations for the coherent FSO system under consideration.

Diversity and multiplexing gains are two performance measures commonly used in the performance analysis of wireless radio-frequency multiple antenna systems [55]. There are two potential gains which can be exploited from a multiple antenna system. If the channels between individual transmit-receive antenna pairs experience independent fading, multiple parallel spatial channels are effectively created. By sending different information through these channels, the data rate can be increased in comparison to a single antenna system. This increase in the data rate is known as *multiplexing gain*. On the other hand, by sending the same information through multiple independent channels, independently faded replicas of the information will be obtained at the receiver. Through proper processing of

these multiple replicas, one can decrease the error probability. The resulting performance advantage is known as *diversity gain*.

In general, a scheme that maximizes one gain over a specific communication channel does not guarantee to maximize the other. In fact, it is shown in [37] that there is a tradeoff between these two gains called *diversity-multiplexing tradeoff* (DMT) which prevents maximizing both gains simultaneously. DMT characterizes the maximum possible diversity gain that can be achieved at a given multiplexing gain over a communication channel. Although, this concept has been originally proposed for multiple-input multiple-output (MIMO) systems, DMT can be defined for any communication system including single-input single-output (SISO) systems [37].

3.2.1 Asymptotic versus Finite-SNR DMT

Conventional definitions of diversity and multiplexing gains apply to the asymptotic case when SNR approaches infinity. The diversity gain is defined as [37]

$$d = -\lim_{\rho\to\infty} \frac{\log P_{out}(\mathcal{R},\rho)}{\log \rho}, \tag{3.10}$$

where $\mathcal{R}$ is the target data rate, ρ is the average SNR, and $P_{out}(\mathcal{R},\rho)$ is the outage probability. If the data rate $\mathcal{R}$ is not fixed and increases with SNR, the multiplexing gain is defined as [37]

$$r = \lim_{\rho\to\infty} \frac{\mathcal{R}(\rho)}{\log \rho}. \tag{3.11}$$

From (3.10) and (3.11), one can observe that d is in fact a function of r when the data rate is variable. In such cases, it is said that the diversity gain $d(r)$ is achieved at the multiplexing gain r. The curve of $d(r)$ is known as (asymptotic) DMT [37].

Since conventional definitions apply to the asymptotically high SNRs, definitions for diversity and multiplexing gains for finite-SNR regimes have been further introduced which are particularly useful in evaluating these gains at practical SNR values. The finite-SNR diversity gain is given by [56]

$$d_f(\mathcal{R},\rho) = -\frac{\partial \log P_{out}(\mathcal{R},\rho)}{\partial \log \rho}. \tag{3.12}$$

It represents the negative slope of the log-log plot of the outage probability versus SNR at a target data rate $\mathcal{R}$. When the data rate increases with SNR, the multiplexing gain in finite-SNR regime is defined as the ratio of the data rate $\mathcal{R}(\rho)$ to the capacity of an AWGN channel at a given SNR. It is given by [56]

$$r_f = \frac{\mathcal{R}(\rho)}{\log(1+\rho)}. \tag{3.13}$$

Inserting (3.13) in (3.12), the finite-SNR DMT can be obtained as

$$d_f(r_f, \rho) = -\frac{\rho}{P_{out}(r_f, \rho)} \frac{\partial P_{out}(r_f, \rho)}{\partial \rho}. \tag{3.14}$$

It can be readily checked that the definitions of finite-SNR diversity and multiplexing gains are consistent with the asymptotic ones, that is, $\lim_{\rho\to\infty} d_f = d$ and $\lim_{\rho\to\infty} r_f = r$.

3.2.2 Derivation of Outage Probability

The outage probability at a given data rate $\mathcal{R}$ is defined as [36]

$$P_{out}(\mathcal{R}) = \Pr\left\{C(\gamma) < \mathcal{R}\right\}, \tag{3.15}$$

where $C(\gamma)$ is the instantaneous capacity of the underlying channel and is given by $C(\gamma) = \log_2(1+\gamma)$ for an AWGN channel. Since $C(\cdot)$ is monotonically increasing with γ, (3.15) can be expressed as

$$P_{out}(\mathcal{R}) = \Pr\left\{\gamma < \gamma_{th}\right\}, \tag{3.16}$$

where $\gamma_{th} = C^{-1}(\mathcal{R})$ denotes the threshold SNR that is required to support the rate $\mathcal{R}$.

Replacing (3.9) in (3.16), we have

$$P_{out}(\mathcal{R}) = \Pr\left\{z < N\gamma_{th}/\rho\right\}, \tag{3.17}$$

where $z = \sum_{k=1}^{N} a_k^2$ is a non-central chi-square random variable with $2N$ degrees of freedom and the non-centrality parameter $2\mathfrak{K}N$ ($\mathfrak{K}$ is the Rician channel parameter given in (2.31)). The pdf of z is given by [57]

$$f_z(z) = \frac{(1+\mathfrak{K})}{\overline{a^2}} \left(\frac{(1+\mathfrak{K})z}{N\mathfrak{K}\overline{a^2}}\right)^{\frac{N-1}{2}} e^{-\mathfrak{K}N-(1+\mathfrak{K})\frac{z}{\overline{a^2}}} \mathbb{I}_{N-1}\left(2\sqrt{\frac{\mathfrak{K}(1+\mathfrak{K})Nz}{\overline{a^2}}}\right), \tag{3.18}$$

where $\mathbb{I}_{N-1}(\cdot)$ is the $(N-1)^{th}$-order modified Bessel function of the first kind [49]. Hence, the outage probability is given by

$$\begin{aligned} P_{out}(\mathcal{R},\rho) &= \int_0^{\frac{N\gamma_{th}}{\rho}} f_z(z)dz \\ &= 1 - Q_N\left(\sqrt{2\mathfrak{K}N}, \sqrt{\frac{2(1+\mathfrak{K})N\gamma_{th}}{\rho\overline{a^2}}}\right), \end{aligned} \tag{3.19}$$

where $Q_N(x,y)$ is the generalized Marcum Q-function of order N defined as [57]

$$Q_N(x,y) = \frac{1}{x^{N-1}} \int_y^{\infty} \omega^N \exp\left(-(\omega^2+x^2)/2\right) \mathbb{I}_{N-1}(x\omega)\, d\omega. \tag{3.20}$$

3.2.3 Derivation of Finite-SNR DMT

When the transmission rate of the system increases with respect to SNR, (3.13) yields $\mathcal{R}(\rho) = r_f \log(1+\rho)$. Consequently, the threshold SNR γ_{th} can be obtained in terms of r_f and ρ as

$$\gamma_{th} = 2^{\mathcal{R}} - 1 = (1+\rho)^{r_f} - 1. \tag{3.21}$$

Substituting (3.21) in (3.19) and replacing the resulting expression in (3.14), we have

$$d_f(r_f,\rho) = \frac{\rho}{1 - Q_N(\zeta,\vartheta)} \frac{\partial Q_N(\zeta,\vartheta)}{\partial \vartheta} \frac{\partial \vartheta}{\partial \rho}, \tag{3.22}$$

where $\zeta = \sqrt{2\mathfrak{K}N}$ and ϑ is given by

$$\vartheta = \sqrt{\frac{2(1+\mathfrak{K})N\left[(1+\rho)^{r_f} - 1\right]}{\rho\overline{a^2}}}. \tag{3.23}$$

Using Leibniz integral rule [58], we have

$$\frac{\partial}{\partial \vartheta} Q_N(\zeta,\vartheta) = -\frac{\vartheta^N}{\zeta^{N-1}} e^{\frac{-\left(\vartheta^2+\zeta^2\right)}{2}} \mathbb{I}_{N-1}(\zeta\vartheta). \tag{3.24}$$

Inserting (3.24) in (3.22) and doing some mathematical manipulations, we obtain

$$d_f(r_f,\rho) = \frac{\vartheta^{N+1} e^{\frac{-\left(\vartheta^2+\zeta^2\right)}{2}} \mathbb{I}_{N-1}(\zeta\vartheta)}{2\zeta^{N-1}\left[1 - Q_N(\zeta,\vartheta)\right]} \left(1 - \frac{r_f \rho (1+\rho)^{r_f-1}}{(1+\rho)^{r_f} - 1}\right). \tag{3.25}$$

Next, we investigate the asymptotic value of the DMT at the high-SNR regime. Expressing the Marcum Q-function in terms of its series form [57] and using the equivalent series form of the modified Bessel function [49], (3.25) can be rewritten as

$$d_f(r_f,\rho)=\frac{\sum\limits_{k=0}^{\infty}\frac{1}{k!(N+k-1)!}\left(\frac{\zeta\vartheta}{2}\right)^{2k}}{\sum\limits_{i=0}^{\infty}\left(\frac{\vartheta^2}{2}\right)^{i}\left[\sum\limits_{k=0}^{\infty}\frac{1}{k!(i+k+N)!}\left(\frac{\zeta\vartheta}{2}\right)^{2k}\right]}\left(1-\frac{r_f\rho(1+\rho)^{r_f-1}}{(1+\rho)^{r_f}-1}\right). \tag{3.26}$$

For $\rho\to\infty$, we have $\vartheta\to\sqrt{\Theta\rho^{r-1}}$,where $\Theta=2(1+\mathfrak{K})N/\overline{a^2}$. Noting $0\leqslant r<\min\{1,N\}$ [37], it can be found out that $\lim_{\rho\to\infty}\vartheta=0$. Therefore, the asymptotic value of DMT at high SNR can be obtained as

$$\lim_{\rho\to\infty} d_f(r_f,\rho)=N(1-r). \tag{3.27}$$

This result agrees with the asymptotic behaviour of the DMT for multiple receive antenna systems analyzed in the context of RF communications [37].

3.2.4 Derivation of Finite-SNR Diversity Gain for a Fixed Data Rate

When the data rate $\mathcal{R}$ is kept fixed, the threshold SNR value γ_{th} is constant (i.e., not a function of ρ). Replacing (3.19) in (3.12), we obtain the finite-SNR diversity gain which turns out to have an identical form of (3.22) where ϑ is now given by $\vartheta=\sqrt{2(1+\mathfrak{K})N\gamma_{th}/(\rho\overline{a^2})}$. Consequently, we obtain

$$d_f(\mathcal{R},\rho)=\frac{\vartheta^{N+1}e^{\frac{-\left(\vartheta^2+\zeta^2\right)}{2}}\mathbb{I}_{N-1}(\zeta\vartheta)}{2\zeta^{N-1}\left[1-Q_N\left(\zeta,\vartheta\right)\right]}. \tag{3.28}$$

At high-SNR regime, we have

$$\lim_{\rho\to\infty} d_f(\mathcal{R},\rho)=N, \tag{3.29}$$

demonstrating that the diversity gain is determined by the number of receive apertures.

For a sanity check, note that, at high-SNR regime, the diversity gain at a fixed rate $\mathcal{R}$ is expected to be equal to the DMT evaluated at $r=0$. For $r=0$, (3.27) yields N which coincides with (3.29).

3.3 Numerical Results and Discussions

In this section, we present numerical results for the outage probability, finite-SNR DMT, and diversity gain derived in the previous sections. We assume an FSO system with wavelength $\lambda = 1.55\,\mu$m operating in turbulence conditions with $\mathbb{C}_n^2 = 5 \times 10^{-14}\,\mathrm{m}^{-2/3}$. The path length is $Z = 1\,$km and the aperture diameter of the equivalent single receiver is chosen as $\mathcal{D} = 25\,$cm.

Before we present information theoretic results, we first validate the underlying statistical model for the system with above characteristics. In Figure 3.2, we use Monte Carlo method to simulate the exact channel of each diversity branch for different numbers of receive apertures (N) assuming that $J = 3$ Zernike modes are compensated in each aperture.The Rician pdf used in the theoretical derivation is provided as well. It is observed from Figure 3.2 that the simulated data and the Rician pdf provide a very good match. To quantify the statistical matching, we have also calculated the overlapping coefficient Δ [59] between the theoretical pdf and the empirical pdf. $\Delta = 1$ means that two pdfs are exactly the same and $\Delta = 0$ means two pdfs are completely distinct. In our case, we have found $\Delta = 0.9992$, $\Delta = 0.9942$, $\Delta = 0.9896$, and $\Delta = 0.9836$ for $N = 1$, 2, 3, and 4, respectively.

Figure 3.3 demonstrates the outage probability given by (3.19) along with the Monte Carlo simulation versus normalized turbulence-free SNR (i.e., ρ/γ_{th}) for various numbers of receive apertures $N = 1$, 2, 3, 4 and $J = 3$ compensated modes in each aperture. Due to the time-consuming nature of the Monte-Carlo simulations, simulation results are provided up to 10^{-6}. We observe a very good match between analytical and simulation results. The required SNR to achieve a target outage probability of 10^{-5} for $N = 1$ is 64 dB (not shown in the figure for the brevity of the presentation). Through the deployment of multiple apertures, we observe impressive performance gains (in terms of the power efficiency) of 30 dB, 42.5 dB, and 48 dB, respectively, for $N = 2$, 3, and 4 in comparison to the benchmark scheme of single receive aperture system. It is also observed that, at high-SNR regime, the diversity gain is determined by the number of receive apertures as expected from our analytical result given by (3.29).

Figure 3.4 illustrates the finite-SNR DMT given by (3.26) for a system with $N = 2$ and $J = 6$ assuming SNR = 10, 20, 30, 60 dB. It is interesting to note that for practical SNR

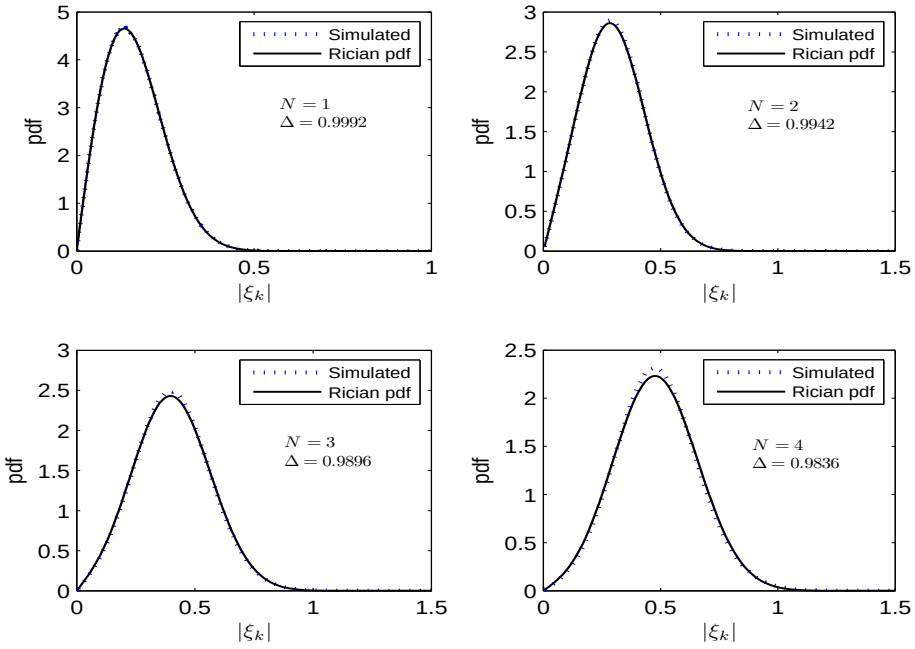

Figure 3.2: Simulated and Rician pdfs for different number of receive apertures.

values, the maximum diversity gain does not occur at zero multiplexing gain. This is mainly due to the presence of the coherent component in the received field which is a phenomenon also observed in wireless RF systems [56, 60]. Recall from (3.25) that the finite-SNR DMT is a function of not only the number of receive apertures but also the channel parameter $\mathfrak{K}$, which is defined as the ratio of the strength of the coherent component to the incoherent one in the detected field. When SNR increases, the incoherent (random) component begins to dominate the system performance and the DMT curve gradually approaches its asymptotic value, i.e., the plot labeled with SNR $= \infty$.

Figure 3.5 depicts the finite-SNR diversity gain for a fixed data rate (given by (3.28)) assuming different number of receive apertures $N = 1$, 2, 3, 4 and $J = 3$. It is observed that, for $N = 1$, the maximum diversity gain is achieved in high-SNR regime. In this case, the strength of the coherent component to the incoherent one in the detected field (quantified by $\mathfrak{K}$) is so small that the effective channel distribution approaches Rayleigh distribution. As N increases, $\mathfrak{K}$ improves and consequently, the maximum diversity gain occurs at a finite value of SNR. In this range of moderate SNRs, the coherent component is the dominating

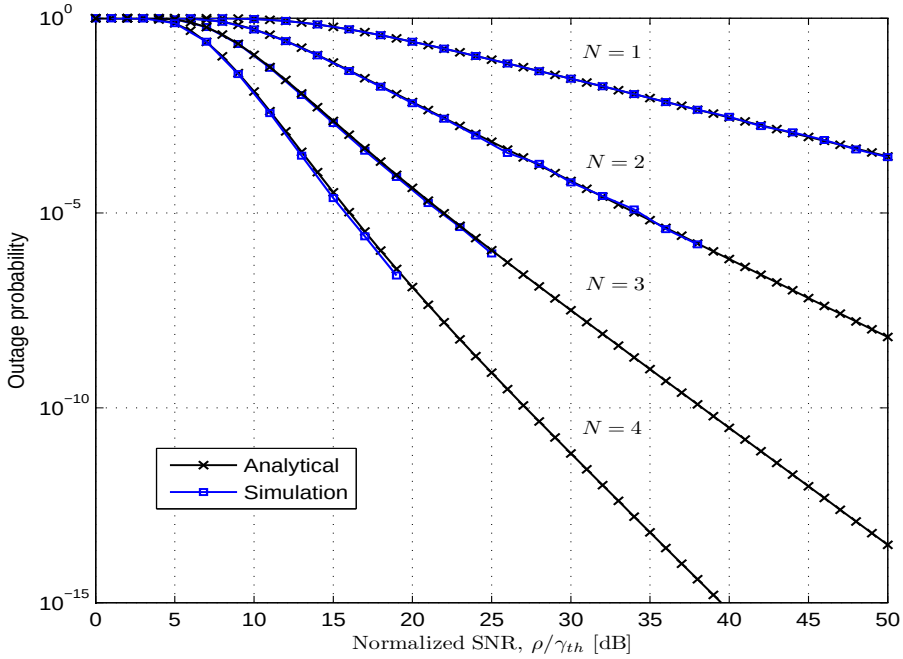

Figure 3.3: Outage probability for different number of receive apertures.

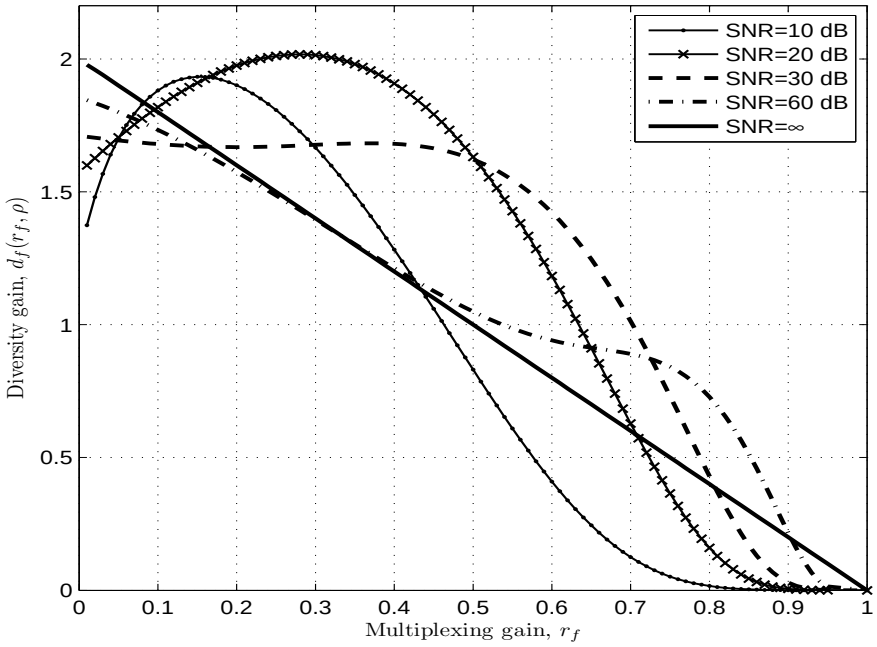

Figure 3.4: Finite-SNR DMT for various values of SNR ($N = 2$).

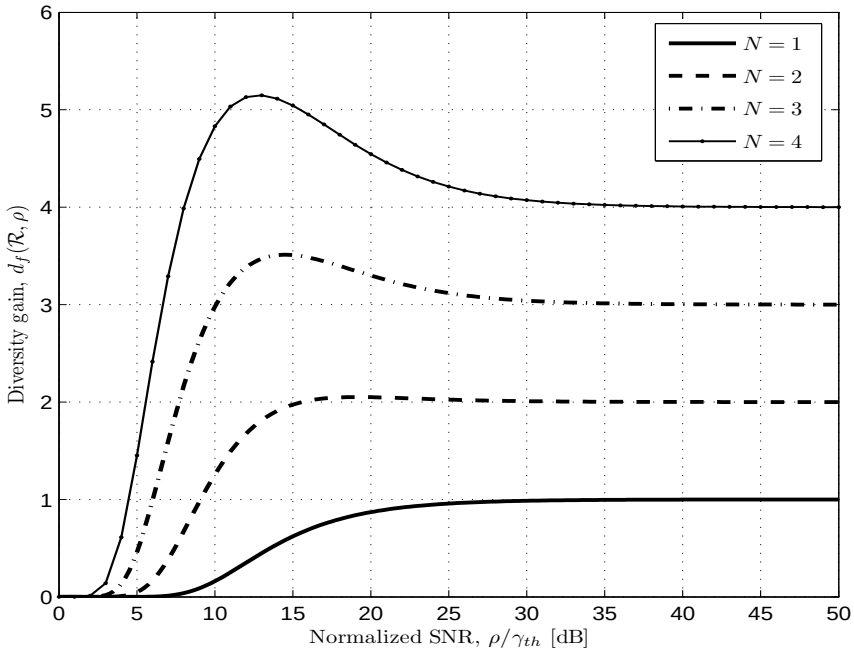

Figure 3.5: Diversity gain (at a fixed transmission rate) for various numbers of receive apertures.

factor and results in a peak in the finite-SNR diversity gain. As SNR increases, the incoherent component begins to dominate and decreases the diversity gain which finally converges to the asymptotic one determined by the number of receive apertures.

In Figure 3.4 and Figure 3.5, we have observed the effect of the coherent component (through dependence on $\mathfrak{K}$) on the system performance. One can check from (2.31) that $\mathfrak{K}$ is a function of channel parameters as well as the number of compensated modes (J) latter of which is in fact a system design parameter. In Figure 3.6, we study the effect of J on the finite-SNR diversity gain. We assume $J = 1, 6, 11, 21$ and consider $N = 1$. Similar to our observations in Figure 3.5 for $N = 1$, when $J = 1$ (only the "piston" mode is compensated), $\mathfrak{K}$ is very small and consequently, the effective channel behaves like Rayleigh distribution and causes maximum diversity gain to occur at high-SNR regime. But, as J increases, the finite-SNR diversity gain takes larger values. This actually indicates that modal compensation acts as an additional diversity source besides multiple apertures in the finite-SNR regime. Nevertheless, the asymptotic value for all cases converges to the

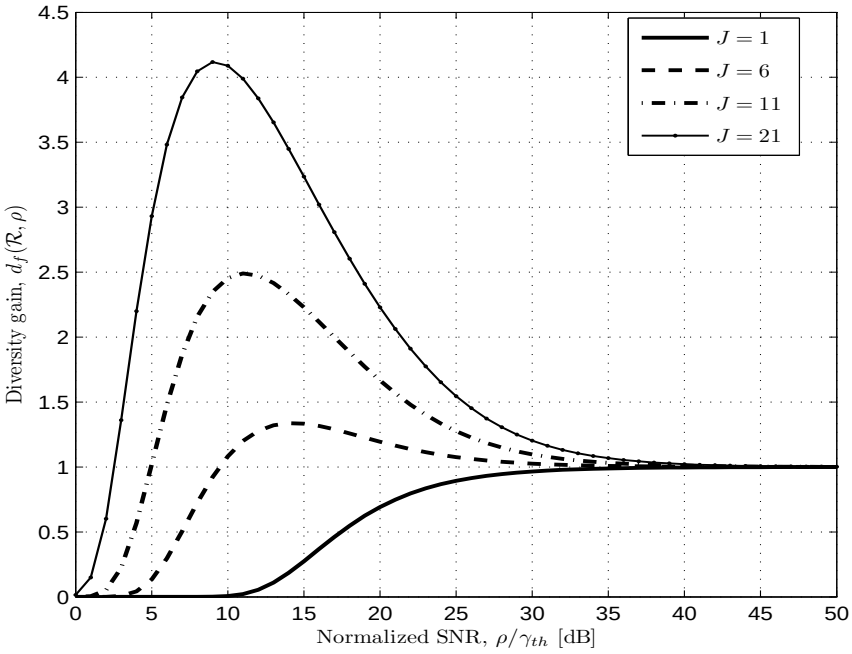

Figure 3.6: The effect of the modal compensation on the finite-SNR diversity gain.

number of receive aperture ($N = 1$ in this example), as expected from (3.29).

As our results demonstrate, both multiple receivers and modal compensation provide diversity gains. Preference of one method to another or simultaneous deployment depends on the cost and complexity issues. In the absence of atmospheric fading, deployment of a large receive aperture increases the total received signal power and therefore improves the system performance. On the other hand, the presence of the atmospheric turbulence causes the incoherency of the received field and results in significant performance degradation particularly for large apertures.

For performance improvement, one can increase the number of compensated modes, but this comes at the cost of higher complexity. Alternatively, one can create an effective large aperture at the receiver by deploying multiple smaller apertures whose total aperture area is equal to that of the large one. When the diameter of each aperture becomes smaller, the received wavefront is more coherent over each aperture compared to the system with a larger aperture. Therefore, only a few first modes can be compensated to yield a desirable

performance and high order compensation is not required.

Chapter 4

Multi-Hop Coherent FSO Communications

In this chapter, we investigate multi-hop relaying in coherent FSO communications over atmospheric channels. We consider an FSO relaying system with DF relay nodes and multiple heterodyne receivers with modal compensation. Considering the combined effects of turbulence-induced amplitude fluctuations and phase aberrations, we derive the outage probability and quantify the potential performance improvements through the derivation of DMT and diversity gain.

4.1 System Model

We consider a coherent multi-hop FSO relaying system as illustrated in Figure 4.1. The source signal arrives at the destination via a sequence of $K+1$ hops through K intermediate relays. The nodes in the network are serially indexed from 0 to $K+1$ where $k=0$ and $k=K+1$ refer to the source and the destination, respectively. We consider full-duplex relaying and assume no interference between individual FSO channels. The link range Z_{SD} (i.e., distance from the source to the destination) is given by $Z_{SD}=\sum_{k=1}^{K+1} Z_k$ where Z_k, $k=1,2,\ldots,K+1$, is the length of the k^{th} hop. All nodes are equipped with single transmitters and each has the transmit-optical power of $P=P_T/(K+1)$ where P_T is the total power budget of the system.

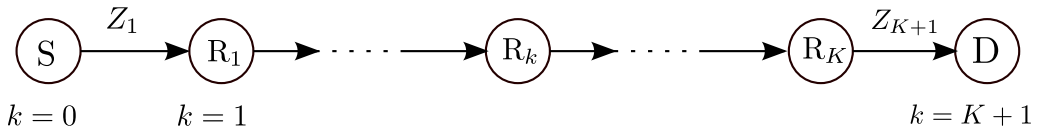

Figure 4.1: Coherent FSO multi-hop relaying configuration.

Relay and destination nodes have more than one heterodyne receiver (not necessarily the same number) to further exploit the receive diversity. Let the k^{th} node, $1 \leqslant k \leqslant K+1$, be equipped with m_k parallel heterodyne receivers. The aperture diameter of each receiver located in the k^{th} node is given by $\mathcal{D}_k = \mathcal{D}/\sqrt{m_k}$ where $\mathcal{D}$ is the total receive aperture diameter. All receive apertures are located within the field-of-view of the previous transmitter. Receive apertures are separated by more than the channel coherence length to ensure independent fading channels.

Each relay first combines the diversity branches using a maximum ratio combiner [57]. Then, it decodes the transmitted information and retransmits it to the next relay (or to the destination in the last hop). The noise term at each receiver's output is dominated by the LO shot noise and can be modeled as AWGN. Using the results of Section 3.1, the IF component of the output signal at the k^{th} node after heterodyning and diversity combining is given by

$$y_k(t) = x_k(t) + n_k(t), \tag{4.1}$$

where $n_k(t)$ is the noise term and the information carrying part $x_k(t)$ is

$$x_k(t) = \frac{\pi}{2}\Re A_L \frac{\mathcal{D}^2}{m_k}\sqrt{\sum_{i=1}^{m_k}|\xi_{k,i}|^2}u_k(t)\cos\left[2\pi\nu_{IF}t + \theta_k(t) - \theta_L\right]. \tag{4.2}$$

Here, $u_k(t)e^{j\theta_k(t)}$ is the complex envelope of the modulation signal received at the k^{th} node, and $\xi_{k,i}$ denotes the effective fading coefficient of the i^{th} diversity branch in the k^{th} hop. As discussed in Section 2.2.3 of Chapter 2, $a_{k,i} = |\xi_{k,i}|$ follows Rician distribution with parameters $\overline{a_{k,i}^2}$ and $\mathfrak{K}_{k,i}$. We assume that the channel coefficients within each hop are i.i.d, i.e., $\mathfrak{K}_{k,i} = \mathfrak{K}_k$ and $\overline{a_{k,i}^2} = \overline{a_k^2}$ for $1 \leqslant i \leqslant m_k$. Sub-channels from one hop to another hop are assumed to be mutually independent, but not necessarily identical.

4.2 Derivation of Outage Probability

In the multi-hop transmission scheme with the DF relaying under consideration, the outage of any intermediate sub-channels causes a failure in the source-destination communication. Hence, using (3.16), the outage probability of the end-to-end scheme, denoted by P_{out}^{SD}, is given by

$$\begin{aligned} P_{out}^{SD} &= \Pr\left\{\bigcup_{k=1}^{K+1}(\gamma_k < \gamma_{th})\right\} \\ &= 1 - \Pr\left\{\bigcap_{k=1}^{K+1}(\gamma_k \geqslant \gamma_{th})\right\} \\ &= 1 - \prod_{k=1}^{K+1}\left(1 - P_{out}^{k}\right) \end{aligned} \tag{4.3}$$

where P_{out}^{k} is the outage probability of the k^{th} intermediate single-input multiple-output (SIMO) link with m_k receive apertures, and $\gamma_k = P_{x_k}/P_{n_k}$ is the output SNR at the k^{th} node. P_{x_k} and P_{n_k} are, respectively, the average received signal power and the noise power at the k^{th} node. Using (4.2), P_{x_k} is calculated as

$$P_{x_k} = \frac{\pi}{2}\frac{\mathcal{D}^2}{m_k^2}\Re^2 A_L^2 P_{r_k}^2 \sum_{i=1}^{m_k} a_{k,i}^2, \tag{4.4}$$

where $P_{r_k} = \overline{|u_k(t)|^2}\pi\mathcal{D}^2/4$ is the average received optical power at the k^{th} node in the absence of the atmospheric fading effect. P_{r_k} is related to the average transmit optical power per transmit aperture (P) by $P_{r_k} = \mathcal{L}_k P$ where $\mathcal{L}_k$ denotes the path loss of the k^{th} hop normalized with respect to the path loss of the end-to-end link, i.e.,

$$\mathcal{L}_k = \frac{\ell\left(Z_k\right)}{\ell\left(Z_{\mathrm{SD}}\right)}. \tag{4.5}$$

On the other hand, the noise power within the signal bandwidth of B_s is given by

$$P_{n_k} = \frac{\pi}{2} q B_s \Re \frac{D^2}{m_k} A_L^2. \tag{4.6}$$

Using (4.4) and (4.6), we have

$$\gamma_k = \frac{\mathcal{L}_k \rho}{m_k\left(K+1\right)} \sum_{i=1}^{m_k} a_{k,i}^2, \tag{4.7}$$

where $\rho = \Re P_T/qB_s$ is the total turbulence-free and path loss-free SNR of the system.

Noting that $a_{k,i}$ has Rician distribution with parameters $\mathfrak{K}_k$ and $\overline{a_k^2}$, we obtain P_{out}^k as

$$P_{out}^k = 1 - Q_{m_k}\left(\sqrt{2m_k\mathfrak{K}_k}, \sqrt{\frac{2m_k(1+\mathfrak{K}_k)(K+1)}{\mathcal{L}_k\rho\overline{a_k^2}}\gamma_{th}}\right). \tag{4.8}$$

Therefore, inserting (4.8) in (4.3), the outage probability of the end-to-end transmission is obtained as

$$P_{out}^{SD} = 1 - \prod_{k=1}^{K+1} Q_{m_k}\left(\sqrt{2m_k\mathfrak{K}_k}, \sqrt{\frac{2m_k(1+\mathfrak{K}_k)(K+1)\gamma_{th}}{\mathcal{L}_k\rho\overline{a_k^2}}}\right). \tag{4.9}$$

4.3 Diversity and Multiplexing Gains

4.3.1 Finite-SNR DMT

When the transmission rate $\mathcal{R}$ increases by SNR as $\mathcal{R}(\rho) = r_f \log(1+\rho)$, the threshold SNR γ_{th} depends on r_f and ρ as $\gamma_{th} = 2^{\mathcal{R}} - 1 = (1+\rho)^{r_f} - 1$. Replacing this in (4.9) yields

$$P_{out}^{SD}(r_f, \rho) = 1 - \prod_{k=1}^{K+1} Q_{m_k}(\zeta_k, \vartheta_k), \tag{4.10}$$

where $\zeta_k = \sqrt{2m_k\mathfrak{K}_k}$ and

$$\vartheta_k = \sqrt{\frac{2m_k(1+\mathfrak{K}_k)(K+1)}{\mathcal{L}_k\rho\overline{a_k^2}}\left((1+\rho)^{r_f} - 1\right)}. \tag{4.11}$$

From (3.14) and (4.10), the finite SNR DMT of the end-to-end scheme can be obtained as

$$\begin{aligned} d_f^{SD}(r_f, \rho) &= -\frac{\rho}{P_{out}^{\mathrm{SD}}(r_f, \rho)}\frac{\partial P_{out}^{\mathrm{SD}}(r_f, \rho)}{\partial \rho} \\ &= \frac{\rho}{1 - \prod_{k=1}^{K+1} Q_{m_k}(\zeta_k, \vartheta_k)} \sum_{k=1}^{K+1}\left(\frac{\partial Q_{m_k}(\zeta_k, \vartheta_k)}{\partial \vartheta_k}\frac{\partial \vartheta_k}{\partial \rho}\prod_{i=1, i\neq k}^{K+1} Q_{m_i}(\zeta_i, \vartheta_i)\right) \end{aligned} \tag{4.12}$$

After some mathematical manipulations, we obtain $d_f^{SD}(r_f,\rho)$ as

$$d_f^{SD}(r_f,\rho)=\left(1-\frac{r_f\rho(1+\rho)^{r_f-1}}{(1+\rho)^{r_f}-1}\right)\frac{\sum_{k=1}^{K+1}\left(\frac{\vartheta_k^{m_k+1}}{\zeta_k^{m_k-1}}e^{\frac{-\left(\vartheta_k^2+\zeta_k^2\right)}{2}}\mathbb{I}_{m_k-1}(\zeta_k\vartheta_k)\prod_{i=1,i\neq k}^{K+1}Q_{m_i}\left(\zeta_i,\vartheta_i\right)\right)}{2\left[1-\prod_{k=1}^{K+1}Q_{m_k}\left(\zeta_k,\vartheta_k\right)\right]}. \tag{4.13}$$

It is also possible to write $d_f^{SD}(r_f,\rho)$ in terms of the finite-SNR DMT of each SIMO sub-channel. Rewriting (4.13) as

$$\begin{aligned}d_f^{SD}(r_f,\rho)=&\frac{\prod_{i=1}^{K+1}Q_{m_i}\left(\zeta_i,\vartheta_i\right)}{\left[1-\prod_{k=1}^{K+1}Q_{m_k}\left(\zeta_k,\vartheta_k\right)\right]}\\&\times\sum_{k=1}^{K+1}\left(\frac{\vartheta_k^{m_k+1}\mathbb{I}_{m_k-1}(\zeta_k\vartheta_k)e^{\frac{-\left(\vartheta_k^2+\zeta_k^2\right)}{2}}}{2\zeta_k^{m_k-1}\left[1-Q_{m_k}\left(\zeta_k,\vartheta_k\right)\right]}\right)\left(1-\frac{r_f\rho(1+\rho)^{r_f-1}}{(1+\rho)^{r_f}-1}\right)\left(\frac{1-Q_{m_k}\left(\zeta_k,\vartheta_k\right)}{Q_{m_k}\left(\zeta_k,\vartheta_k\right)}\right)\end{aligned} \tag{4.14}$$

and using the values of P_{out}^k and P_{out}^{SD} given in (4.8) and (4.9), respectively, we obtain

$$d_f^{SD}(r_f,\rho)=\frac{1-P_{out}^{SD}}{P_{out}^{SD}}\sum_{k=1}^{K+1}d_f^k(r_f,\rho)\frac{P_{out}^k}{1-P_{out}^k}, \tag{4.15}$$

where

$$d_f^k(r_f,\rho)=\frac{\vartheta_k^{m_k+1}}{\zeta_k^{m_k-1}}\frac{e^{\frac{-\left(\vartheta_k^2+\zeta_k^2\right)}{2}}\mathbb{I}_{m_k-1}(\zeta_k\vartheta_k)}{2\left[1-Q_{m_k}\left(\zeta_k,\vartheta_k\right)\right]}\left(1-\frac{r_f\rho(1+\rho)^{r_f-1}}{(1+\rho)^{r_f}-1}\right), \tag{4.16}$$

is the finite-SNR DMT of the k^{th} SIMO sub-channel.

For a sanity check, the asymptotic behavior of the derived DMT at high SNR is investigated in Appendix 4A. It is shown that

$$\lim_{\rho\to\infty}d_f^{SD}(r_f,\rho)=\hat{m}(1-r),\qquad 0\leqslant r<1 \tag{4.17}$$

where $\hat{m}=\min_k\{m_k\}$. This result agrees with the asymptotic DMT of the multi-hop relay channels analyzed in the context of RF communications [61]. It demonstrates that at high SNR regime, the DMT of the end-to-end scheme is determined by the minimum of the underlying sub-channels' DMT values throughout the range of the multiplexing gain.

4.3.2 DMT for the Symmetrical Configuration

In the previous section, we have investigated our system for the general case in which sub-channels from one hop to another hop are independent but not necessarily identically distributed. In the following, we consider a symmetrical scenario in which the relay nodes are evenly distributed between the source and the destination, i.e., $Z_k = Z_{SD}/(K+1)$, $1 \leqslant k \leqslant K+1$. All the relays and the destination are assumed to have equal number of heterodyne receivers denoted by m_o ($m_k = m_o \ \forall k$). It is further assumed that sub-channels from one hop to another hop are independent and identically distributed with parameters $\mathfrak{K}_o$ and $\overline{a_o^2}$ ($\mathfrak{K}_k = \mathfrak{K}_o$ and $\overline{a_k^2} = \overline{a_o^2} \ \forall k$). Under these assumptions, the outage probability in (4.10) can be simplified as

$$P_{out}^{SD} = 1 - \left[Q_m \left(\sqrt{2m_o\mathfrak{K}_o}, \sqrt{\frac{2m_o(1+\mathfrak{K}_o)(K+1)}{\mathcal{L}_o \rho \overline{a_o^2}} \left((1+\rho)^{r_f} - 1 \right)} \right) \right]^{K+1}, \tag{4.18}$$

where $\mathcal{L}_o$ is the normalized path loss for all hops. The finite-SNR DMT in (4.13) can be also simplified as

$$d_f^{SD}(r_f, \rho) = \frac{(K+1)\, \vartheta^{m_o+1} e^{\frac{-\left(\zeta^2+\vartheta^2\right)}{2}} \mathbb{I}_{m_o-1}(\zeta\vartheta)\, Q_{m_o}^K(\zeta, \vartheta)}{2\zeta^{m_o-1}\left(1 - Q_{m_o}^{K+1}(\zeta, \vartheta)\right)} \left(1 - \frac{r_f \rho (1+\rho)^{r_f-1}}{(1+\rho)^{r_f} - 1} \right), \tag{4.19}$$

where $\zeta = \sqrt{2m_o\mathfrak{K}_o}$ and $\vartheta = \sqrt{2m_o(1+\mathfrak{K}_o)(K+1)\left((1+\rho)^{r_f}-1\right)/(\mathcal{L}_o\rho\overline{a_o^2})}$.

For this special case, we prove in Appendix 4B that the finite-SNR DMT of the end-to-end scheme is upper bounded by

$$d_f^{SD}(r_f, \rho) \leqslant d_f^1(r_f, \rho), \tag{4.20}$$

where $d_f^1(r_f, \rho)$ is the finite-SNR DMT of each SIMO sub-channel. This demonstrates that for a target transmission rate, the reliability (indicated by the diversity gain) of the end-to-end scheme is upper bounded by that of each intermediate hop.

4.3.3 Finite SNR Diversity Gain for a Fixed Transmission Rate

In this section, we derive the finite SNR diversity gain when the transmission rate $\mathcal{R}$ is fixed, i.e., it does not vary with SNR. Note that under this assumption, γ_{th} is a constant and

independent of ρ. Using (3.10) and (4.9), the finite SNR diversity gain of the end-to-end scheme for a fixed $\mathcal{R}$ is obtained as

$$d_f^{SD}(\mathcal{R},\rho)=\frac{\sum_{k=1}^{K+1}\left(\frac{\vartheta_k^{m_k+1}}{\zeta_k^{m_k-1}}e^{\frac{-\left(\vartheta_k^2+\zeta_k^2\right)}{2}}\mathbb{I}_{m_k-1}(\zeta_k\vartheta_k)\prod_{i=1,i\neq k}^{K+1}Q_{m_i}\left(\zeta_i,\vartheta_i\right)\right)}{2\left[1-\prod_{k=1}^{K+1}Q_{m_k}\left(\zeta_k,\vartheta_k\right)\right]}, \tag{4.21}$$

in which ϑ_k is now given by $\vartheta_k=\sqrt{2m_k(1+\mathfrak{K}_k)(K+1)\gamma_{th}/(\mathcal{L}_k\rho\overline{a_k^2})}$. From (4.13) and (4.21), it can be readily checked that

$$d_f^{SD}(r_f,\rho)=d_f^{SD}(\mathcal{R},\rho)\big|_{\mathcal{R}=r_f\log(1+\rho)}\times\left(1-\frac{r_f\rho(1+\rho)^{r_f-1}}{(1+\rho)^{r_f}-1}\right). \tag{4.22}$$

Although the derivations of the finite-SNR DMT and the diversity gain at a fixed rate are very similar, they represent two individual performance metrics at practical SNR values and they are not equivalent for any specific value of multiplexing gain r. However, at high SNR regime, it is expected that the diversity gain at a fixed rate $\mathcal{R}$ will be equal to the DMT at $r=0$ [37]. It can be readily checked from (4.17) that the asymptotic DMT at $r=0$ is given by $\hat{m}$ while from (4.21) one can obtain $\lim_{\rho\to\infty}d_f^{SD}(\mathcal{R},\rho)=\hat{m}$, as expected. This result demonstrates that, at high SNR regime, the diversity order of the end-to-end transmission is restricted by the minimum number of receive apertures of each hop.

4.4 Numerical Results and Discussions

In this section, we present numerical results for the outage probability, DMT and diversity gain using the analytical expressions derived in the previous sections. We consider an FSO system with the wavelength $\lambda=1.55\,\mu$m operating in the turbulence conditions with the refractive index structure constant $\mathbb{C}_n^2=1\times10^{-14}\,\mathrm{m}^{-2/3}$ and attenuation of 0.44dB/km (i.e., $\sigma\approx0.1$). The link range is $Z_{SD}=5\,$km and the total receive aperture diameter at each node is $\mathcal{D}=25\,$cm.

In the first three figures (Figure 4.2-Figure 4.4), to demonstrate the diversity advantages extracted from multi-hop transmission in FSO systems, we assume each node is equipped

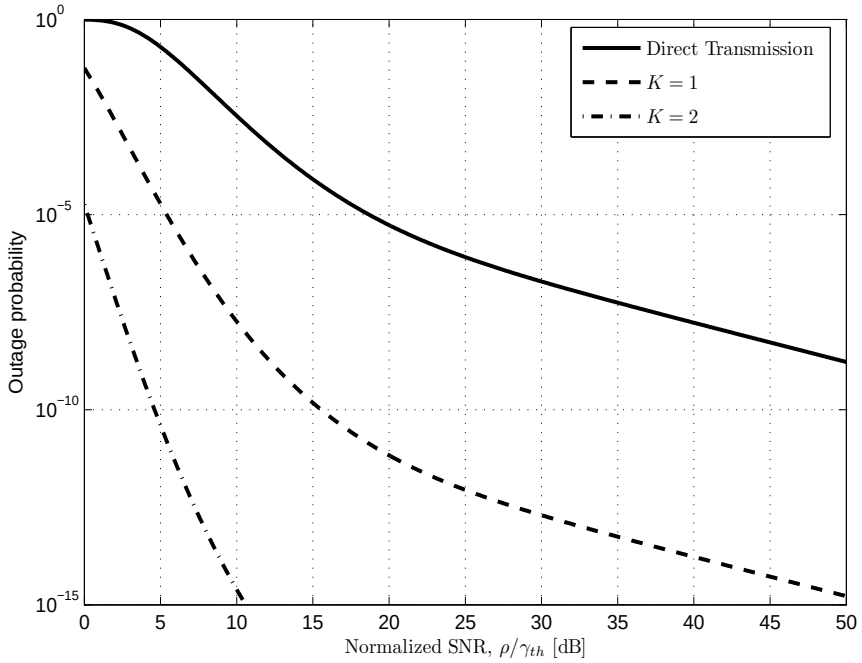

Figure 4.2: Outage probability for multi-hop coherent FSO systems with $K = 1, 2$, and $m_o = 1$.

with single receive aperture i.e., $m_k = 1,\ \ 1 \leqslant k \leqslant K+1$, and therefore, no receive diversity is available. At each receive aperture, $J = 6$ Zernike modes are compensated. We assume a symmetrical scenario for these figures.

Figure 4.2 illustrates the outage probability given by (4.9) versus normalized SNR (ρ/γ_{th}) for $K = 1, 2$. For comparison purposes, the outage probability of the direct transmission is also presented in this figure. It is observed that multi-hop transmission exploits the distance-dependent characteristic of fading variance and significantly improves the system performance. Specifically, at a target outage probability of 10^{-8}, impressive performance improvements of 31.5 dB and 39.2 dB are, respectively, observed with one and two relays in comparison to the benchmark direct transmission system.

Figure 4.3 depicts the finite SNR diversity gain given by (3.28) for a fixed transmission rate $\mathcal{R}$. This actually corresponds to the negative slope of the outage probability curves illustrated in Figure 4.2. It is observed that increasing the number of relays improves the finite-SNR diversity gain. Moreover, the maximum diversity gain occurs at a finite value

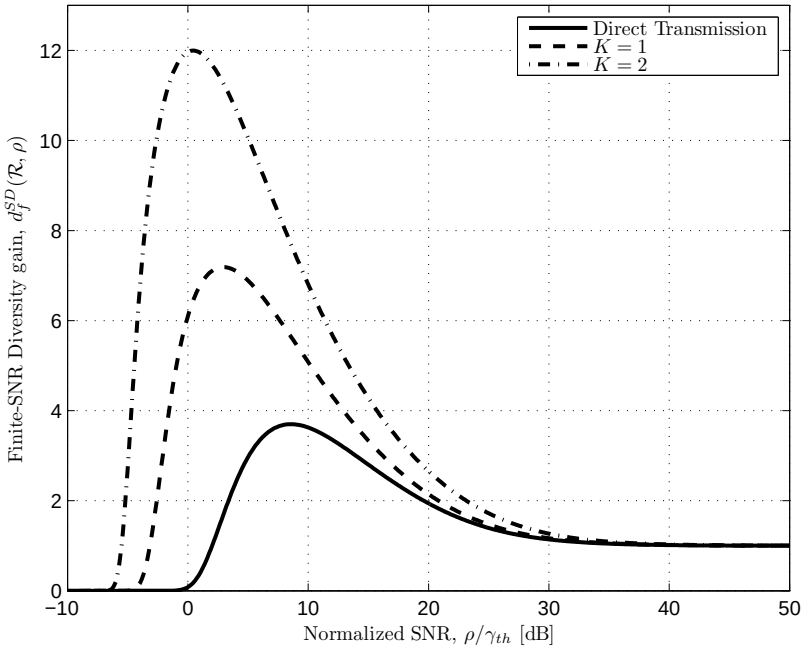

Figure 4.3: Finite SNR diversity gain at a fixed transmission rate $\mathcal{R}$ for $K = 1, 2$, and $m_o = 1$.

of SNR. This is mainly due to the presence of the coherent component in the received field. Indeed, at moderate SNRs, the presence of the coherent component causes a steep drop in the outage probability and results in a peak in the finite SNR diversity gain. As the SNR increases, the incoherent (random) component begins to dominate the system performance and decreases the diversity gain to its asymptotic value which is equal to one in our case.

Figure 4.4 illustrates the finite SNR DMT given by (4.13) for various numbers of relays $K = 1, 2$ assuming a fixed SNR $= 10$ dB. It is observed that multi-hop transmission provides diversity advantages throughout the range of the multiplexing gain. Especially, at high values of multiplexing gain, the diversity gain of the direct transmission approaches zero which can be avoided by the proposed multi-hop transmission.

Figure 4.5 presents a performance comparison between multi-hop coherent and IM/DD systems assuming the deployment of single relay and single receive apertures. For IM/DD systems, it has been shown in [62] through experimental observations that the effective fading amplitude coefficient for a large receive aperture follows log-normal distribution.

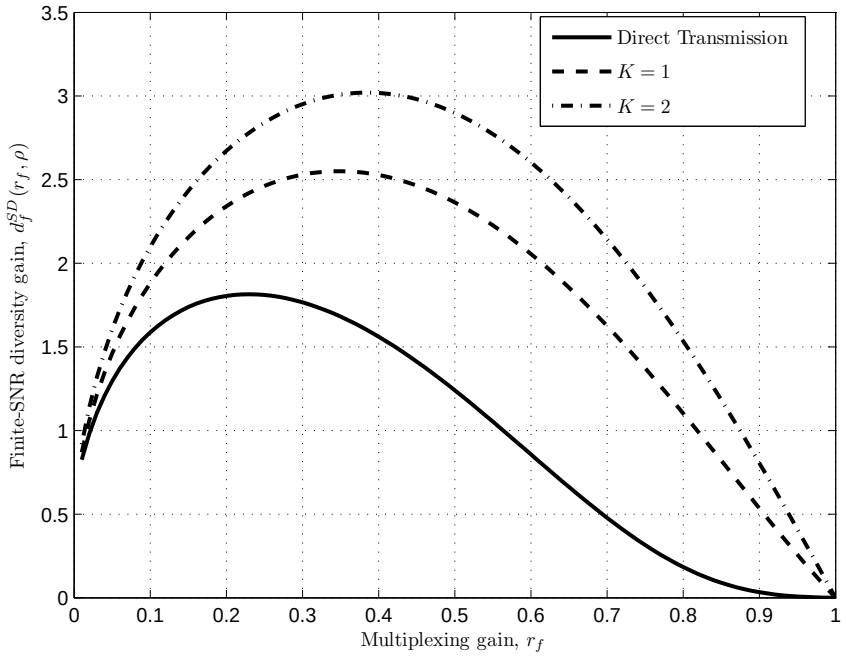

Figure 4.4: Finite-SNR DMT for $K = 1, 2$, and $m_o = 1$ at a fixed SNR = 10 dB.

Under the assumption of background noise-limited receiver and following similar steps as in [24], we obtain the outage probability for the multi-hop IM/DD scheme as

$$P_{out,\mathrm{IM/DD}}^{SD} = 1 - \prod_{k=1}^{K+1} \left[1 - Q\left(\frac{\ln\left(\frac{\Re \mathcal{L}_k P_T}{(K+1)\sqrt{2q\Re B_s P_b \gamma_{th}}} \right) - 2\sigma_\chi^2(\mathcal{D})}{2\sigma_\chi(\mathcal{D})} \right) \right], \tag{4.23}$$

where $Q(\cdot)$ denotes the Gaussian Q-function [57], and P_b is the background noise power in each receiver aperture. In (4.23), $\sigma_\chi^2(\mathcal{D})$ is the log-amplitude variance of a receive aperture with diameter $\mathcal{D}$, and for the plane-wave propagation in the weak turbulence regime with zero inner scale of turbulence ($l_0 \to 0$) and infinite outer scale ($L_0 \to \infty$) can be approximated as [63]

$$\sigma_\chi^2(\mathcal{D}) \approx \sigma_\chi^2(0) \left[1 + 1.062 \left(\frac{\kappa \mathcal{D}^2}{4Z} \right) \right]^{-7/6}, \tag{4.24}$$

where $\sigma_\chi^2(0)$ is the log-amplitude variance for a point receiver ($\mathcal{D} = 0$) given in (2.11).

We assume that $B_s = 1$GHz, $\mathcal{R} = 2$ bits/symbol, and $P_b = 1\,\mathrm{mW}$. Performance plots in Figure 4.5 are provided under the assumption of same transmit power P_T for

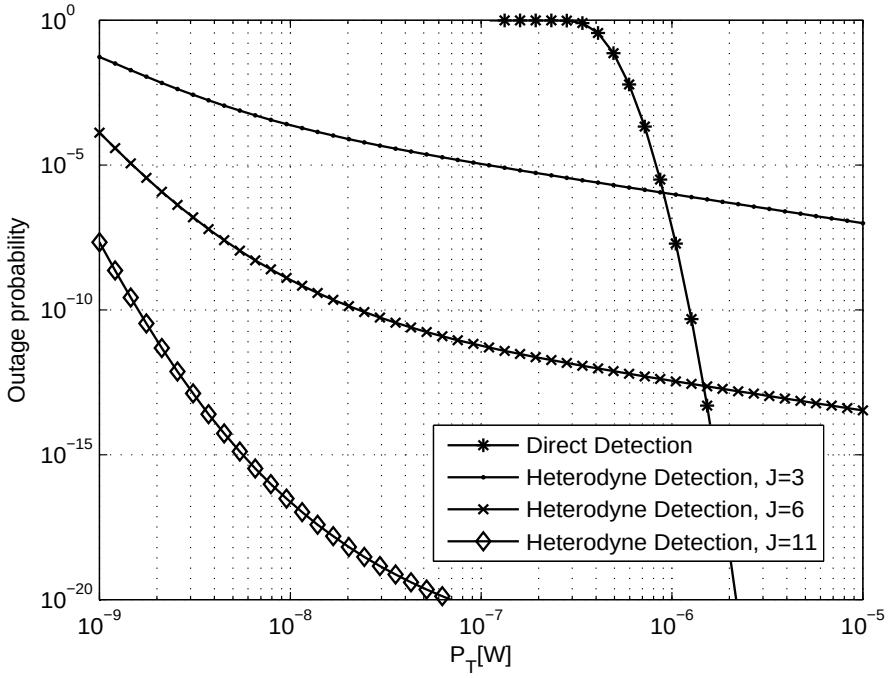

Figure 4.5: Performance comparison of coherent and IM/DD multi-hop systems ($K = 1$ and $m_o = 1$).

both systems. We observe that, for small values of P_T, coherent detection brings better performance compared to the incoherent one, even for low order of compensation ($J = 3$). Performance curves for coherent and incoherent systems intersect for larger values of P_T since the infinite diversity order for a Rician channel (in coherent system) is just one while for a log-normal channel (in IM/DD system) is infinity. However, if the degree of compensation increases at the cost of higher complexity, considerable power gains can be achieved by coherent detection for a desired value of outage probability.

In the following, we consider a coherent FSO system with multiple receive apertures to further exploit the receive diversity advantages. It is assumed that $J = 3$ modes are compensated in each receive aperture. The system is equipped with two relay nodes (i.e., $K = 2$) distributed between the source and the destination with distances $Z_1 = 1\,\text{km}$, $Z_2 = 2.5\,\text{km}$, and $Z_3 = 1.5\,\text{km}$. We consider three different systems based on the number of receive apertures at each node. In the first system (S1), we assume $m_1 = m_2 = m_3 = 2$. In the second system (S2), we have $m_1 = 2$, $m_2 = 3$, and $m_3 = 2$. Finally, in the third

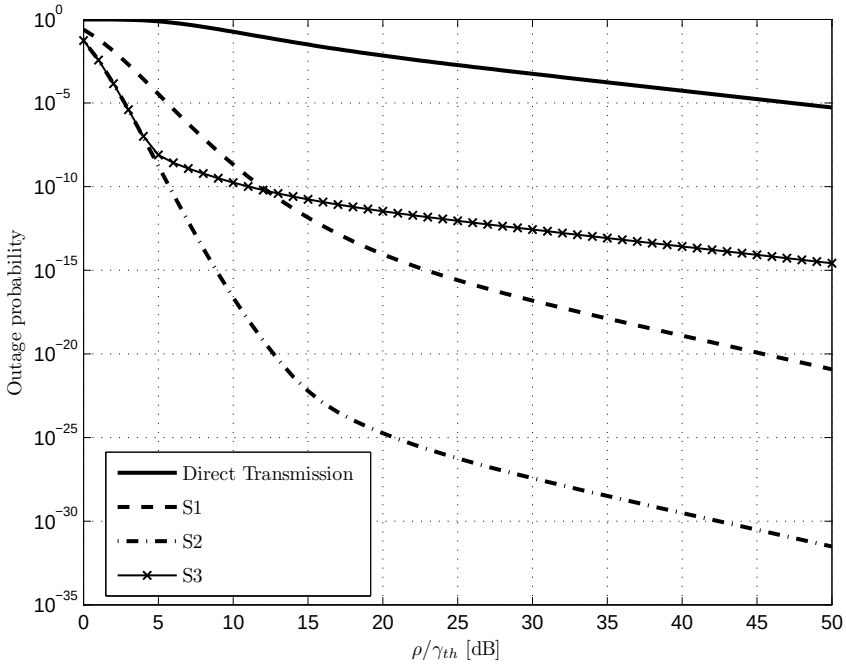

Figure 4.6: Outage probability of asymmetrical systems S1, S2 and S3.

system (S3), we have $m_1 = 1$, $m_2 = 3$, and $m_3 = 2$.

Figure 4.6 depicts the outage probability versus normalized SNR (ρ/γ_{th}) for these three systems. A common observation for all systems is the impressive performance improvements through multi-hop transmission coupled with the receive diversity. For small values of SNR (SNR < 5 dB), the outage performance of S2 and S3 is the same while both outperform S1. In this range, the second sub-channel (i.e., the longest hop which experiences the poorest fading conditions) has the worst outage performance and acts as a bottleneck in the performance of the end-to-end data transmission. Hence, increasing the number of receive apertures at the second relay from two (in S1) to three (in S2 and S3) improves the performance. On the other hand, as SNR increases, performance curves of S2 and S3 deviate from each other because the incoherent component of the Rician channel begins to dominate the system performance and the deployment of receive diversity at the first relay results in S2's additional performance improvement. In this regime, the performance of S3 is restricted by its first relay which has only one receive aperture. It can be readily checked from (4.17) that the asymptotic diversity gain of S1, S2 and S3 is given by two,

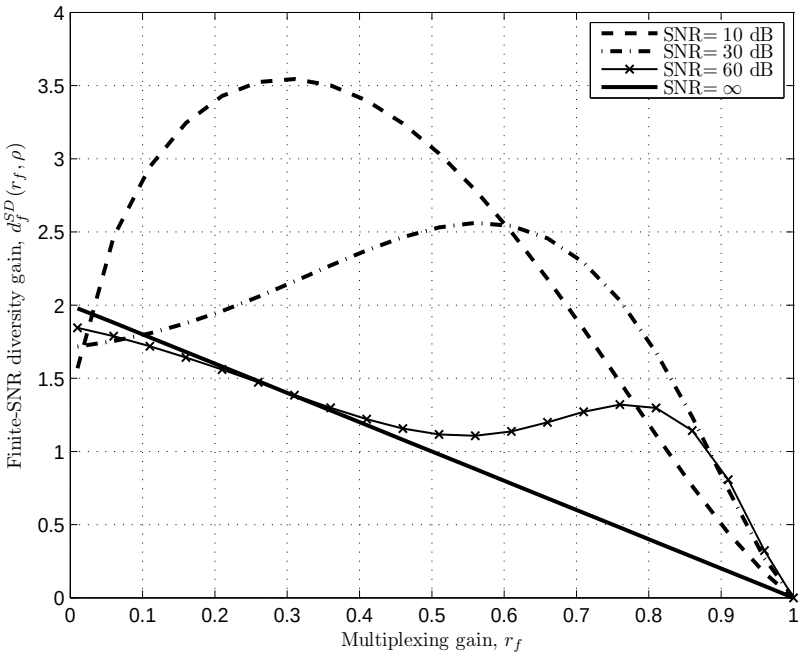

Figure 4.7: DMT of system S2 for different values of SNR.

two, and one, respectively.

Figure 4.7 depicts the finite SNR DMT of S2 for various values of SNR. It is observed that, for finite values of SNR, the maximum diversity gain does not occur at zero multiplexing gain. Similar to our observations in Figure 4.3, this is due to the presence of the coherent component. When SNR increases, the incoherent component begins to dominate the system performance and the DMT curve gradually approaches its asymptotic value. Recall that the number of receive apertures in each hop is given by $m_1 = 2$, $m_2 = 3$, and $m_3 = 2$. It is observed that as SNR increases gradually, the DMT performance approaches $\min\{2, 3, 2\} \times (1-r) = 2(1-r)$. Therefore, the asymptotic DMT of the end-to-end scheme is determined by the minimum of the DMT values of all sub-channels throughout the range of the multiplexing gain.

Appendix 4A. Proof of (4.17)

In this appendix, we derive the asymptotic value of DMT given by (4.17) starting from the finite-SNR DMT expression of (4.13). It can be readily checked that when $\rho \to \infty$, we have $\vartheta_k \to \sqrt{\Theta_k \rho^{r-1}}$, where $\Theta_k = 2m_k(1+\mathfrak{K}_k)(K+1)/(\mathcal{L}_k \overline{a_k^2})$. Since $r < 1$ [37], we have $\lim_{\rho\to\infty} \vartheta_k = 0, \ \forall\, k$. Consequently, we can write

$$\lim_{\rho\to\infty} d_f^{SD}(r_f, \rho) = \lim_{\vartheta_k \to 0} \frac{c_1}{2c_2} \times \lim_{\rho\to\infty} \left[1 - \frac{r_f \rho (1+\rho)^{r_f - 1}}{(1+\rho)^{r_f} - 1}\right], \tag{4.25}$$

where we have defined c_1 and c_2 as

$$c_1 \triangleq \sum_{k=1}^{K+1} \left(\frac{\vartheta_k^{m_k+1}}{\zeta_k^{m_k-1}} e^{\frac{-\left(\vartheta_k^2+\zeta_k^2\right)}{2}} \mathbb{I}_{m_k-1}(\zeta_k \vartheta_k) \prod_{i=1, i\neq k}^{K+1} Q_{m_i}(\zeta_i, \vartheta_i) \right), \tag{4.26}$$

$$c_2 \triangleq 1 - \prod_{k=1}^{K+1} Q_{m_k}(\zeta_k, \vartheta_k). \tag{4.27}$$

It is easy to see that the second limit term in (4.25) yields $1 - r$. For the solution of the first limit expression, we first work with c_2. Replacing the Marcum Q-function by its series form [57], we obtain

$$\lim_{\vartheta_k \to 0} c_2 = \lim_{\vartheta_k \to 0} \left[1 - \prod_{k=1}^{K+1} \left(1 - e^{\frac{-\left(\vartheta_k^2+\zeta_k^2\right)}{2}} \sum_{i=m_k}^{\infty} \left(\frac{\vartheta_k}{\zeta_k}\right)^i \mathbb{I}_i(\zeta_k \vartheta_k) \right) \right]. \tag{4.28}$$

Using the small argument form of the modified Bessel function of the first kind [57], (4.28) can be rewritten as

$$\begin{aligned} \lim_{\vartheta_k \to 0} c_2 &= \lim_{\vartheta_k \to 0} \left[1 - \prod_{k=1}^{K+1} \left(1 - e^{\frac{-\left(\vartheta_k^2+\zeta_k^2\right)}{2}} \sum_{i=m_k}^{\infty} \frac{\left(\vartheta_k^2/2\right)^i}{i!} \right) \right] \\ &= \lim_{\vartheta_k \to 0} \left[1 - \prod_{k=1}^{K+1} \left(1 - \frac{\left(\vartheta_k^2/2\right)^{m_k}}{m_k!} e^{\frac{-\left(\vartheta_k^2+\zeta_k^2\right)}{2}} \right) \right] \\ &= \lim_{\vartheta_k \to 0} \sum_{k=1}^{K+1} \frac{\left(\vartheta_k^2/2\right)^{m_k}}{m_k!} e^{\frac{-\left(\vartheta_k^2+\zeta_k^2\right)}{2}}. \end{aligned} \tag{4.29}$$

Defining $\hat{m} \triangleq \min_k m_k$ and $\hat{k} \triangleq \arg(\min_k m_k)$, we obtain

$$\lim_{\vartheta_k \to 0} c_2 = \lim_{\vartheta_{\hat{k}} \to 0} \frac{\left(\vartheta_{\hat{k}}^2/2\right)^{\hat{m}}}{\hat{m}!} e^{\frac{-\left(\zeta_{\hat{k}}^2+\vartheta_{\hat{k}}^2\right)}{2}}. \tag{4.30}$$

For c_1 given in (4.26), first note that $\lim_{\vartheta_i \to 0} Q_{m_i}(\zeta_i, \vartheta_i) = 1$ [57]. Therefore, using the small argument form of the modified Bessel function [57], we have

$$\begin{aligned} \lim_{\vartheta_k \to 0} c_1 &= \lim_{\vartheta_k \to 0} 2 \sum_{k=1}^{K+1} \frac{\left(\vartheta_k^2/2\right)^{m_k}}{(m_k - 1)!} e^{\frac{-\left(\vartheta_k^2 + \zeta_k^2\right)}{2}} \\ &= \lim_{\vartheta_{\hat{k}} \to 0} 2 \frac{\left(\vartheta_{\hat{k}}^2/2\right)^{\hat{m}}}{(\hat{m} - 1)!} e^{\frac{-\left(\vartheta_{\hat{k}}^2 + \zeta_{\hat{k}}^2\right)}{2}}. \end{aligned} \tag{4.31}$$

Finally, utilizing (4.30) and (4.31) in (4.25), we obtain the asymptotic DMT expression as given by (4.17).

Appendix 4B. Proof of (4.20)

From (4.16), $d_f^1(r_f, \rho)$ can be readily derived as

$$d_f^1(r_f, \rho) = \frac{\vartheta^{m_o+1}}{\zeta^{m-1}} \frac{e^{\frac{-\left(\vartheta^2 + \zeta^2\right)}{2}} \mathbb{I}_{m_o - 1}(\zeta\vartheta)}{2\left[1 - Q_{m_o}(\zeta, \vartheta)\right]} \left(1 - \frac{r_f \rho (1+\rho)^{r_f - 1}}{(1+\rho)^{r_f} - 1}\right). \tag{4.32}$$

Using (4.19) and (4.32), we have

$$\frac{d_f^{SD}(r_f, \rho)}{d_f^1(r_f, \rho)} = \frac{(K+1)\, Q_{m_o}^K(\zeta, \vartheta)}{\sum_{i=0}^{K} Q_{m_o}^i(\zeta, \vartheta)}. \tag{4.33}$$

Since $0 \leqslant Q_{m_o}(\zeta, \vartheta) \leqslant 1$ [57], we have $Q_{m_o}^K(\zeta, \vartheta) \leqslant Q_{m_o}^i(\zeta, \vartheta)$ for $0 \leqslant i \leqslant K$ which yields

$$(K+1)\, Q_{m_0}^K(\zeta, \vartheta) \leqslant \sum_{i=0}^{K} Q_{m_o}^i(\zeta, \vartheta). \tag{4.34}$$

Consequently, using(4.34) in (4.33), we obtain (4.20).

Chapter 5

Hybrid-ARQ protocols in Coherent FSO Communications

In this chapter, we investigate the performance of hybrid-ARQ techniques in coherent FSO communications. Under the assumption of a Gamma-Gamma statistical fading channel model, we derive outage probability and throughput expressions for three H-ARQ protocols. We further characterize the outage performance at high values of SNR through the diversity and coding gains.

5.1 Coherent FSO Systems with H-ARQ

We consider a point-to-point FSO system equipped with a single transmit aperture and multiple receive apertures. The transmitter is assumed to have an infinite buffer of information to send[1] and uses a complex Gaussian codebook with unit average power to encode its message. The transmitted signal passes through the slowly time-varying FSO channel which can be modeled as a non-ergodic block-fading channel wherein the fading coefficient remains constant over each block, but changes independently from one block to another.

The receiver is equipped with N receive apertures that are separated by more than an atmospheric coherence length to ensure independent fading channels. The area of

[1]This simplified scenario allows mathematical tractability and can be considered as a bound on the actual performance [64].

each receive aperture is assumed to be A_{RX}/N where A_{RX} is the aperture area in the benchmark single aperture system. This condition assures that the received signal power remains constant for various values of N. Each aperture is small enough compared to the coherence length so that the received field remains coherent all over the aperture. Furthermore, all receive apertures are assumed to be located within the transmitter field-of-view. Heterodyne detection is employed in each diversity branch. The receiver then uses a maximum ratio combiner [57] to combine the diversity branches' outputs.

Noting that the noise in a practical heterodyne detector is dominated by the LO shot-noise which can be modeled as AWGN, we can write the baseband model of the output electrical signal after heterodyning and diversity combining as

$$y_i^{[l]} = \sqrt{\frac{\rho}{N}\sum_{v=1}^{N} h_{i,v}}\, x_i^{[l]} + \sum_{v=1}^{N} n_{i,v}^{[l]}, \tag{5.1}$$

where $x_i^{[l]}$ and $y_i^{[l]}$ are respectively the input and output signals, $i = 1, 2, \ldots$ indexes the channel's block number, $l = 1, \ldots, L$ counts the channel uses in each block, $v = 1, \ldots, N$ indexes the diversity branches, and $n_{i,v}^{[l]}$ is the circularly symmetric complex Gaussian noise with unit variance. $h_{i,v}$ denotes the atmospheric fading power coefficient which follows the Gamma-Gamma distribution and its pdf is given[2] in (2.12). ρ is the photo-detected electrical SNR over all receive apertures in the absence of turbulence, which is given by $\rho = \Re A_{RX}\mathfrak{I}_s/qB_s$. Under the assumption of i.i.d fading coefficients and i.i.d noise terms, the output instantaneous electrical SNR over the i^{th} block is given by

$$\gamma_i = \frac{\rho}{N}\sum_{v=1}^{N} h_{i,v}. \tag{5.2}$$

We assume that a delay-free error-free feedback channel is available in the underlying system to deploy one of the H-ARQ protocols originally introduced in [64].

In the ALO protocol, the transmitter encodes $\mathcal{K}$ information nats using L symbols and transmits them with the rate $\mathcal{R} = \mathcal{K}/L$ nats per second per Hertz (nps/Hz) in each channel block. If decoding failure occurs, the transmitter sends the same encoded packet in the

[2]We ignore the path loss effect in this chapter and assume that all fading power coefficients are normalized such that $\mu = 1$.

next round[3]. The receiver considers only the last received packet to decode the current message. This process continues until successful decoding is achieved within M rounds or an error is declared.

In the RTD protocol, the transmitter operates the same as that in the ALO protocol. The receiver performs maximum ratio combining on all the packets it has received so far to decode the current message.

In the INR protocol, the transmitter sends additional redundancy symbols in each round until successful decoding occurs. Specifically, $\mathcal{K}$ information nats are encoded by using a mother code with length ML and rate $\mathcal{R}/M$. Each codeword is divided into M packets of L symbols and each packet is transmitted in each ARQ round. The first $m\,(m = 1, \ldots, M)$ packets of each codeword form a codeword of a punctured code of length mL and rate $\mathcal{R}/m$. This punctured code is obtained from the mother code through deleting the last $M - m$ packets. In each round, the receiver tries to decode the current message by using all the packets received until that round. The ACK/NACK procedure is repeated until the receiver decodes the current message successfully or all M packets of the mother code are transmitted.

5.2 Outage Performance, Diversity and Coding Gains

In this section, we first derive the outage performance for each protocol and then, based on the derived expressions, quantify the diversity and coding gains at high-SNR regime.

5.2.1 Basic Definitions and Lemmas

Outage Probability- Let A_m define the event that the per symbol instantaneous mutual information at round m (denoted by I_m) crosses level $\mathcal{R}$ (the transmission rate of the first round), i.e., $A_m = \{I_m > \mathcal{R}\}$. The outage probability after m ARQ rounds is consequently

[3]Each ARQ round spans a channel block. Therefore, the channel remains fixed within each ARQ round, but is i.i.d across ARQ rounds.

given by

$$P_{out}(m) = \Pr\left\{\overline{A_1}, \ldots, \overline{A_m}\right\} = \Pr\left\{I_1 \leq \mathcal{R}, \ldots, I_m \leq \mathcal{R}\right\}. \tag{5.3}$$

An outage event occurs if the mutual information after the maximum number of ARQ rounds is still smaller than $\mathcal{R}$, i.e., $m = M$ is reached in (5.3). In the rest of this chapter, whenever we mention outage probability without specifying the number of ARQ rounds, we implicitly mean $P_{out}(M)$.

Diversity and Coding Gains- At high-SNR regime, the outage probability in most cases can be approximated as [65]

$$P_{out} \sim (O \cdot \rho)^{-d} \tag{5.4}$$

where d and O are respectively inferred as outage diversity gain and outage coding gain. The diversity gain indicates the slope of the outage probability curve versus average SNR (ρ) on a log-log scale while the coding gain determines the relative horizontal shift of this curve.

Lemma 5.1. *Let z denote the sum of k i.i.d Gamma-Gamma random variables with mean μ and parameters α and β. The distribution of z can be efficiently approximated*[4] *by a single Gamma-Gamma random variable with mean $k\mu$ and parameters ϕ_k and ψ_k, i.e.,*

$$f_z(z) \approx \frac{2}{\Gamma(\phi_k)\Gamma(\psi_k)z}\left(\frac{\phi_k\psi_k}{k\mu}z\right)^{\frac{(\phi_k+\psi_k)}{2}} \mathbb{K}_{\phi_k-\psi_k}\left(2\sqrt{\frac{\phi_k\psi_k}{k\mu}z}\right), \tag{5.5}$$

where $f_z(z)$ denotes the pdf of z, and ϕ_k and ψ_k are respectively given by

$$\phi_k = k\upsilon + \varepsilon_k, \tag{5.6}$$

$$\psi_k = k\tau, \tag{5.7}$$

with $\upsilon = \max\{\alpha, \beta\}$ and $\tau = \min\{\alpha, \beta\}$. In (5.6), ε_k denotes an appropriately chosen adjustment parameter given by

$$\varepsilon_k = (k-1)\frac{-0.127 - 0.95\upsilon - 0.0058\tau}{1 + 0.00124\upsilon + 0.98\tau}. \tag{5.8}$$

[4]To evaluate the validity of such a statistical approximation, a goodness-of-fit statistical test, such as Kolmogrov- Smrinov (KS) test can be used [66, 67].

See [66] for the proof.

Lemma 5.2. *Let z denote the sum of k i.i.d Gamma-Gamma random variables with mean μ and shaping parameters α and β. The pdf of z can be approximated by a single-term polynomial for small values of z ($z \to 0^+$), i.e.,*

$$f_z(z) \sim \left(\frac{\Gamma(\upsilon-\tau)(\upsilon\tau/\mu)^\tau}{\Gamma(\upsilon)}\right)^k \frac{z^{k\tau-1}}{\Gamma(k\tau)}. \tag{5.9}$$

The proof is given in Appendix 5A.

5.2.2 ALO Protocol

In the ALO protocol, the receiver considers only the most recently received packet and has no memory of the past packets. Therefore, the events A_ms in (5.3) are i.i.d and the per symbol instantaneous mutual information at round m for this protocol is given by [64]

$$I_{m,ALO} = \log(1+\gamma_m), \tag{5.10}$$

where γ_m is the output instantaneous electrical SNR at round m and given by (5.2).

Consequently, from (5.3), the outage probability of the ALO protocol after m rounds, denoted by $P_{out,ALO}(m)$, is obtained as

$$\begin{aligned} P_{out,ALO}(m) &= \prod_{i=1}^{m} \Pr\{I_{i,ALO} \le \mathcal{R}\} \\ &= [\Pr\{I_{1,ALO} \le \mathcal{R}\}]^m \\ &= \left[\Pr\left\{\log\left(1+\frac{\rho}{N}\sum_{v=1}^{N} h_{1,v}\right) \le \mathcal{R}\right\}\right]^m. \end{aligned} \tag{5.11}$$

An accurate approximation of $P_{out,ALO}(m)$ for finite values of ρ can be obtained by using Lemma 5.1. Rewriting the Bessel function in (5.5) in terms of the Meijer-G function [68, p. 665, Eq. 8.4.23.1] and using [68, p. 46, Eq. 1.16.2.1], we obtain

$$P_{out,ALO}(m) \approx \left[\frac{1}{\Gamma(\phi_N)\Gamma(\psi_N)} G_{1,3}^{2,1}\Big(\phi_N\psi_N\gamma_{th}/\rho \Big| \begin{matrix} 1 \\ \phi_N, \psi_N, 0 \end{matrix}\Big)\right]^m, \tag{5.12}$$

where $G(\cdot)$ denotes the Meijer G-function [69], ϕ_N and ψ_N are obtained by replacing $k = N$ in (5.6) and (5.7), respectively, and γ_{th} is defined as $\gamma_{th} = \exp(\mathcal{R}) - 1$.

It should be noted that for one receive-aperture ($N = 1$), there is no need to use the approximation given in Lemma 5.1, and $P_{out,ALO}(m)$ has an exact expression given by

$$P_{out,ALO}(m)|_{N=1} = \left[\frac{1}{\Gamma(\alpha)\Gamma(\beta)} G_{1,3}^{2,1}\Big(\alpha\beta\gamma_{th}/\rho \Big| \begin{matrix} 1 \\ \alpha, \beta, 0 \end{matrix}\Big)\right]^m, \tag{5.13}$$

To analyze the asymptotic outage performance at large values of SNR, we employ Lemma 5.2. Substituting $k = N$ and $\mu = 1$ in (5.9), and using the result in (5.11), we have

$$\begin{aligned} P_{out,ALO}(M) &\sim \left[\int_0^{N\gamma_{th}/\rho} \frac{\Gamma^N(\upsilon - \tau)(\upsilon\tau)^{N\tau}}{\Gamma^N(\upsilon)\Gamma\left(N\tau\right)} z^{N\tau-1} dz\right]^M \\ &= \left(\frac{\Gamma^N(\upsilon - \tau)(N\upsilon\tau\gamma_{th})^{N\tau}}{\Gamma^N(\upsilon)\Gamma\left(N\tau + 1\right)}\right)^M \rho^{-MN\tau}. \end{aligned} \tag{5.14}$$

Thus, using (5.4), we obtain the outage diversity and coding gains of the ALO protocol, respectively, as

$$d_{ALO} = MN\tau, \tag{5.15}$$

$$O_{ALO} = \frac{1}{N\tau\upsilon\gamma_{th}} \left(\frac{\Gamma(\upsilon)\Gamma^{1/N}\left(N\tau + 1\right)}{\Gamma(\upsilon - \tau)}\right)^{1/\tau}. \tag{5.16}$$

5.2.3 RTD Protocol

Since the receiver performs maximum ratio combining on all received packets in the RTD protocol, the SNR is accumulated over H-ARQ rounds. Therefore, the per symbol instantaneous mutual information at round m for this protocol is given by [64]

$$I_{m,RTD} = \log\Big(1 + \sum_{i=1}^{m} \gamma_i\Big). \tag{5.17}$$

Because γ_i is nonnegative, $\{I_{m,RTD}\}$ is a non-decreasing sequence which results in [64]

$$\begin{aligned} P_{out,RTD}(m) &= \Pr\left\{I_{1,RTD} \leq \mathcal{R}, \ldots, I_{m,RTD} \leq \mathcal{R}\right\} \\ &= \Pr\left\{I_{m,RTD} \leq \mathcal{R}\right\}, \end{aligned} \tag{5.18}$$

where $P_{out,RTD}(m)$ denotes the outage probability of the RTD protocol after m rounds. Substituting (5.2) in (5.17) and (5.18) yields

$$P_{out,RTD}(m) = \Pr\left\{\log\left(1+\frac{\rho}{N}\sum_{i=1}^{m}\sum_{v=1}^{N}h_{i,v}\right) \leq \mathcal{R}\right\}. \tag{5.19}$$

By using Lemma 5.1, [68, p. 665, Eq. 8.4.23.1], and [68, p. 46, Eq. 1.16.2.1], an accurate approximation of $P_{out,RTD}(m)$ at finite SNR values is obtained as

$$P_{out,RTD}(m) \approx \frac{1}{\Gamma(\phi_{mN})\Gamma(\psi_{mN})} G_{1,3}^{2,1}\left(\phi_{mN}\psi_{mN}\frac{\gamma_{th}}{m\rho}\,\middle|\, \begin{matrix} 1 \\ \phi_{mN},\psi_{mN},0 \end{matrix}\right), \tag{5.20}$$

where ϕ_{mN} and ψ_{mN} are obtained by replacing $k = mN$ in (5.6) and (5.7), respectively.

The asymptotic approximation of $P_{out,RTD}(M)$ at high-SNR regime can be obtained by using Lemma 5.2 with $k = MN$ as

$$\begin{aligned} P_{out,RTD}(M) &\sim \int_0^{N\gamma_{th}/\rho}\left(\frac{\Gamma(\upsilon-\tau)(\upsilon\tau)^{\tau}}{\Gamma(\upsilon)}\right)^{MN}\frac{z^{MN\tau-1}}{\Gamma\left(MN\tau\right)}dz \\ &= \frac{\Gamma^{MN}(\upsilon-\tau)(N\upsilon\tau\gamma_{th})^{MN\tau}}{\Gamma^{MN}\left(\upsilon\right)\Gamma\left(MN\tau+1\right)}\rho^{-MN\tau}. \end{aligned} \tag{5.21}$$

Consequently, the outage diversity and coding gains of the RTD protocol at high-SNR regime are respectively obtained as

$$d_{RTD} = MN\tau, \tag{5.22}$$

$$O_{RTD} = \frac{1}{N\tau\upsilon\gamma_{th}}\left(\frac{\Gamma\left(\upsilon\right)\Gamma^{1/MN}\left(MN\tau+1\right)}{\Gamma(\upsilon-\tau)}\right)^{1/\tau}. \tag{5.23}$$

5.2.4 INR Protocol

In the INR protocol, the mutual information is accumulated over H-ARQ rounds at the receiver. Therefore, for this protocol, the instantaneous mutual information at round m is given by [64]

$$I_{m,INR} = \sum_{i=1}^{m}\log\left(1+\gamma_i\right). \tag{5.24}$$

Similar to (5.18) for the RTD protocol, we have $P_{out,INR}(m) = \Pr\{I_{m,INR} \leq \mathcal{R}\}$ where $P_{out,INR}(m)$ denotes the outage probability of the INR protocol after m rounds. Using (5.2) and (5.24), we have

$$P_{out,INR}(m) = \Pr\left\{\sum_{i=1}^{m} J_i \leq \mathcal{R}\right\}, \tag{5.25}$$

where

$$J_i = \log\Big(1 + \frac{\rho}{N}\sum_{v=1}^{N} h_{i,v}\Big). \tag{5.26}$$

The probability distribution of $\sum_{i=1}^{m} J_i$ can be calculated from the m-fold convolution of the pdf of J_i. Unfortunately, the exact pdf of J_i is not available. However, we can use Lemma 5.1 to derive an accurate approximation of the pdf of J_i, i.e.,

$$\begin{aligned} f_{J_i}(J_i) \approx & \frac{2(\phi_N\psi_N/\rho)^{(\phi_N+\psi_N)/2}}{\Gamma(\phi_N)\Gamma(\psi_N)}\exp(J_i) \\ & \times (\exp(J_i)-1)^{(\phi_N+\psi_N)/2-1}\mathbb{K}_{\phi_N-\psi_N}\left(2\sqrt{\frac{1}{\rho}\phi_N\psi_N\left(\exp(J_i)-1\right)}\right). \end{aligned} \tag{5.27}$$

It should be noted that for a system with single receive aperture ($N = 1$), $f_{J_i}(J_i)$ can be exactly derived from (2.12) as

$$f_{J_i}(J_i)|_{N=1} = \frac{2(\alpha\beta/\rho)^{(\alpha+\beta)/2}}{\Gamma(\alpha)\Gamma(\beta)}\exp(J_i)(\exp(J_i)-1)^{(\alpha+\beta)/2-1}\mathbb{K}_{\alpha-\beta}\left(2\sqrt{\frac{\alpha\beta}{\rho}\left(\exp(J_i)-1\right)}\right). \tag{5.28}$$

Finding a closed form expression for the distribution of $\sum_{i=1}^{m} J_i$ with the help of (5.27) is still a difficult task. In the following, we derive lower and upper bounds on $P_{out,INR}(m)$.

Lower Bound - Using Jensen's inequality for the logarithm function [54], we have

$$\frac{1}{m}\sum_{i=1}^{m}\log\Big(1+\gamma_i\Big) \leqslant \log\Big(\frac{1}{m}\sum_{i=1}^{m}(1+\gamma_i)\Big). \tag{5.29}$$

Replacing γ_i from (5.2), we obtain

$$\Pr\left\{m\log\left(\frac{1}{m}\sum_{i=1}^{m}\Big(1+\frac{\rho}{N}\sum_{v=1}^{N}h_{i,v}\Big)\right)\leqslant\mathcal{R}\right\} \leqslant \Pr\left\{\sum_{i=1}^{m}\log\Big(1+\frac{\rho}{N}\sum_{v=1}^{N}h_{i,v}\Big)\leqslant\mathcal{R}\right\}. \tag{5.30}$$

It can be figured out that the right-hand side of (5.30) is $P_{out,INR}(m)$ in (5.25). Let us denote the left-hand side of (5.30) by $P_{out,LB}(m)$, i.e.,

$$P_{out,LB}(m) = \Pr\left\{ m \log\left(\frac{1}{m} \sum_{i=1}^{m} \left(1 + \frac{\rho}{N} \sum_{v=1}^{N} h_{i,v} \right) \right) \leqslant \mathcal{R} \right\}. \tag{5.31}$$

This can be approximately obtained by using Lemma 5.1 as

$$P_{out,LB}(m) \approx \frac{1}{\Gamma(\phi_{mN})\Gamma(\psi_{mN})} G_{1,3}^{2,1}\left(\phi_{mN}\psi_{mN}\gamma_{th,m}/\rho \,\middle|\, \begin{matrix} 1 \\ \phi_{mN}, \psi_{mN}, 0 \end{matrix} \right), \tag{5.32}$$

where ϕ_{mN} and ψ_{mN} are obtained by replacing $k = mN$ in (5.6) and (5.7), respectively, and $\gamma_{th,m}$ is defined as $\gamma_{th,m} = \exp(\mathcal{R}/m) - 1$.

Upper bound - We use following lemmas to derive the upper bound.

Lemma 5.3. ***(Minkowski Inequality)*** *For $z_i, w_i \geqslant 0$, $i = 1, 2, \ldots, m$, we have*

$$\left[\prod_{i=1}^{m} z_i \right]^{1/m} + \left[\prod_{i=1}^{m} w_i \right]^{1/m} \leqslant \left[\prod_{i=1}^{m} (z_i + w_i) \right]^{1/m}. \tag{5.33}$$

See [54] for the proof.

Lemma 5.4. *Let q_is denote i.i.d Gamma-Gamma random variables with mean μ and shaping parameters α and β. The cumulative distribution function (cdf) of the random variable $w = \prod_{i=1}^{m} q_i$ is given by*

$$\mathbb{F}_w(w) = \frac{1}{\Gamma^m(\alpha)\Gamma^m(\beta)} G_{1,2m+1}^{2m,1}\left((\alpha\beta/\mu)^m w \,\middle|\, \begin{matrix} 1 \\ \underbrace{\alpha, \ldots, \alpha}_{m \text{ times}}, \underbrace{\beta, \ldots, \beta}_{m \text{ times}}, 0 \end{matrix} \right). \tag{5.34}$$

The proof is given in Appendix 5B.

Using Lemma 5.3 with $z_i = \gamma_i$ and $w_i = 1$, we have

$$\left[\left(\prod_{i=1}^{m} \gamma_i \right)^{1/m} + 1 \right]^m \leqslant \prod_{i=1}^{m} (1 + \gamma_i). \tag{5.35}$$

Replacing γ_i from (5.2) in (5.35) yields

$$\Pr\left\{ \sum_{i=1}^{m} \log\left(1 + \frac{\rho}{N} \sum_{\nu=1}^{N} h_{i,\nu} \right) \leqslant \mathcal{R} \right\} \leqslant \Pr\left\{ m \log\left(1 + \frac{\rho}{N} \left(\prod_{i=1}^{m} \sum_{\nu=1}^{N} h_{i,\nu} \right)^{1/m} \right) \leqslant \mathcal{R} \right\}. \tag{5.36}$$

It is clear from (5.25) that the left-hand side of (5.36) is $P_{out,INR}(m)$. We denote the right-hand side of (5.36) by $P_{out,UB}(m)$, i.e.,

$$P_{out,UB}(m) = \Pr\left\{ m \log\left(1 + \frac{\rho}{N}\Big(\prod_{i=1}^{m}\sum_{\nu=1}^{N} h_{i,\nu}\Big)^{1/m}\right) \leqslant \mathcal{R} \right\}. \tag{5.37}$$

An approximation of $P_{out,UB}(m)$ is calculated by using Lemma 5.1 and Lemma 5.4 as

$$P_{out,UB}(m) \approx \frac{1}{\Gamma^m(\phi_N)\Gamma^m(\psi_N)} G_{1,2m+1}^{2m,1}\left((\phi_N\psi_N\gamma_{th,m}/\rho)^m \middle| \begin{matrix} 1 \\ \underbrace{\phi_N,\ldots,\phi_N}_{m\ times}, \underbrace{\psi_N,\ldots,\psi_N}_{m\ times}, 0 \end{matrix} \right), \tag{5.38}$$

where ϕ_N and ψ_N are obtained by replacing $k = N$ in (5.6) and (5.7), respectively.

For a system with single receive-aperture, an exact expression for $P_{out,UB}(m)$ can be obtained by using Lemma 5.4 as

$$P_{out,UB}(m)|_{N=1} = \frac{1}{\Gamma^m(\alpha)\Gamma^m(\beta)} G_{1,2m+1}^{2m,1}\left((\alpha\beta\gamma_{th,m}/\rho)^m \middle| \begin{matrix} 1 \\ \underbrace{\alpha,\ldots,\alpha}_{m\ times}, \underbrace{\beta,\ldots,\beta}_{m\ times}, 0 \end{matrix} \right). \tag{5.39}$$

At high-SNR regime, the outage lower bound given in (5.31) can be approximated as

$$P_{out,LB}(M) \sim \frac{\Gamma^{MN}(\upsilon-\tau)(MN\tau\upsilon\gamma_{th,M})^{MN\tau}}{\Gamma^{MN}(\upsilon)\,\Gamma(MN\tau+1)} \rho^{-MN\tau}, \tag{5.40}$$

by using Lemma 5.2. Hence, the outage diversity and coding gains of $P_{out,LB}(M)$ are respectively given by

$$d_{LB} = MN\tau, \tag{5.41}$$

$$O_{LB} = \frac{1}{MN\tau\upsilon\gamma_{th,M}} \left(\frac{\Gamma(\upsilon)\,\Gamma^{1/MN}(MN\tau+1)}{\Gamma(\upsilon-\tau)} \right)^{1/\tau}. \tag{5.42}$$

Evaluating the asymptotic approximation and, consequently, the diversity and coding gains based on $P_{out,UB}(M)$ is not an easy task. However, it can be proven that [64]

$$P_{out,INR}(M) \leqslant P_{out,RTD}(M) \leqslant P_{out,ALO}(M), \tag{5.43}$$

i.e., the outage probability of the INR protocol is upper bounded by that of the RTD and ALO protocols. Therefore, from the definition of the outage diversity gain given in (3.10),

the diversity gain of the INR protocol is lower bounded by that of the ALO and RTD protocols which is given by $MN\tau$ (according to (5.15) and (5.22)). This result, together with (5.41) and the squeeze theorem [70], yields the diversity gain of the INR protocol as

$$d_{INR} = MN\tau. \tag{5.44}$$

5.2.5 Remarks on Diversity and Coding Gains

Our asymptotic analysis above demonstrates that all considered protocols provide the same diversity order, which is the product of the maximum number of ARQ rounds (M), the number of receive apertures (N), and the minimum of the Gamma-Gamma channel parameters, i.e., $\tau = \min\{\alpha, \beta\}$. On the other hand, the coding gains of three protocols are different. As can be observed from (5.16), the coding gain of the ALO protocol is a constant independent of M and is simply equal to that of a system without any H-ARQ protocol. This result is expected since the ALO protocol does not have memory. However, since the transmission of the same information packet is repeated over M independent channel realizations, this protocol provides as much diversity order as the other protocols.

Different from ALO, the coding gains of the RTD and INR protocols depend on M. As shown in Appendix 5C, the coding gains of the RTD and INR protocols increase linearly with respect to M for the large values of M, i.e.,

$$O_{\{RTD,INR\}} \doteq M. \tag{5.45}$$

However, they show different behavior with respect to the transmission rate, $\mathcal{R}$. From (5.23) and (5.42), we have

$$\frac{O_{LB}}{O_{RTD}} = \frac{1}{M}\left(e^{\frac{(M-1)\mathcal{R}}{M}} + \cdots + 1\right). \tag{5.46}$$

This demonstrates that, for a given M, the ratio between the coding gain of the lower bound and that of RTD increases exponentially with respect to $\mathcal{R}$. Later, we will show numerically in Section 5.4 that O_{INR}/O_{RTD} (where O_{INR} is the exact outage coding gain of the INR protocol) has similar behavior. In other words, by increasing the transmission rate, asymptotic outage performance of the RTD protocol degrades exponentially compared to that of the INR protocol. This degraded performance behavior of the RTD protocol is

due to its sub-optimal coding structure. The code structure in the RTD protocol is in fact equivalent to a concatenated code where the outer code has a length of L symbols and the inner code is a repetition code of length M. Therefore, the RTD protocol can be basically interpreted as a repetition code which is spectrally inefficient at high-SNR regime.

5.3 Throughput Analysis

Throughput is the average rate of the data successfully decoded at the receiver side. The overall throughput of an H-ARQ protocol expressed in nps/Hz is given by [64]

$$\mathcal{T} = \frac{\mathcal{R}\left[1 - p(M)\right]}{1 + \sum_{m=1}^{M-1} p(m)}, \tag{5.47}$$

where $\mathcal{R}$ is the transmission rate of the first round and $p(m)$ is the probability that the message is not correctly decoded at the receiver after m H-ARQ rounds. Assuming random coding and typical set decoding under the assumption of large packet lengths ($L \to \infty$), the probability that the message is not correctly decoded at the receiver after m H-ARQ rounds is equivalent to the outage probability after m H-ARQ rounds [64], i.e., $p(m) = P_{out}(m)$ where $P_{out}(m)$ is given by (5.3). In the sequel, we use this equivalency and evaluate the throughput of each protocol.

ALO Protocol- Substituting (5.12) in (5.47), the throughput of the ALO protocol is obtained as

$$\mathcal{T}_{ALO} \approx \mathcal{R}\left[1 - \frac{1}{\Gamma(\phi_N)\Gamma(\psi_N)} G_{1,3}^{2,1}\Big(\phi_N\psi_N\gamma_{th}/\rho\Big|\begin{array}{c}1\\ \phi_N, \psi_N, 0\end{array}\Big)\right]. \tag{5.48}$$

For a single receive aperture system, $\mathcal{T}_{ALO}$ can be exactly obtained by using (5.13) in (5.47) which yields

$$\mathcal{T}_{ALO}|_{N=1} = \mathcal{R}\left[1 - \frac{1}{\Gamma(\alpha)\Gamma(\beta)} G_{1,3}^{2,1}\Big(\alpha\beta\gamma_{th}/\rho\Big|\begin{array}{c}1\\ \alpha, \beta, 0\end{array}\Big)\right]. \tag{5.49}$$

It is clear from both (5.48) and (5.49) that the throughput of the ALO protocol is independent of M (i.e., the maximum number of H-ARQ rounds). This is expected due to the memoryless nature of this protocol.

RTD Protocol- Inserting (5.20) in (5.47), we obtain a closed-form approximation for the throughput of the RTD protocol as

$$\mathcal{T}_{RTD} \approx \mathcal{R}\frac{1-\frac{1}{\Gamma(\phi_{MN})\Gamma(\psi_{MN})}G_{1,3}^{2,1}\left(\phi_{MN}\psi_{MN}\frac{\gamma_{th}}{M\rho}\middle|\begin{matrix}1\\ \phi_{MN},\psi_{MN},0\end{matrix}\right)}{1+\sum_{m=1}^{M-1}\frac{1}{\Gamma(\phi_{mN})\Gamma(\psi_{mN})}G_{1,3}^{2,1}\left(\phi_{mN}\psi_{mN}\frac{\gamma_{th}}{m\rho}\middle|\begin{matrix}1\\ \phi_{mN},\psi_{mN},0\end{matrix}\right)}. \tag{5.50}$$

This indicates that the throughput of the RTD protocol, unlike that of ALO, is a function of M. In fact, $\mathcal{T}_{RTD}$ increases with respect to M.

INR Protocol- As earlier discussed in Section 5.2.4, obtaining a closed form analytical expression for $P_{out,INR}(m)$ is a difficult task. However, we can bound the throughput of the INR protocol using the derived bounds on $P_{out,INR}(m)$ in Section 5.2.4. Specifically, using the lower bound (given by (5.32)) in (5.47), we obtain an upper bound on the throughput as

$$\mathcal{T}_{UB} \approx \mathcal{R}\frac{1-P_{out,LB}(M)}{1+\sum_{m=1}^{M-1}P_{out,LB}(m)}. \tag{5.51}$$

On the other hand, using (5.38) in (5.47) yields a lower bound for $\mathcal{T}_{INR}$ as

$$\mathcal{T}_{LB} \approx \mathcal{R}\frac{1-P_{out,UB}(M)}{1+\sum_{m=1}^{M-1}P_{out,UB}(m)}. \tag{5.52}$$

In addition, comparing the expressions of $I_{m,ALO}$, $I_{m,RTD}$, and $I_{m,INR}$, given respectively in (5.10), (5.17), and (5.24), one can show that [64]

$$\mathcal{T}_{ALO} \leqslant \mathcal{T}_{RTD} \leqslant \mathcal{T}_{INR}. \tag{5.53}$$

The above inequalities indicate that $\mathcal{T}_{INR}$ is also lower bounded by $\mathcal{T}_{RTD}$. Later, through numerical results, we will see in Section 5.4 that $\mathcal{T}_{LB}$ is much tighter than $\mathcal{T}_{RTD}$ as a lower bound for $\mathcal{T}_{INR}$. We should also note that similar to $\mathcal{T}_{RTD}$, $\mathcal{T}_{INR}$ increases with respect to the maximum number of ARQ rounds, M, i.e., both RTD and INR protocols have the property that "the longer we wait, the more we gain" [64].

5.4 Numerical Results and Discussions

In this section, we illustrate the analytical results derived in the previous sections and evaluate the effects of various system parameters on the performance. In all figures, unless otherwise stated, we assume plane-wave propagation and moderate turbulence regime with Rytov variance $\sigma_R^2 = 1$ ($\alpha = 4.3939$ and $\beta = 2.5636$).

Figure 5.1 demonstrates the outage probability[5] versus average SNR (ρ) for the H-ARQ protocols under consideration assuming a single receive aperture, the transmission rate at the first round equal to $\mathcal{R} = 3$ nps/Hz, and the maximum number of ARQ rounds equal to $M = 3$. In this figure, plots are obtained as follows.

- For the ALO protocol, the outage probability for the single receive-aperture case is exactly given by (5.13).
- For the RTD protocol, the exact expression for $P_{out,RTD}(M)$ is obtained by inserting $N = 1$ in (5.19) and performing the M-fold convolution of the Gamma-Gamma pdf given in (2.12). The approximate expression for $P_{out,RTD}(M)$, which is obtained by using Lemma 5.1, is given in (5.20) with $N = 1$.
- For the INR protocol, the outage probability (according to (5.25)) is obtained by the M-fold convolution of the exact pdf of J_i given in (5.28). The lower and upper bounds are calculated based on (5.32) (with $N = 1$) and (5.39), respectively.

From Figure 5.1, it is observed that the INR protocol has the best outage performance among all protocols. That is followed by RTD. The asymptotic outage approximations obtained from Lemma 5.2 are also sketched in this figure. As observed, the asymptotic approximations are very accurate at high-SNR regime. In addition, the slope of all these curves is 7.69 confirming that all protocols achieve the same diversity gain of $M \min\{\alpha, \beta\}$. However, since they provide different coding gains, the corresponding asymptotic curves have horizontal shift respect to each other. Our results also demonstrate that the exact INR performance curve is very close to its lower bound indicating that the lower bound in (5.32) is considerably tight.

[5]To highlight the accuracy of the derived asymptotic approximations at high-SNR regime, the numerical results are provided for very small values of the outage probability as well as its practical values.

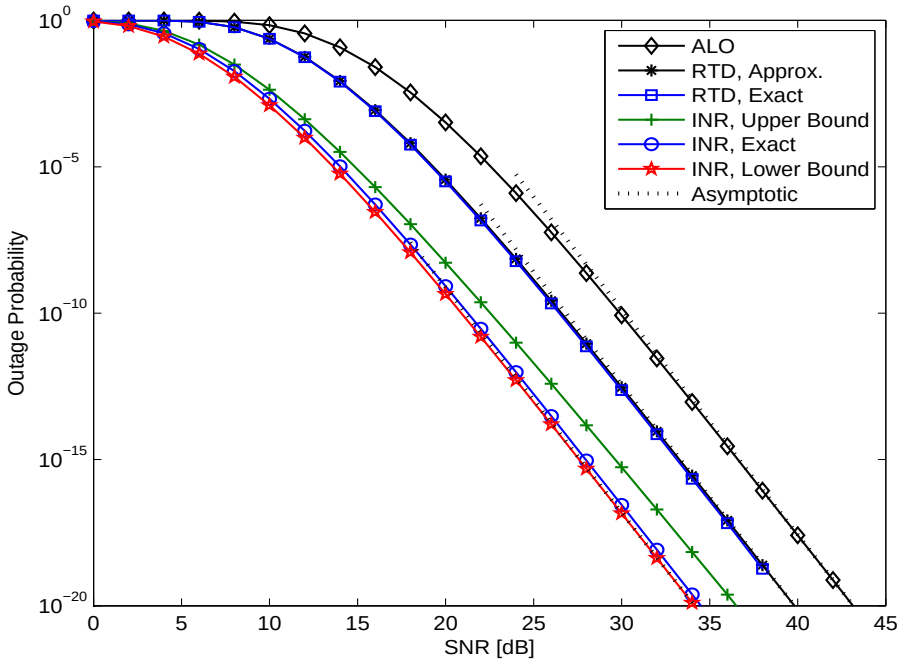

Figure 5.1: Outage probability versus average SNR (ρ) assuming $N = 1$, $M = 3$, and $\mathcal{R} = 3$.

Figure 5.2 depicts the outage probability versus SNR with similar assumptions to Figure 5.1 except that the receiver is now equipped with two apertures ($N = 2$). In this figure, plots are obtained as follows.

- For the ALO protocol, the exact outage probability (according to (5.11)) is obtained by the N-fold convolution of the Gamma-Gamma pdf. The approximate expression is given in (5.12).
- For the RTD protocol, the exact $P_{out,RTD}(M)$ in (5.19) is obtained through the MN-fold convolution of the Gamma-Gamma pdf. The approximate expression of $P_{out,RTD}(M)$ is given in (5.20).
- For the INR protocol, the exact $P_{out,INR}(M)$ in (5.25) is obtained by the Monte Carlo simulation. The approximate value of $P_{out,INR}(M)$ is derived through the M-fold convolution of the approximated pdf of J_i given in (5.27). Lower and upper bounds are calculated based on (5.32) and (5.38), respectively.

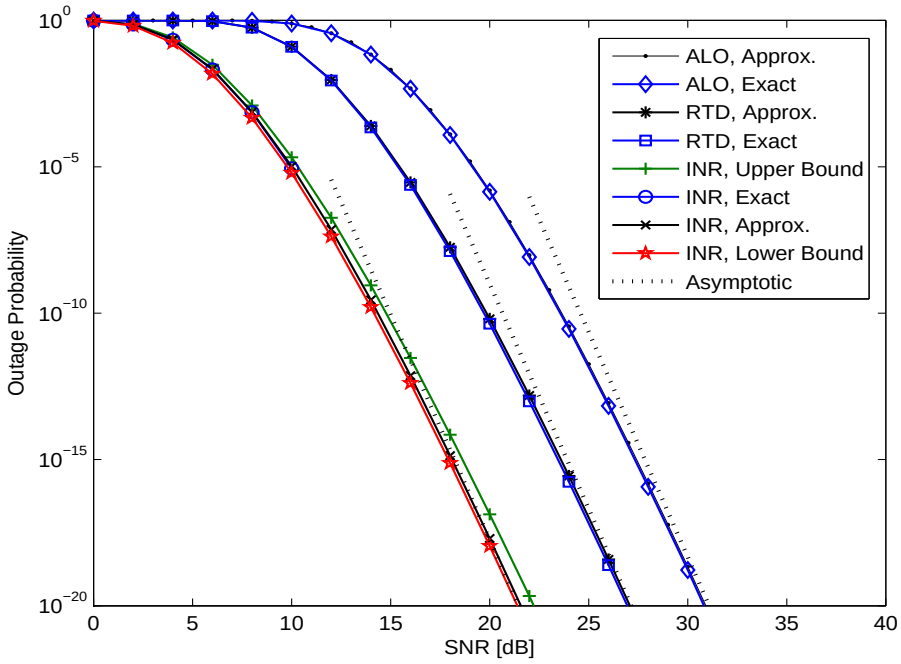

Figure 5.2: Outage probability versus average SNR assuming $N = 2$, $M = 3$, and $\mathcal{R} = 3$.

As observed, the "exact" curves precisely match with the corresponding "approximation" ones, demonstrating the accuracy of the approximation in Lemma 5.1. In addition, all protocols achieve the same diversity gain of 15.38, as expected from the derived expression $MN \min\{\alpha, \beta\}$.

Figure 5.3 demonstrates the outage performance versus SNR for different values of M in a single receive-aperture system ($N = 1$), assuming $\mathcal{R} = 3$ nps/Hz. As expected, the outage probability curves[6] of different protocols coincide for $M = 1$. In addition, comparing the curves corresponding to $M = 1$ with those for $M > 1$ clearly shows that H-ARQ improves the outage performance of FSO systems at the cost of delay and rate loss. Precisely, at a target outage probability of 10^{-6}, we observe impressive performance gains of 16.4 dB, 19.7 dB, and 25 dB, respectively, by using the ALO, RTD, and INR protocols with $M = 3$ in comparison to a system without H-ARQ ($M = 1$). The slope of curves also indicates that the diversity order at high-SNR regime is proportional to M.

[6]In the following, if a curve is not labeled by "exact" or "approximation", it indicates an "exact" one.

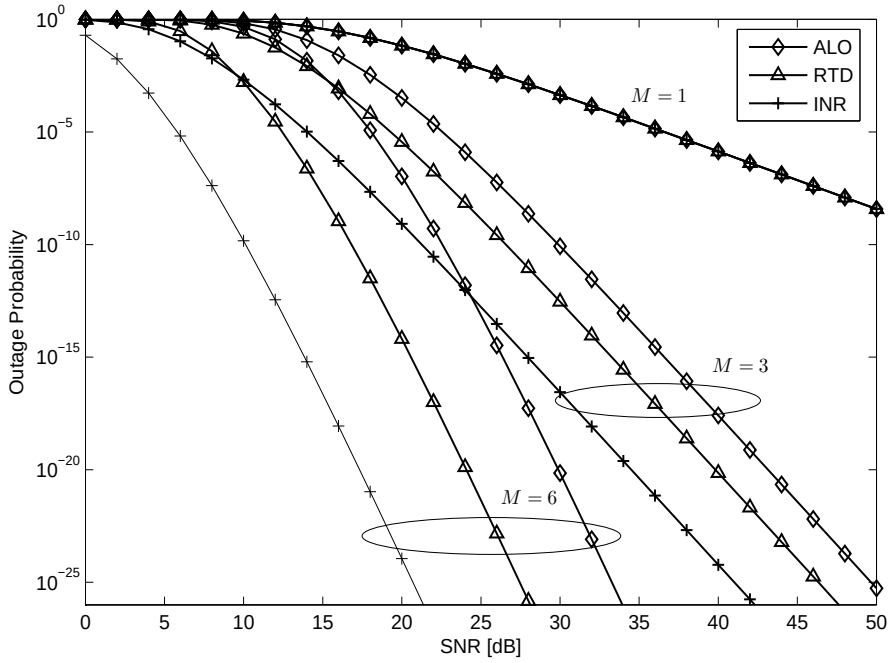

Figure 5.3: Outage performance versus SNR for various values of M ($N = 1$ and $\mathcal{R} = 3$).

Figure 5.4 depicts the outage probability versus SNR for different values of $\mathcal{R}$, assuming $M = 3$ and $N = 1$. As expected, the performance of the RTD and ALO protocols deteriorates considerably by increasing $\mathcal{R}$. On the other hand, the benefit of INR respect to other protocols becomes more evident at larger values of $\mathcal{R}$. To be more precise, consider the curves associated with $\mathcal{R} = 0.5$ nps/Hz. For this rate, to achieve a target outage probability of 10^{-6}, INR brings, respectively, 4.1 dB and 0.8 dB SNR gains compared to ALO and RTD. As $\mathcal{R}$ increases to 6 nps/Hz, these gains increase drastically to 15.7 dB and 12.4 dB, respectively. This indicates that INR significantly outperforms other protocols particularly for high rates at the cost of higher complexity.

Figure 5.5 demonstrates the outage probability of the ALO protocol versus SNR for two different turbulence conditions: weak turbulence regime with $\sigma_R^2 = 0.1$ ($\alpha = 21.5890$, $\beta = 19.8208$) and strong turbulence regime with $\sigma_R^2 = 10$ ($\alpha = 5.6893$, $\beta = 1.1016$). We assume $\mathcal{R} = 2$ and $N = 1$ in this figure. As observed, for an FSO system operating at weak turbulence regime, the ALO protocol with $M = 3$ brings 4 dB performance improvement compared to a system without ARQ ($M = 1$) to achieve a target outage probability of

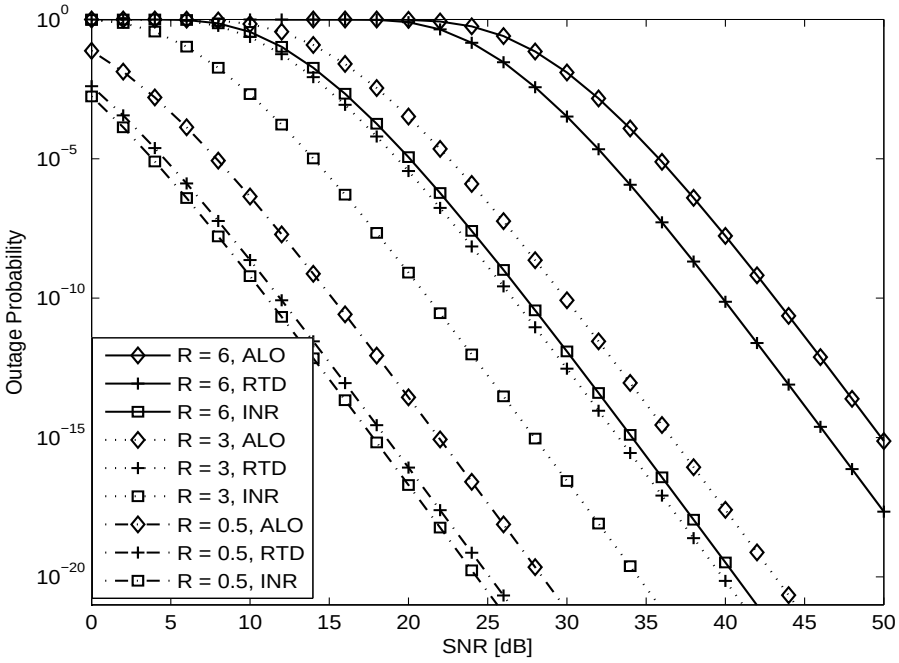

Figure 5.4: Outage probability versus SNR for various values of $\mathcal{R}$ ($N = 1$ and $M = 3$).

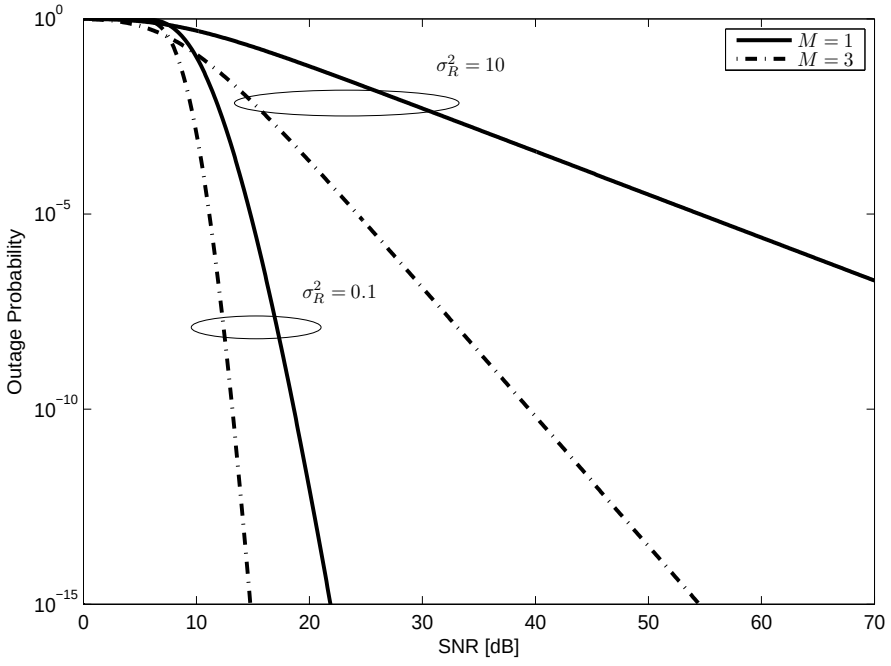

Figure 5.5: Outage probability of ALO protocol versus SNR for two different turbulence conditions ($N = 1$, $\mathcal{R} = 2$).

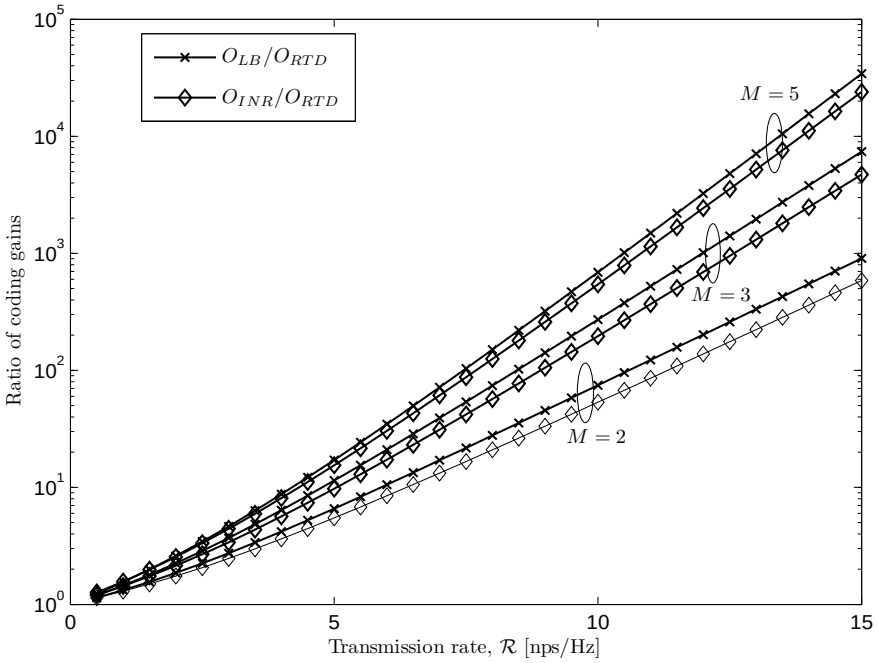

Figure 5.6: Ratio of RTD and INR coding gains versus $\mathcal{R}$.

10^{-6}. Nevertheless, this performance improvement increases considerably to 36.3 dB at strong turbulence regime. Similar results can be readily observed for the RTD and INR protocols. Therefore, it is figured out that H-ARQ improves the performance of a coherent FSO system in the strong turbulence regime more drastically than in the weak turbulence regime. This is due to the fact that H-ARQ increases the reliability of a communication system and this beneficial property is more demanded in the strong turbulence regime.

Figure 5.6 depicts the ratio of the coding gains in the INR and RTD protocols (i.e., O_{INR}/O_{RTD})[7] for a single-aperture system versus $\mathcal{R}$ for $M = 2, 3, 5$. The ratio O_{LB}/O_{RTD}, given by (5.46), is also demonstrated in this figure. We observe that O_{INR}/O_{RTD} follows similar trend as O_{LB}/O_{RTD}, i.e., the outage coding gain of INR grows exponentially with respect to $\mathcal{R}$ compared to that of RTD. This again confirms that INR brings much more outage performance improvement than RTD at high transmission rate.

[7]To obtain O_{INR}, we first obtain $P_{out,INR}$ at a large value of SNR, e.g., $\rho = 100$ dB, by M-fold convolution of the exact pdf of J_i in (5.28) and then compute $O_{INR} = (P_{out,INR})^{-1/d_{INR}}/\rho$, according to (5.4).

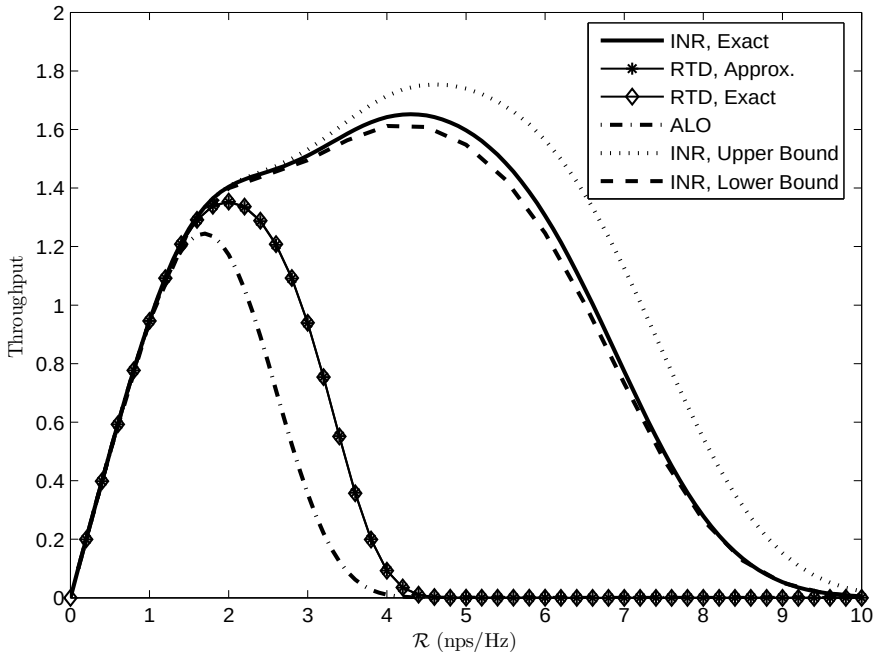

Figure 5.7: Throughput versus $\mathcal{R}$ for $N = 1$, $M = 3$, and $\rho = 10$ dB.

Figure 5.7 illustrates the throughput of three protocols versus $\mathcal{R}$ assuming $M = 3$ and $\rho = 10$ dB. The upper and lower bounds of $\mathcal{T}_{INR}$, respectively given by (5.51) and (5.52), are also included in this figure. It is observed that $\mathcal{T}_{LB}$ is much tighter than $\mathcal{T}_{RTD}$ as a lower bound on $\mathcal{T}_{INR}$. In addition, we observe that the curves of different schemes overlap for small values of $\mathcal{R}$ since one round of transmission is enough for decoding when $\mathcal{R}$ is small. However, as $\mathcal{R}$ increases, due to the sub-optimality of ALO and RTD protocols, their curves are considerably below the INR curve.

Appendix 5A. Proof of Lemma 5.2

In our proof, we use the small argument approximation approach of [71]. In this approximation, the term corresponding to the smallest exponent of z in the power series expansion of $f_z(z)$ becomes our focus. To derive this term, we first evaluate the Laplace transform of

$f_z(z)$ as

$$\begin{aligned} F_z(s) &= \int_0^\infty \exp(-sz) f_z(z) dz \\ &= \left(F_h(s)\right)^k, \end{aligned} \tag{5.54}$$

where $F_h(s)$ is the Laplace transform of the Gamma-Gamma pdf with unit mean and shaping parameters α and β. $F_h(s)$ can be calculated from

$$F_h(s) = \int_0^\infty \exp(-sh) f_h(h) dh, \tag{5.55}$$

where $f_h(h)$ is given in (2.12). Rewriting the integrand in terms of the Meijer G-function using [68, p. 633, Eq. 8.4.3.1] and [68, p. 665, Eq. 8.4.23.1], i.e.,

$$\exp(-sh) = G_{0,1}^{1,0}\Big(sh \Big| \begin{array}{c} - \\ 0 \end{array}\Big), \tag{5.56}$$

$$\mathbb{K}_{\alpha-\beta}\left(2\sqrt{\alpha\beta h/\mu}\right) = \frac{1}{2} G_{0,2}^{2,0}\left(\alpha\beta h/\mu \,\middle|\, \begin{array}{c} - \\ (\alpha-\beta)/2,\, (\beta-\alpha)/2 \end{array}\right), \tag{5.57}$$

and then further using [68, p. 346, Eq. 2.24.1.1], we obtain

$$F_h(s) = \frac{1}{\Gamma(\alpha)\Gamma(\beta)} G_{1,2}^{2,1}\left(\frac{\alpha\beta}{\mu s} \,\middle|\, \begin{array}{c} 1 \\ \alpha, \beta \end{array}\right). \tag{5.58}$$

The convergent series expansion for the Meijer G-function is given by [72, p. 1033, Eq. 9.303]

$$\begin{aligned} G_{p,q}^{m,n}\left(z \,\middle|\, \begin{array}{c} (r_p) \\ (t_q) \end{array}\right) = \sum_{i=1}^{m} & \frac{\prod_{v=1}^{m} \Gamma(t_v - t_i)' \prod_{v=1}^{n} \Gamma(1 + t_i - r_v)}{\prod_{v=m+1}^{q} \Gamma(1 + t_i - t_v) \prod_{v=n+1}^{p} \Gamma(r_v - t_i)} z^{t_i} \\ & \times {}_p\mathcal{F}_{q-1}\left((-1)^{p-m-n} z \,\middle|\, \begin{array}{c} (1 + t_i - r_p) \\ (1 + t_i - t_q)' \end{array}\right), \end{aligned} \tag{5.59}$$

for $p < q$, $z \neq 0$, and no two of the t_i terms ($i = 1, \ldots, m$) differ by an integer. The symbol (r_p) denotes the sequence $r_1, r_2, \ldots, r_p$, the sign $(\cdot)'$ indicates that the term corresponding

to $v = i$ is absent, and ${}_p\mathcal{F}_{q-1}(\cdot)$ is the generalized hyper-geometric function [69]. We assume that $\alpha - \beta \notin \mathbb{Z}$, where $\mathbb{Z}$ denotes the set of integers[8].

Utilizing (5.59) in (5.58), we have

$$F_h(s) = \frac{\Gamma(\beta-\alpha)}{\Gamma(\beta)}\left(\frac{\alpha\beta}{\mu s}\right)^{\alpha} {}_1\mathcal{F}_1\left(\frac{\alpha\beta}{\mu s}\middle| \begin{matrix} \alpha \\ 1+\alpha-\beta \end{matrix}\right) + \frac{\Gamma(\alpha-\beta)}{\Gamma(\alpha)}\left(\frac{\alpha\beta}{\mu s}\right)^{\beta} {}_1\mathcal{F}_1\left(\frac{\alpha\beta}{\mu s}\middle| \begin{matrix} \beta \\ 1+\beta-\alpha \end{matrix}\right). \tag{5.60}$$

Substituting ${}_1\mathcal{F}_1(\cdot)$ by its series form [69], we obtain the following convergent series for $F_h(s)$

$$F_h(s) = \sum_{i=0}^{\infty} \frac{a_i(\alpha,\beta)}{s^{\alpha+i}} + \sum_{i=0}^{\infty} \frac{a_i(\beta,\alpha)}{s^{\beta+i}}, \tag{5.61}$$

where

$$a_i(\alpha,\beta) = \frac{\Gamma(\beta-\alpha)\Gamma(1+\alpha-\beta)\Gamma(\alpha+i)}{i!\Gamma(\alpha)\Gamma(\beta)\Gamma(1+\alpha-\beta+i)}\left(\frac{\alpha\beta}{\mu}\right)^{\alpha+i}. \tag{5.62}$$

Substituting (5.61) in (5.54), $F_z(s)$ is expressed as

$$F_z(s) = \sum_{n=0}^{k}\binom{k}{n}\sum_{i=0}^{\infty}\frac{b_i(k-n,n)}{s^{n\alpha+(k-n)\beta+i}}, \tag{5.63}$$

where $b_i(p,q) = a_i^{(p)}(\alpha,\beta) * a_i^{(q)}(\beta,\alpha)$ [72, p. 18, Eq. 0.316]. Here, $*$ denotes the convolution operator and $a_i^{(p)}(\alpha,\beta)$ means that $a_i(\alpha,\beta)$ is convolved p times with itself.

The pdf of z is derived by the inverse Laplace transform of $F_z(s)$ as

$$f_z(z) = \sum_{n=0}^{k}\binom{k}{n}\sum_{i=0}^{\infty}\frac{b_i(k-n,n)}{\Gamma\left(n\alpha+(k-n)\beta+i\right)}x^{n\alpha+(k-n)\beta+i-1}. \tag{5.64}$$

Now, confining our attention only to the term corresponding to the smallest exponent of z in the series (5.64), the small argument approximation of $f_z(z)$ is obtained as

$$f_z(z) \sim \left(\frac{a_0(\tau,\upsilon)}{\Gamma(\tau)\Gamma(\upsilon)}\right)^{k}\frac{z^{k\tau-1}}{\Gamma(k\tau)}, \tag{5.65}$$

where $\tau = \min\{\alpha,\beta\}$ and $\upsilon = \max\{\alpha,\beta\}$. Finally, substituting $a_0(\tau,\upsilon)$ from (5.62) in (5.65), we obtain (5.9).

[8]This assumption is not a limiting restriction because it holds for typical values of α and β [2]. Furthermore, if necessary, α and β can be selected such that $\alpha - \beta + \varepsilon \in \mathbb{Z}$ with some small constant ε to approximate the case $\alpha - \beta \in \mathbb{Z}$ [16].

Appendix 5B. Proof of Lemma 5.4

We want to derive the cdf of the random variable $w = \prod_{i=1}^{m} q_i$ where q_is are i.i.d. Gamma-Gamma random variables with mean μ and shaping parameters α and β. We use Mellin transform technique [69] to derive the pdf of w, denoted by $f_w(w)$. The Mellin transform of $f_w(w)$ is defined as the $(s-1)$th moment of w, i.e., $E[w^{s-1}]$. Hence, $f_w(w)$ can be obtained by the inverse Mellin transform of $E[w^{s-1}]$ as

$$f_w(w) = \frac{1}{2\pi j} \int_{\mathcal{C}} E[w^{s-1}] w^{-s} ds, \tag{5.66}$$

where $\mathcal{C}$ is an appropriate contour [69].

Since q_is are i.i.d, $E[w^{s-1}]$ can be obtained as

$$E[w^{s-1}] = \prod_{i=1}^{m} E\left[q_i^{s-1}\right], \tag{5.67}$$

where $E[q_i^{s-1}]$ is the $(s-1)$th moment of q_i, and is obtained by using (2.12) and [72, p. 676, Eq. 6.561.16] as

$$E\left[q_i^{s-1}\right] = \left(\frac{\alpha\beta}{\mu}\right)^{1-s} \frac{\Gamma\left(\alpha+s-1\right)\Gamma\left(\beta+s-1\right)}{\Gamma(\alpha)\Gamma(\beta)}. \tag{5.68}$$

Inserting (5.67) and (5.68) in (5.66), we obtain $f_w(w)$ as

$$f_w(w) = \frac{w^{-1}}{\Gamma^m(\alpha)\Gamma^m(\beta)} \times \frac{1}{2\pi j} \int_{\mathcal{C}} \Gamma^m\left(\alpha+s-1\right)\Gamma^m\left(\beta+s-1\right) \left(\left(\frac{\alpha\beta}{\mu}\right)^m w\right)^{-(s-1)} ds. \tag{5.69}$$

Using the definition of the Meijer G-function [69], i.e.,

$$G_{p,q}^{m,n}\left(z \left| \begin{matrix}(r_p)\\(t_q)\end{matrix}\right.\right) = \frac{1}{2\pi j} \int_{\mathcal{C}} \frac{\prod_{i=1}^{m}\Gamma(t_i+s)\prod_{i=1}^{n}\Gamma(1-r_i-s)}{\prod_{i=n+1}^{p}\Gamma(r_i+s)\prod_{i=m+1}^{q}\Gamma(1-t_i-s)} z^{-s} ds, \tag{5.70}$$

$f_w(w)$ in (5.69) can be represented as

$$f_w(w) = \frac{w^{-1}}{\Gamma^m(\alpha)\Gamma^m(\beta)} G_{0,2m}^{2m,0}\left(\left(\frac{\alpha\beta}{\mu}\right)^m w \left| \begin{matrix} - \\ \underbrace{\alpha,\ldots,\alpha}_{m\ times}, \underbrace{\beta,\ldots,\beta}_{m\ times}\end{matrix}\right.\right). \tag{5.71}$$

Therefore, the cdf of w, denoted by $\mathbb{F}_w(w)$, is obtained by using (5.71) and [68, p. 46, Eq. 1.16.2.1] as

$$\begin{aligned}\mathbb{F}_w(w) &= \int_0^w f_w(t)dt \\ &= \frac{1}{\Gamma^m(\alpha)\Gamma^m(\beta)} G_{1,2m+1}^{2m,1}\left(\left(\frac{\alpha\beta}{\mu}\right)^m w \middle| \begin{matrix} 1 \\ \underbrace{\alpha,\ldots,\alpha}_{m\ times}, \underbrace{\beta,\ldots,\beta}_{m\ times}, 0 \end{matrix}\right).\end{aligned} \tag{5.72}$$

Appendix 5C. Proof of (5.45)

First we start with the RTD protocol. Using (5.23), we have

$$\begin{aligned}\lim_{M\to\infty} \frac{\ln O_{RTD}}{\ln M} &= \lim_{M\to\infty} \frac{\ln\Gamma(\upsilon)}{\tau \ln M} + \lim_{M\to\infty} \frac{\ln\Gamma\left(MN\tau+1\right)}{MN\tau \ln M} \\ &\quad - \lim_{M\to\infty} \frac{\ln\Gamma\left(\upsilon-\tau\right)}{\tau \ln M} - \lim_{M\to\infty} \frac{N\tau\upsilon\gamma_{th}}{\ln M} \\ &= \lim_{M\to\infty} \frac{\ln\Gamma\left(MN\tau+1\right)}{MN\tau \ln M}.\end{aligned} \tag{5.73}$$

From Stirling's approximation, we have $\ln\Gamma(x) \approx (x-1/2)\ln x - x$ for $x \to \infty$ [69]. Employing this approximation in (5.73), we have

$$\begin{aligned}\lim_{M\to\infty} \frac{\ln O_{RTD}}{\ln M} &= \lim_{M\to\infty} \frac{MN\tau \ln\left(MN\tau\right)}{MN\tau \ln M} \\ &= 1,\end{aligned} \tag{5.74}$$

which results in $O_{RTD} \doteq M$.

Likewise, it can be shown from (5.42) that $O_{LB} \doteq M$. In addition, as observed in (5.43), the outage probability of the RTD protocol is an upper bound for that of the INR protocol. Therefore, we have a lower bound (O_{RTD}) and an upper bound (O_{LB}) for O_{INR} both of which grow linearly respect to M for its large values. Hence, noting that the limits of functions preserve inequalities [70], we have $C_{INR} \doteq M$ and the proof is completed.

Chapter 6

Parallel Relaying in IM/DD FSO Communications

In this chapter, we return our focus to IM/DD FSO communications and investigate the performance of parallel relaying over the Gamma-Gamma fading channels. We consider an IM/DD FSO system with a single relay and a line-of-sight link between the source and the destination. We analyze two classes of cooperation; DF and AF. Focusing on high-SNR regime, we develop performance characterizations of each cooperation mode in terms of the outage probability, outage diversity and coding gains, and DMT.

6.1 System Model

Consider the parallel FSO relaying scheme in Figure 6.1. Information is to be transmitted from the source terminal S to the destination terminal D with the assistance of the relay terminal R. We assume full-duplex (bi-directional) transceivers which are the common choice in commercial FSO links. The relay node utilizes either DF strategy or AF strategy to relay the received signal to the destination. The destination makes its final decision by maximum ratio combining [57] the received signals from the direct (source-destination) link and the indirect (relay-destination) link. Let P_T denote the average transmitted optical power in a direct transmission system that we will use as the benchmark scheme. For a fair comparison, we assume that each of the three transmitting terminals ($\mathrm{TRX}_{S,1}, \mathrm{TRX}_{S,2}$, and

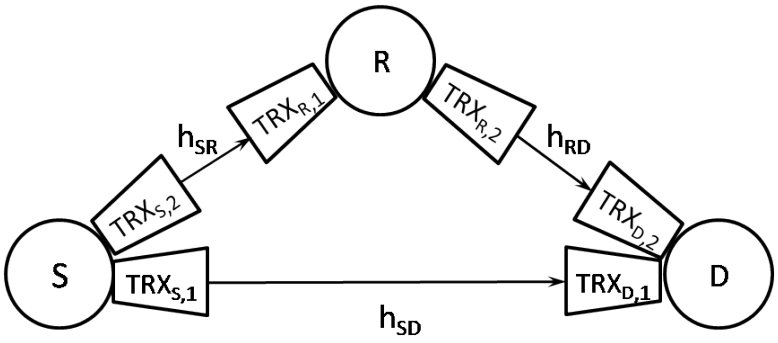

Figure 6.1: Parallel FSO relaying system.

$\mathrm{TRX}_{R,2}$) in each cooperation cycle uses an average transmitted optical power of $P_T/3$. Let $y_{D,1}$ and $y_{D,2}$ respectively denote the detected electrical signals at the $\mathrm{TRX}_{D,1}$ and $\mathrm{TRX}_{D,2}$ terminals of the destination, and let y_R be the detected electrical signal at $\mathrm{TRX}_{R,1}$ terminal of the relay. These signals are respectively given by

$$y_{D,1} = \Re h_{SD} x_S + n_{D,1}, \tag{6.1}$$

$$y_{D,2} = \Re h_{RD} x_R + n_{D,2}, \tag{6.2}$$

$$y_R = \Re h_{SR} x_S + n_R, \tag{6.3}$$

where x_S is the intensity modulated source signal with $E[x_S] = P_T/3$, and x_R is the relay transmitted signal. $n_{D,1}$, $n_{D,2}$, and n_R are the noise terms in $\mathrm{TRX}_{\mathrm{D},1}$, $\mathrm{TRX}_{\mathrm{D},2}$, and $\mathrm{TRX}_{\mathrm{R},1}$ terminals, respectively. Each noise term is the superposition of the thermal noise and the background light induced shot noise, and is modeled as zero-mean signal-independent Gaussian noise [11] with variance σ_n^2. The noise terms are assumed to be mutually independent.

In (6.1)-(6.3), h_{SR}, h_{RD}, and h_{SD} respectively denote the atmospheric fading power coefficients of the source-relay (S-R), relay-destination (R-D), and source-destination (S-D) links. We assume that h_{SR}, h_{RD}, and h_{SD} respectively follow $\Gamma\Gamma(\alpha_1, \beta_1, \mathcal{L}_1)$, $\Gamma\Gamma(\alpha_2, \beta_2, \mathcal{L}_2)$, and $\Gamma\Gamma(\alpha_3, \beta_3, 1)$ distributions where $\mathcal{L}_1$ and $\mathcal{L}_2$ are, respectively, the path losses of S-R and R-D links normalized by the path loss of S-D link.

The value of x_R in (6.2) depends on the relaying strategy. In the DF mode, the relay first decodes the received signal after direct detection and then repeats the source transmission with optical power $P_T/3$. We assume that the relay is allowed to forward only if it has

decoded correctly. Otherwise, it remains silent. Hence, we have $x_R = x_S$ when the relay is active.

In the AF mode, the relay first normalizes the detected electrical signal y_R by factor $\sqrt{h_{SR}^2 \Re^2 P_T^2/9 + \sigma_n^2}$ to satisfy its average power constraint, then modulates the normalized signal by optical power $P_T/3$, and retransmits it to the destination. Therefore, x_R in (6.2) is given by $x_R = \Phi_R y_R$ where Φ_R is given by

$$\Phi_R = \frac{P_T/3}{\sqrt{h_{SR}^2 \Re^2 P_T^2/9 + \sigma_n^2}}. \tag{6.4}$$

6.2 Outage Analysis

As given by (3.15), the outage probability is defined as the probability that the instantaneous capacity of the underlying channel is below the transmission rate $\mathcal{R}$. The exact capacity of an FSO IM/DD channel corrupted by AWGN is still an open problem. However, upper and lower bounds on this channel's capacity under different power constrains have been recently derived [73, 74]. Using the results of [73], the capacity of an IM/DD FSO channel at high-SNR regime satisfies

$$C(\gamma) \sim \frac{1}{2}\log(\gamma), \tag{6.5}$$

where γ denotes the instantaneous electrical SNR.

The following lemma and its corollary are used in the outage analysis of this section.

Lemma 6.1. *Let V be a random variable with $\Gamma\Gamma^2(\alpha, \beta, \mu)$ distribution and the pdf of $f_V(V)$. The Laplace transform of $f_V(V)$, denoted by $F_V(s)$, satisfies*

$$F_V(s) = \frac{\Gamma(\upsilon - \tau)(\upsilon\tau/\mu)^\tau}{2\Gamma(\upsilon)\Gamma(\tau)} \frac{\Gamma(\tau/2)}{s^{\tau/2}} + o\left((1/s)^{\tau/2}\right), \tag{6.6}$$

where $\tau = \min\{\alpha, \beta\}$ and $\upsilon = \max\{\alpha, \beta\}$.

The proof is given in Appendix 6A.

Corollary 6.1. *The pdf of the random variable V with $\Gamma\Gamma^2(\alpha, \beta, \mu)$ distribution can be approximated by a single-term polynomial for small values of V ($V \to 0^+$), i.e.,*

$$f_V(V) = \frac{\Gamma(\upsilon - \tau)}{2\Gamma(\upsilon)\Gamma(\tau)} (\upsilon\tau/\mu)^\tau V^{\tau/2-1} + o\left(V^{\tau/2-1}\right). \tag{6.7}$$

6.2.1 Direct Transmission

As a benchmark scheme, we first investigate the outage performance of the direct transmission (DT), i.e., no relay is used. In this case, the instantaneous electrical SNR at the destination, denoted by γ_D^{DT} , can be obtained by using (6.1) as

$$\gamma_D^{DT} = \rho h_{SD}^2, \tag{6.8}$$

where $\rho = (\Re P_T)^2/\sigma_n^2$ is the average electrical SNR in the absence of atmospheric channel effect. Substituting γ_D^{DT} in (3.16) and using [68, p. 665, Eq. 8.4.23.1], [68, p. 665, Eq. 8.4.23.1], and [68, p. 46, Eq. 1.16.2.1], the outage probability of direct transmission is obtained as

$$P_{out}^{DT} = \frac{1}{\Gamma(\alpha_3)\Gamma(\beta_3)} G_{1,3}^{2,1}\left(\alpha_3\beta_3\sqrt{\gamma_{th}/\rho}\,\middle|\,\begin{matrix}1\\ \alpha_3, \beta_3, 0\end{matrix}\right) \tag{6.9}$$

with $\gamma_{th} = C^{-1}(\mathcal{R})$, where $C(\cdot)$ is the instantaneous capacity of IM/DD FSO channels.

By using Corollary 6.1, the outage probability of the direct transmission at high-SNR regime can be approximated as

$$P_{out}^{DT} \sim (O_{DT} \cdot \rho)^{-d_{DT}}, \tag{6.10}$$

wherein the diversity gain (d_{DT}) and the coding gain (O_{DT}) are respectively given by

$$d_{DT} = \tau_3/2, \tag{6.11}$$

$$O_{DT} = \frac{1}{\gamma_{th}(\upsilon_3\tau_3)^2}\left(\frac{\Gamma(\upsilon_3 - \tau_3)}{\Gamma(\upsilon_3)\,\Gamma(\tau_3+1)}\right)^{-1/d_{DT}}. \tag{6.12}$$

with $\tau_3 = \min\{\alpha_3, \beta_3\}$ and $\upsilon_3 = \max\{\alpha_3, \beta_3\}$.

On-off keying (OOK) and pulse position modulation (PPM) are two binary-level modulation schemes which are most popular in IM/DD FSO systems. Although these schemes typically have simple and inexpensive implementations, they are spectrally inefficient. To overcome this deficiency, the direct detection of $\mathcal{M}$-level intensity modulation, also referred as $\mathcal{M}$-level pulse amplitude modulation ($\mathcal{M}$-PAM), can be employed in IM/DD FSO systems which provides higher bandwidth than binary level schemes. For more details on different modulation schemes in FSO communications please refer to [75].

The DMT concept presented in Section 3.2 of Chapter 3 is obtained based on the outage probability wherein the only performance limiting factor is the channel fading. This DMT is referred as the optimal DMT that can be achieved in the underlying system and is independent of the coding/modulation scheme employed at the transmitter. In reality, however, the system performance is limited by both the fading and the noise. In other words, due to use of imperfect channel codes, some symbols might be detected erroneous at the presence of the noise.

Hence, to consider the malicious effect of the noise, the average error probability is used which is obviously lower bounded by the outage probability. Therefore, the DMT of a practical scheme is upper bounded by the optimal DMT obtained by the outage expression. A coding/modulation scheme is called DMT achieving if it achieves the optimal DMT, i.e., at a given multiplexing gain, the decaying rate of the average error probability versus SNR at high-SNR regime mimics that of the outage probability. In the following, we first derive the optimal DMT of the direct transmission at high-SNR regime and then, demonstrate that $\mathcal{M}$-PAM achieves the optimal DMT of a point-to-point IM/DD FSO system.

Let the data rate of the system increase with respect to SNR as $\mathcal{R} \sim r \log \rho$ for large values of ρ, where r denotes the multiplexing gain. Utilizing (6.5) in the outage expression of (3.15) and then using (6.8), we have

$$\begin{aligned} P_{out}^{DT} &\doteq \Pr\left\{\frac{1}{2}\log(\gamma_D^{DT}) < r\log\rho\right\} \\ &= \Pr\left\{h_{SD}^2 < \rho^{-(1-2r)}\right\} \\ &\doteq \rho^{\frac{-\tau_3}{2}(1-2r)}, \qquad \text{for} \qquad 0 \leqslant r < 1/2 \end{aligned} \tag{6.13}$$

where we have used Corollary 6.1 in the last exponential equality.

Therefore, from the definition of (asymptotic) DMT given in (3.10), it can be realized that the optimal DMT of the direct transmission is given by

$$d_{DT}(r) = \frac{\tau_3}{2}(1-2r), \qquad 0 \leqslant r < 1/2 \tag{6.14}$$

As can be observed, the multiplexing gain in a point-to-point IM/DD FSO channel goes only up to 1/2 instead of one. This is in contrast to the fact that the maximum multiplexing gain achieved in a point-to-point RF channel [37] (and also in a point-to-point coherent

FSO channel) is one. Such a different result is due to the square-law operation of the direct detection on the received optical signal in IM/DD FSO channels.

Theorem 6.1. *$\mathcal{M}$-PAM achieves the optimal DMT of the direct transmission, i.e.,*

$$P_E^{DT} \doteq \rho^{-d_{DT}(r)}, \tag{6.15}$$

where P_E^{DT} is the average error probability at the destination when the source uses $\mathcal{M}$-PAM.

The proof is given in Appendix 6B.

6.2.2 Decode-and-Forward Mode

By using (6.1)-(6.3), the instantaneous electrical SNR at the destination for the DF mode can be obtained as

$$\gamma_D^{DF} = \begin{cases} h_{SD}^2 \rho/9, & \gamma_R^{DF} < \gamma_{th} \\ \left(h_{RD}^2 + h_{SD}^2\right) \rho/9, & \gamma_R^{DF} \geqslant \gamma_{th} \end{cases} \tag{6.16}$$

where $\gamma_R^{DF} = h_{SR}^2 \rho/9$ is the instantaneous electrical SNR at the relay. The first condition in (6.16), i.e., $\gamma_R^{DF} < \gamma_{th}$, indicates that the relay was not able to decode the source signal and therefore remained silent. On the other hand, $\gamma_R^{DF} \geq \gamma_{th}$ means that the relay successfully decoded the source signal and retransmitted it to the destination. Note that in (6.16), we have assumed that the relay cannot decode successfully if and only if an outage event occurs in S-R channel.

Using (6.16) and (3.16), the outage probability of the DF mode can be expressed as

$$\begin{aligned} P_{out}^{DF} = &\Pr\left\{h_{SD}^2 \rho/9 < \gamma_{th}\right\} \Pr\left\{h_{SR}^2 \rho/9 < \gamma_{th}\right\} \\ &+ \Pr\left\{\left(h_{SD}^2 + h_{RD}^2\right) \rho/9 < \gamma_{th}\right\} \Pr\left\{h_{SR}^2 \rho/9 \geqslant \gamma_{th}\right\}. \end{aligned} \tag{6.17}$$

Deriving a closed form expression for P_{out}^{DF} is a difficult task, if not impossible. However, an asymptotic approximation can be obtained as follows.

Theorem 6.2. *The outage probability of the DF mode at high-SNR regime can be approximated as*

$$P_{out}^{DF} \sim \left(O_{DF} \cdot \rho\right)^{-d_{DF}}, \tag{6.18}$$

wherein the diversity gain (d_{DF}) and the coding gain (O_{DF}) are respectively given by

$$d_{DF} = (\tau_n + \tau_3)/2, \tag{6.19}$$

$$O_{DF} = \begin{cases} O_n^{DF} & \tau_1 \neq \tau_2 \\ \left(\sum_{i=1}^{2} \left(O_i^{DF}\right)^{-d_{DF}}\right)^{-1/d_{DF}} & \tau_1 = \tau_2 \end{cases} \tag{6.20}$$

with $\tau_i = \min\{\alpha_i, \beta_i\}$ *for* $i = 1, 2, 3$, *and* $n = \arg\min_{i\in\{1,2\}} \{\tau_i\}$.

O_1^{DF} *and* O_2^{DF} *in (6.20) are respectively given by*

$$O_1^{DF} = \frac{1}{9\gamma_{th}} \left(\frac{\Gamma(\upsilon_1 - \tau_1)(\upsilon_1\tau_1/\mathcal{L}_1)^{\tau_1}}{\Gamma(\upsilon_1)\Gamma(\tau_1+1)} \times \frac{\Gamma(\upsilon_3 - \tau_3)(\upsilon_3\tau_3)^{\tau_3}}{\Gamma(\upsilon_3)\Gamma(\tau_3+1)} \right)^{-2/(\tau_1+\tau_3)}, \tag{6.21}$$

$$O_2^{DF} = \frac{1}{9\gamma_{th}} \left(\frac{\Gamma(\upsilon_2 - \tau_2)(\upsilon_2\tau_2/\mathcal{L}_2)^{\tau_2}}{\Gamma(\upsilon_2)\Gamma(\tau_2)} \times \frac{\Gamma(\upsilon_3 - \tau_3)(\upsilon_3\tau_3)^{\tau_3}}{\Gamma(\upsilon_3)\Gamma(\tau_3)} \times \frac{\mathrm{B}(\tau_2/2, \tau_3/2)}{2(\tau_2+\tau_3)} \right)^{-2/(\tau_2+\tau_3)}, \tag{6.22}$$

where $\upsilon_i = \max\{\alpha_i, \beta_i\}$ *for* $i = 1, 2, 3$, *and* $B(x, y)$ *is the Beta function [72].*

The proof is given in Appendix 6C.

When the transmission rate $\mathcal{R}$ increases with respect to SNR as $\mathcal{R} \sim r \log \rho$, utilizing (6.5) and (6.16) in (3.15), we have

$$\begin{aligned} P_{out}^{DF} \doteq{}& \Pr\left\{h_{SD}^2 < \rho^{-(1-2r)}\right\} \Pr\left\{h_{SR}^2 < \rho^{-(1-2r)}\right\} \\ &+ \Pr\left\{h_{SD}^2 + h_{RD}^2 < \rho^{-(1-2r)}\right\} \Pr\left\{h_{SR}^2 \geqslant \rho^{-(1-2r)}\right\}. \end{aligned} \tag{6.23}$$

Consequently, for $0 \leqslant r < 1/2$, P_{out}^{DF} at high-SNR regime satisfies

$$P_{out}^{DF} \doteq \rho^{-\frac{1}{2}(\sigma_n+\sigma_3)(1-2r)}, \tag{6.24}$$

where we have used the results of Appendix 6C.

Therefore, from (3.10), the optimal DMT of the DF mode is given by

$$d_{DF}(r) = \frac{1}{2}(\tau_n + \tau_3)(1-2r), \qquad 0 \leqslant r < 1/2. \tag{6.25}$$

It is observed that since the underlying cooperative system is full-duplex, the maximum multiplexing gain of 1/2 for IM/DD FSO channels (see (6.14)) is achieved.

Theorem 6.3. *If both source and relay utilize $\mathcal{M}$-PAM for the data transmission, the optimal DMT of the DF mode is achieved, i.e.,*

$$P_E^{DF} \doteq \rho^{-d_{DF}(r)}, \tag{6.26}$$

where P_E^{DF} is the average error probability at the destination when $\mathcal{M}$-PAM is used.

The proof is given in Appendix 6D.

6.2.3 Amplify-and-Forward Mode

The instantaneous electrical SNR at the destination for the AF mode can be obtained by using (6.1)-(6.3) as

$$\gamma_D^{AF} = \frac{\Re^2 P_T^2}{9\sigma_n^2}\left(h_{SD}^2 + \frac{\left(\Re\Phi_R h_{SR} h_{RD}\right)^2}{\left(\Re\Phi_R h_{RD}\right)^2 + 1}\right). \tag{6.27}$$

Replacing the relay's amplification factor Φ_R from (6.4) and noting that $\rho = (\Re P_T)^2/\sigma_n^2$, we obtain

$$\gamma_D^{AF} = h_{SD}^2\rho/9 + \mathcal{H}\left(h_{SR}^2\rho/9, h_{RD}^2\rho/9\right), \tag{6.28}$$

where $\mathcal{H}(x,y) \triangleq xy/(x+y+1)$.

Therefore, the outage probability of the AF mode can be expressed as

$$P_{out}^{AF} = \Pr\left\{h_{SD}^2 + \frac{9}{\rho}\mathcal{H}\left(h_{SR}^2\rho/9, h_{RD}^2\rho/9\right) \leqslant 9\gamma_{th}/\rho\right\}. \tag{6.29}$$

Deriving a closed form expression for the outage probability of the AF mode becomes complicated. In the following, we analyze its performance at high-SNR regime.

Theorem 6.4. *The outage probability of the AF mode at high-SNR regime can be approximated as*

$$P_{out}^{AF} \sim \left(O_{AF}\cdot\rho\right)^{-d_{AF}}, \tag{6.30}$$

wherein the diversity gain (d_{AF}) and the coding gain (O_{AF}) are respectively given by

$$d_{AF} = \left(\tau_n + \tau_3\right)/2, \tag{6.31}$$

$$O_{AF} = \begin{cases} O_n^{AF} & \tau_1 \neq \tau_2 \\ \left(\sum_{i=1}^{2}\left(O_i^{AF}\right)^{-d_{AF}}\right)^{-1/d_{AF}} & \tau_1 = \tau_2 \end{cases} \tag{6.32}$$

with $n = \arg\min_{i\in\{1,2\}} \{\tau_i\}$, *and* O_i^{AF} *for* $i = 1, 2$ *is given by*

$$O_i^{AF} = \frac{1}{9\gamma_{th}} \left(\frac{\Gamma(\upsilon_i - \tau_i)\left(\upsilon_i \tau_i / \mathcal{L}_i\right)^{\tau_i}}{\Gamma(\upsilon_i)\Gamma(\tau_i)} \times \frac{\Gamma(\upsilon_3 - \tau_3)\left(\upsilon_3 \tau_3\right)^{\tau_3}}{\Gamma(\upsilon_3)\Gamma(\tau_3)} \times \frac{\mathrm{B}(\tau_i/2, \tau_3/2)}{2(\tau_i + \tau_3)} \right)^{-2/(\tau_i+\tau_3)}. \tag{6.33}$$

The proof is given in Appendix 6E.

When the data rate of the system increases with respect to SNR as $R \sim r \log \rho$ at high-SNR regime, using (6.28), (6.5), and (3.15) results in

$$P_{out}^{AF} \doteq \Pr\left\{ h_{SD}^2 + \frac{9}{\rho}\mathcal{H}\left(h_{SR}^2\rho/9, h_{RD}^2\rho/9\right) < \rho^{-(1-2r)} \right\}. \tag{6.34}$$

Using the results of Appendix 6.E with $\omega(\varepsilon) = \varepsilon^{(1-2r)}$, we have

$$P_{out}^{AF} \doteq \rho^{\frac{-1}{2}(\sigma_n+\sigma_3)(1-2r)}, \qquad 0 \leqslant r < 1/2. \tag{6.35}$$

Consequently, from (3.10), the optimal DMT of the AF mode is given by

$$d_{AF}(r) = \frac{1}{2}(\tau_n + \tau_3)(1-2r), \qquad 0 \leqslant r < 1/2. \tag{6.36}$$

Comparing (6.36) with (6.25), one can realize that both cooperation modes provide the same optimal DMT.

6.2.4 Remarks on Diversity and Coding Gains

Our asymptotic analysis above demonstrates that both cooperation modes provide the same diversity order, which is the diversity of the direct transmission plus the minimum of the diversities of S-R and R-D channels[1]. In addition, as observed in (6.21) and (6.33), O_1^{DF} and O_1^{AF} are just functions of S-R and S-D links' parameters, and are independent of the R-D link's parameters. Similarly, as observed in (6.22) and (6.33), O_2^{DF} and O_2^{AF} are just functions of R-D and S-D links' parameters, and are independent of the S-R link's parameters. It indicates that when S-R channel is worse than R-D channel statistically, which corresponds to $\sigma_1 < \sigma_2$ $(n = 1)$, we have $P_{out}^{DF} \sim \left(O_1^{DF}\rho\right)^{-(\tau_1+\tau_3)/2}$ and $P_{out}^{AF} \sim \left(O_1^{AF}\rho\right)^{-(\tau_1+\tau_3)/2}$,

[1]Using corollary 6.1, it can be shown that the diversity orders of S-R and R-D channels are respectively given by $\tau_1/2$ and $\tau_2/2$.

and consequently, the asymptotic outage probabilities of both modes are independent of R-D link's characteristics. On the other hand, when R-D channel is worse than S-R channel statistically, i.e., $\sigma_2 < \sigma_1$ ($n = 2$), we have $P_{out}^{DF} \sim \left(O_2^{DF}\rho\right)^{-(\tau_2+\tau_3)/2}$ and $P_{out}^{AF} \sim \left(O_2^{AF}\rho\right)^{-(\tau_2+\tau_3)/2}$, and therefore, the asymptotic outage performances are independent of S-R link's characteristics. Hence, the outage performance at high-SNR regime in both modes is dominated by either S-R or R-D link that has the worse statistical characteristic. Note that if S-R and R-D channels have the same statistical characteristics, both channels affect the high-SNR outage performance.

In addition, it can be observed that O_1^{DF} (see (6.21)) is different from O_1^{AF}(see (6.33)). However, O_2^{DF} and O_2^{AF} (see (6.22) and (6.33)) are the same. Therefore, depending on the underlying channels' conditions, two modes may provide different coding gains despite the same diversity gain. More precisely, when R-D channel is statistically worse than S-R channel and dominates the outage performance at high-SNR regime (which corresponds to $n = 2$), both modes provide the same coding gains. On the other hand, when S-R channel is statistically worse than R-D channel and dominates the asymptotic outage performance (which corresponds to $n = 1$), we show in Appendix 6F that the AF mode outperforms the DF mode at high-SNR regime in the sense that

$$O_1^{DF} \leqslant O_1^{AF}. \tag{6.37}$$

This result can be interpreted as follows. When the S-R channel is statistically worse than the R-D channel, it is more probable that the instantaneous S-R channel goes in the fade such that the relay cannot decode its received signal correctly. Therefore, the relay is not helpful in the DF mode, but can at least amplify and forward the received signal in the AF mode.

6.3 Numerical Results and Discussions

In this section, we illustrate the analytical results derived in the previous sections and evaluate the effect of underlying channels' characteristics on the performance of two cooperation modes. We assume plane-wave propagation in turbulence conditions with refractive-index structure constant $\mathbb{C}_n^2 = 2.5 \times 10^{-14}\mathrm{m}^{-2/3}$ and attenuation of 0.44 dB/km. The system

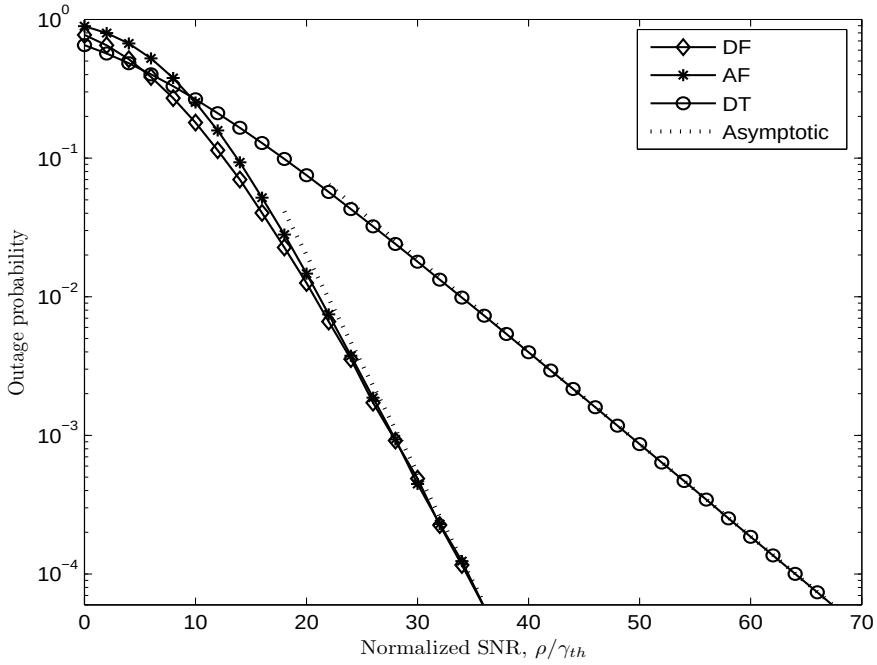

Figure 6.2: Outage probability versus normalized SNR, $Z_{SR} = 1.5$ km, $Z_{RD} = 2$ km, and $Z_{SD} = 3$ km .

is operating in the wavelength of $\lambda = 1.55$ μm. Note that since we assume the same refractive-index structure constant and wavelength for all S-R, R-D, and S-D channels in this section, only the links' lengths dominate the channels' characteristics (see (2.13) and (2.14)), i.e., the channel with the longest (shortest) length has the worst (best) statistical characteristics.

Figure 6.2 depicts the outage probabilities of the DF and AF modes versus normalized average SNR (ρ/γ_{th}). The path lengths of S-R, R-D, and S-D links are respectively assumed $Z_{SR} = 1.5\,\text{km}$, $Z_{RD} = 2\,\text{km}$, and $Z_{SD} = 3\,\text{km}$. The outage probability of direct transmission is also presented in this figure as a benchmark. Both exact outage probability and derived asymptotic approximation are displayed. The exact outage curves of the DF and AF modes are respectively obtained from (6.17) and (6.29) via the Monte Carlo simulation. It is observed that the diversity gain of both cooperation modes (i.e., the slope of the corresponding outage probability curve) is 1.57 confirming the observation of $(\tau_2 + \tau_3)/2$ from (6.19) and (6.31) respectively for the DF mode and the AF mode. This is a significant

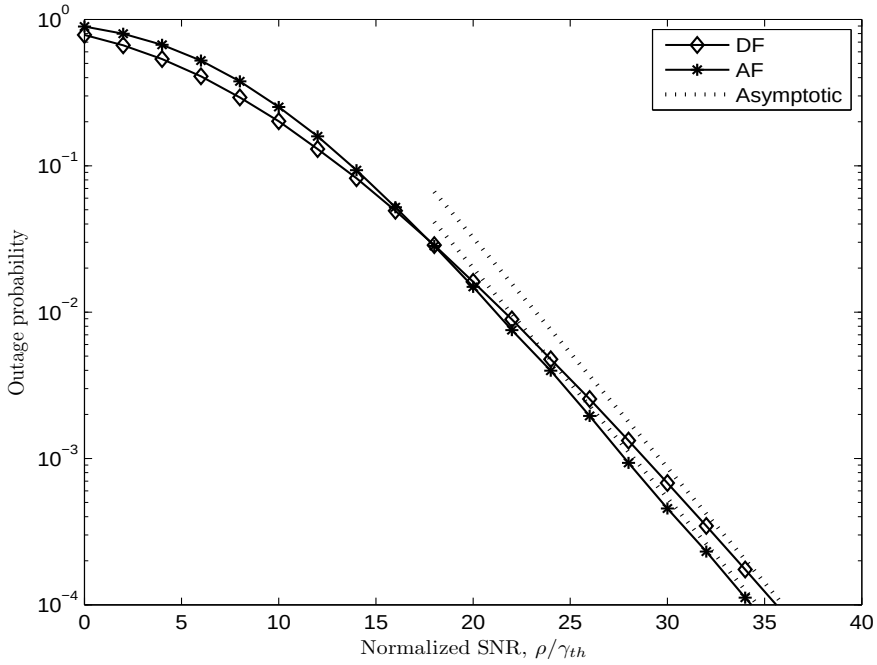

Figure 6.3: Outage probability versus normalized SNR, $Z_{SR} = 2$ km, $Z_{RD} = 1.5$ km, and $Z_{SD} = 3$ km .

increase over the diversity gain of $\tau_3/2 = 0.67$ obtained from the direct transmission. The diversity advantages obtained by cooperation modes considerably improve the system performance. For instance, at a target outage probability of 10^{-4}, cooperation modes[2] bring 28 dB energy savings compared to the direct transmission. We note that, in this figure, since the relay is closer to the source than to the destination, R-D channel is worse than S-R channel statistically ($\tau_2 < \tau_1$) and consequently dominates the outage performance of both cooperation modes at high-SNR regime. In addition, as illustrated in Section 6.2.4, since R-D channel dominates the outage performance, both modes achieve the same coding gain (besides the same diversity gain) and consequently bring the same outage performance at high-SNR regime.

Figure 6.3 depicts the outage probability versus normalized average SNR for cooperation modes under consideration assuming $Z_{SR} = 2\,\text{km}$, $Z_{RD} = 1.5\,\text{km}$, and $Z_{SD} = 3\,\text{km}$. With this configuration, the relay is closer to the destination than to the source, and con-

[2]Both modes have the same asymptotic performance at this point.

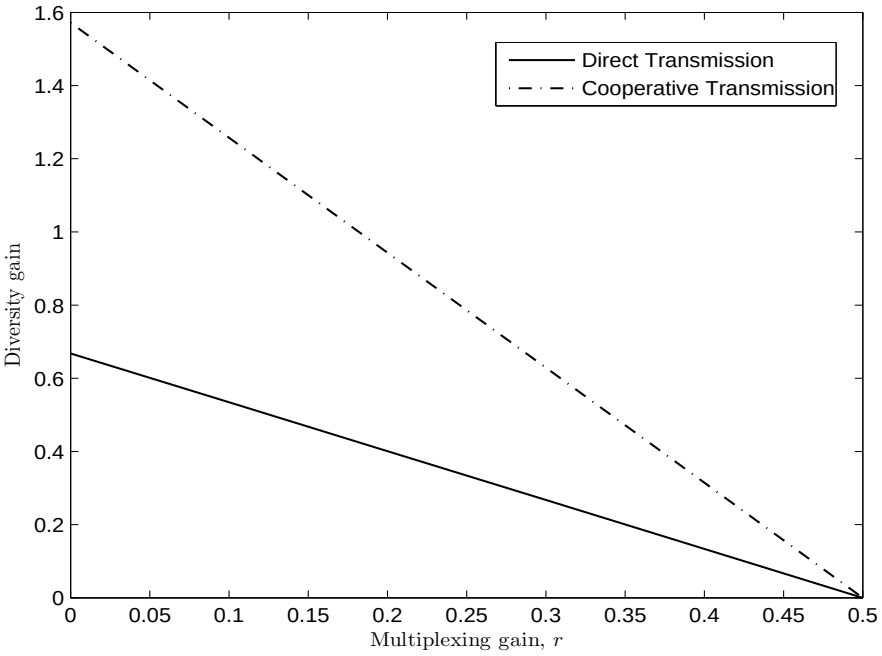

Figure 6.4: DMT curves for direct transmission and cooperative transmission.

sequently, S-R channel is statistically worse than R-D channel. It is observed that both cooperation modes achieve the same diversity gain of $(\tau_1 + \tau_3)/2$. However, since S-R channel dominates the asymptotic outage performance ($n = 1$), the AF mode provides higher coding gain than the DF mode and consequently brings better outage performance at high-SNR regime, as expected from (6.37).

Figure 6.4 demonstrates the optimal DMT curves of direct transmission and cooperation modes assuming $Z_{SR} = 1.5\,\text{km}$, $Z_{RD} = 2\,\text{km}$, and $Z_{SD} = 3\,\text{km}$. As can be seen, cooperative transmission improves the diversity gain throughout the range of the multiplexing gain. Note that both modes (see (6.25) and (6.36)) provide the same optimal DMT. In addition, as mentioned earlier, due to the square-law operation of the direct detection on the received optical power, the multiplexing gain goes only up to 1/2. This maximum multiplexing gain is achieved by the underlying cooperation modes since they are full-duplex. The maximum achievable diversity gains of direct transmission and cooperation modes are obtained at $r = 0$ which are obviously $\tau_3/2 = 0.67$ and $(\tau_2 + \tau_3)/2 = 1.57$, respectively.

Appendix 6A. Proof of Lemma 6.1

Before proceeding, for simplicity in notation, we define new random variables $u \triangleq h_{SD}^2$, $v \triangleq h_{SR}^2$, $w \triangleq h_{RD}^2$, and $z \triangleq u + w$ with pdfs $f_u(u)$, $f_v(v)$, $f_w(w)$, and $f_z(z)$, respectively. These random variables will be also used in the next appendices. We take the similar approach as Appendix 5A in this appendix.

$F_V(s)$ can be obtained by utilizing (2.12) as

$$\begin{aligned} F_V(s) &= \int_0^\infty \exp\left(-sh^2\right) \frac{2(\alpha\beta/\mu)^{(\alpha+\beta)/2}}{\Gamma(\alpha)\Gamma(\beta)} h^{(\alpha+\beta)/2-1} \mathbb{K}_{\alpha-\beta}\left(2\sqrt{\alpha\beta h}\right) dh \\ &= \frac{1}{4\pi} \frac{2^{\alpha+\beta}}{\Gamma(\alpha)\Gamma(\beta)} G_{1,4}^{4,1}\left(\frac{(\alpha\beta/\mu)^2}{16s} \middle| \begin{matrix} 1 \\ \frac{\alpha}{2}, \frac{\alpha+1}{2}, \frac{\beta}{2}, \frac{\beta+1}{2} \end{matrix} \right), \end{aligned} \tag{6.38}$$

where we have used (5.56), (5.57), and [68, p. 346, Eq. 2.24.1.1].

In the following, we assume that $\alpha - \beta \notin \mathbb{Z}$[3]. Using the series expansion of the Meijer G-function given in (5.59) and doing some mathematical manipulations, we obtain the following convergent series for $F_V(s)$

$$F_V(s) = \sum_{m=0}^{\infty} \frac{a_m(\alpha,\beta,\mu)}{s^{m+\alpha/2}} + \frac{b_m(\alpha,\beta,\mu)}{s^{m+(\alpha+1)/2}} + \frac{a_m(\beta,\alpha,\mu)}{s^{m+\beta/2}} + \frac{b_m(\beta,\alpha,\mu)}{s^{m+(\beta+1)/2}}, \tag{6.39}$$

where

$$a_m(x,y,\mu) = \frac{\sqrt{\pi}\Gamma(y-x)}{\Gamma(x)\Gamma(y)} \frac{(xy/\mu)^{2m+x}}{m!2^{2m+1}} \frac{\Gamma(1+x-y)}{\Gamma(1+x-y+2m)} \frac{\Gamma(m+x/2)}{\Gamma(m+1/2)}, \tag{6.40}$$

$$b_m(x,y,\mu) = \frac{-\sqrt{\pi}\Gamma(y-x-1)}{\Gamma(x)\Gamma(y)} \frac{(xy/\mu)^{2m+x+1}}{m!2^{2m+2}} \frac{\Gamma(2+x-y)}{\Gamma(2+x-y+2m)} \frac{\Gamma\left(m+(x+1)/2\right)}{\Gamma(m+3/2)}. \tag{6.41}$$

Consequently using (6.39), we can rewrite $F_V(s)$ as

$$F_V(s) = \frac{a_0(\tau,\upsilon,\mu)}{s^{\tau/2}} + o\left((1/s)^{\tau/2}\right), \tag{6.42}$$

where $\tau = \min\{\alpha,\beta\}$ and $\upsilon = \max\{\alpha,\beta\}$. Substituting $a_0(\tau,\upsilon,\mu)$ from (6.40) in (6.42), the lemma is proved.

[3]We make this assumption for all the Gamma-Gamma channels under consideration, i.e., $\alpha_i - \beta_i \notin \mathbb{Z}$ for $i = 1, 2, 3$.

Appendix 6B. Proof of Theorem 6.1

The average symbol error probability for the direct transmission system, when the source uses $\mathcal{M}$-PAM, is given by [76, 77]

$$P_E^{DT} = \frac{2(\mathcal{M}-1)}{\mathcal{M}} \int_0^\infty Q\left(\sqrt{A\rho u}\right) f_u(u) du, \tag{6.43}$$

where $A = 3/(\mathcal{M}-1)(2\mathcal{M}-1)$, and $Q(\cdot)$ is the Gaussian Q-function [57]. Replacing the Q-function with its definite integral form [57], P_E^{DT} can be rewritten as

$$\begin{aligned} P_E^{DT} &= \frac{2(\mathcal{M}-1)}{\pi\mathcal{M}} \int_0^\infty \left(\int_0^{\pi/2} \exp\left(-\frac{A\rho u}{2\sin^2\phi}\right) d\phi \right) f_u(u) du \\ &= \frac{2(\mathcal{M}-1)}{\pi\mathcal{M}} \int_0^{\pi/2} F_u\left(\frac{A\rho}{2\sin^2\phi}\right) d\phi, \end{aligned} \tag{6.44}$$

where $F_u(s)$ is the Laplace transform of $f_u(u)$. Using Lemma 6.1 and noting that u follows $\Gamma\Gamma^2(\alpha_3, \beta_3, 1)$ distribution, we have

$$F_u(s) = \frac{a_0(\tau_3, \upsilon_3, 1)}{s^{\tau_3/2}} + o\left((1/s)^{\tau_3/2}\right), \tag{6.45}$$

where $\tau_3 = \min\{\alpha_3, \beta_3\}$, $\upsilon_3 = \max\{\alpha_3, \beta_3\}$, and $a_m(x, y, \mu)$ is given in (6.40).

Substituting $s = A\rho/(2\sin^2\phi)$ in (6.45) and then utilizing the result in (6.44), we obtain the following approximation for P_E^{DT} at high-SNR regime

$$P_E^{DT} \sim \frac{(\mathcal{M}-1)}{\pi\mathcal{M}A^{\tau_3/2}} 2^{3\tau_3/2} a_0(\tau_3, \upsilon_3, 1) \mathrm{B}\left(\frac{(\tau_3+1)}{2}, \frac{(\tau_3+1)}{2}\right) \rho^{-\tau_3/2}, \tag{6.46}$$

where $\mathrm{B}(x, y)$ is the Beta function [72], and we have used [72, p. 395, Eq. 3.621.1]. Noting that $A = 3/(\mathcal{M}-1)(2\mathcal{M}-1)$ and $\mathcal{M} = 2^{\mathcal{R}} \sim \rho^r$, we obtain

$$P_E^{DT} \doteq \rho^{\frac{-\tau_3}{2}(1-2r)}. \tag{6.47}$$

This concludes the proof.

Appendix 6C. Proof of Theorem 6.2

Using the new notation, the outage probability of the DF mode in (6.17) can be rewritten as

$$\begin{aligned} P_{out}^{DF} &= \Pr\left\{v < 9\gamma_{th}/\rho\right\} \times \Pr\left\{u < 9\gamma_{th}/\rho\right\} \\ &\quad + \Pr\left\{v \geq 9\gamma_{th}/\rho\right\} \times \Pr\left\{z < 9\gamma_{th}/\rho\right\}. \end{aligned} \tag{6.48}$$

Noting that v follows $\Gamma\Gamma^2(\alpha_1, \beta_1, \mathcal{L}_1)$ distribution and using Corollary 6.1, $\Pr\left\{v < 9\gamma_{th}/\rho\right\}$ in (6.48) can be approximated at high-SNR regime as

$$\begin{aligned} \Pr\left\{v < 9\gamma_{th}/\rho\right\} &\sim \int_0^{9\gamma_{th}/\rho} \frac{\Gamma(\upsilon_1 - \tau_1)}{2\Gamma(\upsilon_1)\Gamma(\tau_1)} (\upsilon_1\tau_1/\mathcal{L}_1)^{\tau_1} v^{\tau_1/2-1} dv \\ &= \frac{\Gamma(\upsilon_1 - \tau_1)(\upsilon_1\tau_1/\mathcal{L}_1)^{\tau_1}}{\Gamma(\upsilon_1)\Gamma(\tau_1+1)} (9\gamma_{th}/\rho)^{\tau_1/2}. \end{aligned} \tag{6.49}$$

where $\tau_1 = \min\left\{\alpha_1, \beta_1\right\}$, $\upsilon_1 = \max\left\{\alpha_1, \beta_1\right\}$.

Similarly, $\Pr\left\{u < 9\gamma_{th}/\rho\right\}$ can be approximated at high-SNR regime as

$$\Pr\left\{u < 9\gamma_{th}/\rho\right\} \sim \frac{\Gamma(\upsilon_3 - \tau_3)(\upsilon_3\tau_3)^{\tau_3}}{\Gamma(\upsilon_3)\Gamma(\tau_3+1)} (9\gamma_{th}/\rho)^{\tau_3/2}. \tag{6.50}$$

The high-SNR approximation of $\Pr\left(z < 9\gamma_{th}/\rho\right)$ is obtained as follows. The smallest exponent of z in the power series expansion of $f_z(z)$ is in our interest at high-SNR regime. To derive this term, we first evaluate the Laplace transform of $f_z(z)$ as

$$\begin{aligned} F_z(s) &= \int_0^{\infty} \exp(-sz) f_z(z) du \\ &= F_u(s) \times F_w(s), \end{aligned} \tag{6.51}$$

where $F_u(s)$ and $F_w(s)$ are the Laplace transforms of $f_u(u)$ and $f_w(w)$, respectively. Using Lemma 6.1, we have

$$F_u(s) = \frac{a_0(\tau_3, \upsilon_3, 1)}{s^{\tau_3/2}} + o\left((1/s)^{\tau_3/2}\right), \tag{6.52}$$

$$F_w(s) = \frac{a_0(\tau_2, \upsilon_2, \mathcal{L}_2)}{s^{\tau_2/2}} + o\left((1/s)^{\tau_2/2}\right), \tag{6.53}$$

where $\tau_i = \min\left\{\alpha_i, \beta_i\right\}$, $\upsilon_i = \max\left\{\alpha_i, \beta_i\right\}$ for $i = 1, 2, 3$, and $a_m(x, y, \mu)$ is given in (6.40).

Utilizing (6.52) and (6.53) in (6.51) results in

$$F_z(s) = \frac{a_0(\tau_3, \upsilon_3, 1) a_0(\tau_2, \upsilon_2, \mathcal{L}_2)}{s^{(\tau_2+\tau_3)/2}} + o\left((1/s)^{(\tau_2+\tau_3)/2}\right). \tag{6.54}$$

By taking the inverse Laplace transform of (6.54), $f_z(z)$ can be written as

$$f_z(z) = \frac{a_0(\tau_3, \upsilon_3, 1) a_0(\tau_2, \upsilon_2, \mathcal{L}_2)}{\Gamma\left((\tau_2+\tau_3)/2\right)} z^{\frac{(\tau_2+\tau_3)}{2}-1} + o\left(z^{\frac{(\tau_2+\tau_3)}{2}-1}\right). \tag{6.55}$$

Consequently, by replacing $a_0(\tau_3, \upsilon_3, 1)$ and $a_0(\tau_2, \upsilon_2, \mathcal{L}_2)$ from (6.40) in (6.55), $\Pr\{z < 9\gamma_{th}/\rho\}$ for large values of ρ satisfies

$$\begin{aligned} \Pr\{z < 9\gamma_{th}/\rho\} \sim{}& \frac{\Gamma(\upsilon_2 - \tau_2)\left(\upsilon_2\tau_2/\mathcal{L}_2\right)^{\tau_2}}{\Gamma(\upsilon_2)\Gamma(\tau_2)} \times \frac{\Gamma(\upsilon_3 - \tau_3)\left(\upsilon_3\tau_3\right)^{\tau_3}}{\Gamma(\upsilon_3)\Gamma(\tau_3)} \\ &\times \frac{\mathrm{B}(\tau_2/2, \tau_3/2)}{2(\tau_2+\tau_3)} \times \left(9\gamma_{th}/\rho\right)^{(\tau_2+\tau_3)/2}, \end{aligned} \tag{6.56}$$

wherein we have used $\mathrm{B}(x, y) = \Gamma(x)\Gamma(y)/\Gamma(x+y)$ [72, p. 909, Eq. 8.384.1].

Inserting (6.49), (6.50), and (6.56) in (6.48) and noting that $\Pr\{v \geq 9\gamma_{th}/\rho\} \to 1$ as $\rho \to \infty$, we obtain the asymptotic approximation of P_{out}^{DF} as in Theorem 6.2.

Appendix 6D. Proof of Theorem 6.3

In this practical scenario, the relay determines whether it decodes the source signal correctly or not using a cyclic redundancy check (CRC) code [29]; the source first segments its data bits into blocks that are augmented with a CRC code. Each block of bits is then modulated using optical $\mathcal{M}$-PAM and transmitted. If the relay decodes correctly, it retransmits the source signal to the destination using the same $\mathcal{M}$-PAM. Otherwise, the relay remains silent. Hence, the symbol error probability at the destination can be obtained as

$$\begin{aligned} P_E^{DF} = {}& \Pr\{\text{Error} \,|\text{Relay cannot decode correctly}\} \times \Pr\{\text{Relay cannot decode correctly}\} \\ &+ \Pr\{\text{Error} \,|\text{Relay decodes correctly}\} \times \Pr\{\text{Relay decodes correctly}\} \\ ={}& \left(\frac{2(\mathcal{M}-1)}{\mathcal{M}}\right)^2 \int_0^\infty Q\left(\sqrt{A\rho u/9}\right) f_u(u)du \times \int_0^\infty Q\left(\sqrt{A\rho v/9}\right) f_v(v)dv \\ &+ \left(\frac{2(\mathcal{M}-1)}{\mathcal{M}}\right) \int_0^\infty \int_0^\infty Q\left(\sqrt{A\rho z/9}\right) f_z(z)dz \\ &\times \left(1 - \frac{2(\mathcal{M}-1)}{\mathcal{M}} \int_0^\infty Q\left(\sqrt{A\rho v/9}\right) f_v(v)dv\right) \end{aligned} \tag{6.57}$$

where $A = 3/(\mathcal{M}-1)(2\mathcal{M}-1)$. Using the definite integral form of Q-function [57], we have

$$P_E^{DF} = \left(\frac{2(\mathcal{M}-1)}{\pi\mathcal{M}}\right)^2 \left(\int_0^{\pi/2} F_u\left(\frac{A\rho}{18\sin^2\phi}\right)d\phi\right) \times \left(\int_0^{\pi/2} F_v\left(\frac{A\rho}{18\sin^2\phi}\right)d\phi\right) + \frac{2(\mathcal{M}-1)}{\pi\mathcal{M}}\int_0^{\pi/2} F_z\left(\frac{A\rho}{18\sin^2\phi}\right)d\phi \times \left(1 - \frac{2(\mathcal{M}-1)}{\pi\mathcal{M}}\int_0^{\pi/2} F_v\left(\frac{A\rho}{18\sin^2\phi}\right)d\phi\right) \tag{6.58}$$

where $F_u(s)$, $F_v(s)$, and $F_z(s)$ are the Laplace transforms of $f_u(u)$, $f_v(v)$, and $f_z(z)$, respectively. Utilizing Lemma 6.1 with $s = A\rho/(18\sin^2\phi)$, we have

$$\int_0^{\pi/2} F_u\left(\frac{A\rho}{18\sin^2\phi}\right)d\phi = \frac{a_0(\tau_3,\upsilon_3,1)}{(A\rho/9)^{\tau_3/2}}2^{3\tau_3/2-1}\mathrm{B}\left(\frac{\tau_3+1}{2},\frac{\tau_3+1}{2}\right), \tag{6.59}$$

$$\int_0^{\pi/2} F_v\left(\frac{A\rho}{18\sin^2\phi}\right)d\phi = \frac{a_0(\tau_1,\upsilon_1,\mathcal{L}_1)}{(A\rho/9)^{\tau_1/2}}2^{3\tau_1/2-1}\mathrm{B}\left(\frac{\tau_1+1}{2},\frac{\tau_1+1}{2}\right), \tag{6.60}$$

where we have used [72, p. 395, Eq. 3.621.1].

In addition, using (6.54) with $s = A\rho/(18\sin^2\phi)$ and [72, p. 395, Eq. 3.621.1], we obtain

$$\int_0^{\pi/2} F_z\left(\frac{A\rho}{18\sin^2\phi}\right)d\phi = \frac{a_0(\tau_2,\upsilon_2,\mathcal{L}_2)a_0(\tau_3,\upsilon_3,1)}{(A/9)^{(\tau_2+\tau_3)/2}}2^{3(\tau_2+\tau_3)/2-1}\mathrm{B}\left(\frac{\tau_2+\tau_3+1}{2},\frac{\tau_2+\tau_3+1}{2}\right). \tag{6.61}$$

Consequently, inserting (6.59)-(6.61) in (6.58), we obtain the high-SNR approximation of P_E^{DF} as

$$P_E^{DF} \sim \begin{cases} C_n\rho^{-(\tau_n+\tau_3)/2} & \tau_1 \neq \tau_2 \\ (C_1+C_2)\,\rho^{-(\tau_n+\tau_3)/2} & \tau_1 = \tau_2 \end{cases}, \tag{6.62}$$

where $n = \arg\min_{i\in\{1,2\}}\{\tau_i\}$ and

$$C_1 = \frac{(\mathcal{M}-1)^2}{\pi^2\mathcal{M}^2}\frac{a_0(\tau_1,\upsilon_1,\mathcal{L}_1)a_0(\tau_3,\upsilon_3,1)}{(A/9)^{(\tau_1+\tau_3)/2}}\mathrm{B}\left(\frac{\tau_1+1}{2},\frac{\tau_1+1}{2}\right)\mathrm{B}\left(\frac{\tau_3+1}{2},\frac{\tau_3+1}{2}\right)2^{3(\tau_1+\tau_3)/2}, \tag{6.63}$$

$$C_2 = \frac{\mathcal{M}-1}{\pi\mathcal{M}}\frac{a_0(\tau_2,\upsilon_2,\mathcal{L}_2)a_0(\tau_3,\upsilon_3,1)}{(A/9)^{(\tau_3+\tau_2)/2}}\mathrm{B}\left(\frac{\tau_2+\tau_3+1}{2},\frac{\tau_2+\tau_3+1}{2}\right)2^{3(\tau_2+\tau_3)/2}. \tag{6.64}$$

By substituting $A = 3/(\mathcal{M}-1)(2\mathcal{M}-1)$ and $\mathcal{M} = 2^{\mathcal{R}} \sim \rho^r$, the proof is completed.

Appendix 6E. Proof of Theorem 6.4

Following lemma is used to prove Theorem 6.4[4].

Lemma 6.2. *For a positive δ, let us define $r_\delta \triangleq \delta\mathcal{H}(v/\delta, w/\delta)$, where v and w are two independent random variables with distributions $\Gamma\Gamma^2(\alpha_1, \beta_1, \mathcal{L}_1)$ and $\Gamma\Gamma^2(\alpha_2, \beta_2, \mathcal{L}_2)$, respectively, and $\mathcal{H}(x, y) \triangleq xy/(x + y + 1)$. Let $\psi(\delta) > 0$ be a continuous function of δ with $\lim_{\delta\to 0} \psi(\delta) = 0$ and $\lim_{\delta\to 0} \delta/\psi(\delta) = c < \infty$. Then, for $\delta \to 0$, we have*

$$\Pr\{r_\delta < \psi(\delta)\} \sim Y(\psi(\delta))^{\tau_n/2}, \tag{6.65}$$

where $\tau_i = \min\{\alpha_i, \beta_i\}$ for $i = 1, 2$, $n = \arg\min_{i\in\{1,2\}} \{\tau_i\}$, and Y is a constant given by

$$Y = \begin{cases} X_n & \tau_1 \neq \tau_2 \\ X_1 + X_2 & \tau_1 = \tau_2 \end{cases}, \tag{6.66}$$

wherein X_i for $i = 1, 2$ is given by

$$X_i = \frac{\Gamma(\upsilon_i - \tau_i)\left(\upsilon_i\tau_i/\mathcal{L}_i\right)^{\tau_i}}{\Gamma(\upsilon_i)\,\Gamma(\tau_i + 1)}, \tag{6.67}$$

with $\upsilon_i = \max\{\alpha_i, \beta_i\}$ for $i = 1, 2$.

Proof. We start with a lower bound.

$$\begin{aligned} \Pr\{r_\delta < \psi(\delta)\} &= \Pr\{1/v + 1/w + \delta/(vw) > 1/\psi(\delta)\} \\ &> \Pr\{1/v + 1/w > 1/\psi(\delta)\} \\ &\geq \Pr\{\max(1/v, 1/w) > 1/\psi(\delta)\} \\ &= 1 - \Pr\{v \geq \psi(\delta)\}\Pr\{w \geq \psi(\delta)\} \\ &= \Pr\{v < \psi(\delta)\} + \Pr\{w < \psi(\delta)\} - \Pr\{v < \psi(\delta)\}\Pr\{w < \psi(\delta)\}. \end{aligned} \tag{6.68}$$

Using Corollary 6.1, for $\delta \to 0$ we have

$$\Pr\{v < \psi(\delta)\} \sim \frac{\Gamma(\upsilon_1 - \tau_1)(\upsilon_1\tau_1/\mathcal{L}_1)^{\tau_1}}{\Gamma(\upsilon_1)\Gamma(\tau_1 + 1)}(\psi(\delta))^{\tau_1/2}, \tag{6.69}$$

$$\Pr\{w < \psi(\delta)\} \sim \frac{\Gamma(\upsilon_2 - \tau_2)(\upsilon_2\tau_2/\mathcal{L}_2)^{\tau_2}}{\Gamma(\upsilon_2)\Gamma(\tau_2 + 1)}(\psi(\delta))^{\tau_2/2}. \tag{6.70}$$

[4]We take the similar approach as [20, Appendix I] in this appendix.

Consequently, utilizing (6.69) and (6.70) in the bound of (6.68), we obtain

$$\liminf_{\delta\to 0} \frac{\Pr\{r_\delta < \psi(\delta)\}}{(\psi(\delta))^{\tau_n/2}} \geq Y, \tag{6.71}$$

where Y is given in (6.66).

For the other direction, we have

$$\begin{aligned}\Pr\{r_\delta < \psi(\delta)\} &= \Pr\{1/v + 1/w + \delta/(vw) > 1/\psi(\delta)\} \\ &= \int_0^\infty \Pr\left\{1/v > \frac{1/\psi(\delta) - 1/w}{1+\delta/w}\right\} f_w(w)dw \\ &\leq \Pr\{w < \Omega\psi(\delta)\} + \int_{\Omega\psi(\delta)}^\infty \Pr\left\{1/v > \frac{1/\psi(\delta) - 1/w}{1+\delta/w}\right\} f_w(w)dw,\end{aligned} \tag{6.72}$$

where $\Omega > 1$ is a constant. Let $\Theta > \Omega$ be another constant. We break the integral in the bound of (6.72) into two integrals as

$$\begin{aligned}\Pr\{r_\delta < \psi(\delta)\} &\leq \Pr\{w < \Omega\psi(\delta)\} + \int_{\Theta\psi(\delta)}^\infty \Pr\left\{1/v > \frac{1/\psi(\delta) - 1/w}{1+\delta/w}\right\} f_w(w)dw \\ &\quad + \int_{\Omega\psi(\delta)}^{\Theta\psi(\delta)} \Pr\left\{1/v > \frac{1/\psi(\delta) - 1/w}{1+\delta/w}\right\} f_w(w)dw \\ &\leq \underbrace{\Pr\{w < \Omega\psi(\delta)\}}_{\text{(I)}} + \underbrace{\Pr\left\{1/v > \frac{1-1/\Theta}{\psi(\delta)+\delta/\Theta}\right\}}_{\text{(II)}} \\ &\quad + \underbrace{\int_{\Omega\psi(\delta)}^{\Theta\psi(\delta)} \Pr\left\{1/v > \frac{1/\psi(\delta) - 1/w}{1+\delta/w}\right\} f_w(w)dw}_{\text{(III)}},\end{aligned} \tag{6.73}$$

where the second inequality follows from the fact that $\Pr\{1/v > (1/\psi(\delta) - 1/w)/(1+\delta/w)\}$ is non-increasing in w. Using Corollary 6.1, terms (I) and (II) of (6.73) for $\delta \to 0$ satisfy

$$\text{(I)} \sim \frac{\Gamma(\upsilon_2 - \tau_2)(\upsilon_2\tau_2/\mathcal{L}_2)^{\tau_2}\Omega^{\tau_2/2}}{\Gamma(\upsilon_2)\Gamma(\tau_2+1)}(\psi(\delta))^{\tau_2/2}, \tag{6.74}$$

$$\text{(II)} \sim \frac{\Gamma(\upsilon_1 - \tau_1)(\upsilon_1\tau_1/\mathcal{L}_1)^{\tau_1}}{\Gamma(\upsilon_1)\Gamma(\tau_1+1)}\left(\frac{1+c/\Theta}{1-1/\Theta}\right)^{\tau_1/2}(\psi(\delta))^{\tau_1/2}. \tag{6.75}$$

By a change of variable $w' = w/\psi(\delta)$, term (III) in the bound of (6.73) can be rewritten as

$$\text{(III)} = \psi(\delta)\int_\Omega^\Theta \Pr\left\{v < \frac{\psi(\delta)+\delta/w'}{1-1/w'}\right\} f_w(w'\psi(\delta))\,dw'. \tag{6.76}$$

Using Corollary 6.1, for $\delta \to 0$ we have

$$\Pr\left\{v < \frac{\psi(\delta)+\delta/w'}{1-1/w'}\right\} \sim \frac{\Gamma\left(\upsilon_1-\tau_1\right)\left(\upsilon_1\tau_1\right)^{\tau_1}}{\Gamma\left(\upsilon_1\right)\Gamma\left(\tau_1+1\right)}\left(\frac{1+c/w'}{1-1/w'}\right)^{\tau_1/2}(\psi(\delta))^{\tau_1/2}, \tag{6.77}$$

$$f_w\left(w'\psi(\delta)\right) \sim \frac{\Gamma(\upsilon_2-\tau_2)(\upsilon_2\tau_2/\mathcal{L}_2)^{\tau_2}}{2\Gamma(\upsilon_2)\Gamma(\tau_2)}(w'\psi(\delta))^{\tau_2/2-1}. \tag{6.78}$$

By utilizing (6.77) and (6.78) in (6.76), term (III) for $\delta \to 0$ satisfies

$$\begin{aligned}\text{(III)} \sim (\psi(\delta))^{(\tau_1+\tau_2)/2}&\frac{\Gamma\left(\upsilon_1-\tau_1\right)\left(\upsilon_1\tau_1/\mathcal{L}_1\right)^{\tau_1}}{\Gamma\left(\upsilon_1\right)\Gamma\left(\tau_1+1\right)}\frac{\Gamma\left(\upsilon_2-\tau_2\right)\left(\upsilon_2\tau_2/\mathcal{L}_2\right)^{\tau_2}}{\Gamma\left(\upsilon_2\right)\Gamma\left(\tau_2+1\right)} \\ &\times \underbrace{\int_{\Omega}^{\Theta}\frac{1}{2}(w')^{\tau_2/2}\left(\frac{1+c/w'}{1-1/w'}\right)^{\tau_1/2}dw'}_{\Lambda(\Omega,\Theta,c)},\end{aligned} \tag{6.79}$$

where $\Lambda(\Omega,\Theta,c)$ is finite for any $\Theta > \Omega > 1$ and $c < \infty$.

Consequently, inserting (6.74), (6.75), and (6.79) in (6.73), we obtain

$$\limsup_{\delta\to 0}\frac{\Pr\left\{r_\delta < \psi(\delta)\right\}}{\left(\psi(\delta)\right)^{\tau_n/2}} \le Y' \tag{6.80}$$

where

$$Y' = \begin{cases} {X'}_n & \tau_1 \neq \tau_2 \\ {X'}_1 + {X'}_2 & \tau_1 = \tau_2 \end{cases}, \tag{6.81}$$

with $n = \arg\min\limits_{i\in\{1,2\}}\{\tau_i\}$, and X_1' and X_2' are respectively given by

$$X_1' = \frac{\Gamma\left(\upsilon_1-\tau_1\right)\left(\upsilon_1\tau_1/\mathcal{L}_1\right)^{\tau_1}}{\Gamma\left(\upsilon_1\right)\Gamma\left(\tau_1+1\right)}\left(\frac{1+c/\Theta}{1-1/\Theta}\right)^{\tau_1/2}, \tag{6.82}$$

$$X_2' = \frac{\Gamma\left(\upsilon_2-\tau_2\right)\left(\upsilon_2\tau_2/\mathcal{L}_2\right)^{\tau_2}\Omega^{\tau_2/2}}{\Gamma\left(\upsilon_2\right)\Gamma\left(\tau_2+1\right)}. \tag{6.83}$$

The constants $\Theta > \Omega > 1$ are arbitrary. Choosing Θ arbitrarily large and Ω arbitrarily close to one, we obtain $X_i' = X_i$ for $i = 1, 2$, where X_i is given in (6.67), and $Y' = Y$, where Y is given in (6.66). Consequently, from (6.80), we have

$$\limsup_{\delta\to 0}\frac{\Pr\left(r_\delta < \psi(\delta)\right)}{\left(\psi(\delta)\right)^{\tau_n/2}} \le Y. \tag{6.84}$$

Combining (6.71) with (6.84), the lemma is proved. □

Defining $\varepsilon = 9/\rho$ and $\omega(\varepsilon) = \gamma_{th}\varepsilon$ as a function of ε, the outage probability of the AF mode in (6.29) can be rewritten as

$$\begin{aligned} P_{out}^{AF} &= \Pr\left\{u + \varepsilon\mathcal{H}\left(v/\varepsilon, w/\varepsilon\right) < \omega(\varepsilon)\right\} \\ &= \Pr\left\{u + r_\varepsilon < \omega(\varepsilon)\right\} \\ &= \int_0^{\omega(\varepsilon)} \Pr\left\{r_\varepsilon < \omega(\varepsilon) - u\right\} f_u(u)du \\ &= \omega(\varepsilon)\int_0^1 \Pr\left\{r_\varepsilon < \omega(\varepsilon)(1-u')\right\} f_u\left(\omega(\varepsilon)u'\right)du', \end{aligned} \tag{6.85}$$

where we have used a change of variable $u' = u/\omega(\varepsilon)$ in the forth equality. By using Lemma 6.2 with $\delta = \varepsilon$ and $\psi(\delta) = \omega(\delta)(1-u')$, $\Pr\left\{r_\varepsilon < \omega(\varepsilon)(1-u')\right\}$ for $\varepsilon \to 0$ satisfies

$$\Pr\left\{r_\varepsilon < \omega(\varepsilon)(1-u')\right\} \sim Y((1-u')\omega(\varepsilon))^{\tau_n/2}. \tag{6.86}$$

In addition, using Corollary 6.1, for $\varepsilon \to 0$ we have

$$f_u\left(\omega(\varepsilon)u'\right) \sim \frac{\Gamma(\upsilon_3 - \tau_3)}{2\Gamma(\upsilon_3)\Gamma(\tau_3)}(\upsilon_3\tau_3)^{\tau_3}(\omega(\varepsilon)u')^{\tau_3/2-1}. \tag{6.87}$$

Inserting (6.86) and (6.87) in (6.85), we have

$$\begin{aligned} \Pr\left\{u + r_\varepsilon < \omega(\varepsilon)\right\} &\sim Y\frac{\Gamma\left(\upsilon_3 - \tau_3\right)\left(\upsilon_3\tau_3\right)^{\tau_3}}{2\Gamma\left(\upsilon_3\right)\Gamma\left(\tau_3\right)}(\omega(\varepsilon))^{(\tau_n+\tau_3)/2}\int_0^1 u'^{\tau_3/2-1}(1-u')^{\tau_n/2}du' \\ &= Y\frac{\Gamma\left(\upsilon_3 - \tau_3\right)\left(\upsilon_3\tau_3\right)^{\tau_3}}{2\Gamma\left(\upsilon_3\right)\Gamma\left(\tau_3\right)}\mathrm{B}\left(1+\tau_n/2, \tau_3/2\right)(\omega(\varepsilon))^{(\tau_n+\tau_3)/2}, \end{aligned} \tag{6.88}$$

where we have used [72, p. 315, Eq. 3.191.1]. By substituting Y from (6.66), $\omega(\varepsilon) = \gamma_{th}\varepsilon$, and $\varepsilon = 9/\rho$, the proof is completed.

Appendix 6F. Proof of (6.37)

Following lemma and its corollary are used to prove the inequality of (6.37).

Lemma 6.3. *Let m, l, p, and q be positive real numbers, such that $(p-m)(q-l) \leq (\geq)\, 0$. Then*

$$\Gamma(p+l+1)\Gamma(m+q) \geq (\leq)\,\Gamma(p+q+1)\Gamma(m+l). \tag{6.89}$$

See [78] for the proof.

Corollary 6.2. *For every pair of positive real numbers x and y, we have*

$$\Gamma(x+1)\Gamma(y+1) \leq \Gamma(x+y+1). \tag{6.90}$$

Proof. First, we assume $x \geq 1$ and $y > \varepsilon$, where ε is an arbitrary small number. Hence, we have $(x-1)(y-\varepsilon) \geq 0$. Putting $p = x$, $m = 1$, $q = y$, and $l = \varepsilon$ in Lemma 6.3 results in

$$\Gamma(x+\varepsilon+1)\Gamma(y+1) \leq \Gamma(x+y+1)\Gamma(1+\varepsilon). \tag{6.91}$$

Choosing ε arbitrarily close to zero, we obtain

$$\Gamma(x+1)\Gamma(y+1) \leq \Gamma(x+y+1), \qquad \text{if} \qquad x \geq 1,\ y > 0 \tag{6.92}$$

Similarly, putting $p = y$, $m = 1$, $q = x$, and $l = \varepsilon$ in Lemma 6.3, one can obtain

$$\Gamma(x+1)\Gamma(y+1) \leq \Gamma(x+y+1), \qquad \text{if} \quad x > 0,\ y \geq 1 \tag{6.93}$$

Finally, we assume that $0 < x < 1$, and $0 < y < 1$. Therefore $(y-1)(1-x) \leq 0$. Putting $p = y$, $m = 1$, $q = 1$, and $l = x$ in Lemma 6.3, we have

$$\begin{aligned} \Gamma(y+x+1)\Gamma(2) &\geq \Gamma(y+2)\Gamma(x+1) \\ &= (y+1)\Gamma(y+1)\Gamma(x+1) \\ &\geq \Gamma(y+1)\Gamma(x+1), \end{aligned} \tag{6.94}$$

where the second inequality follows from the assumption that $y > 0$. Noting that $\Gamma(2) = 1$, (6.94) yields

$$\Gamma(x+1)\Gamma(y+1) \leq \Gamma(x+y+1), \qquad \text{if} \quad 0 < x < 1,\ 0 < y < 1 \tag{6.95}$$

Combining (6.92), (6.93), and (6.95), the corollary is proved. □

Using (6.21) and (6.33), we obtain

$$\begin{aligned} \frac{O_1^{AF}}{O_1^{DF}} &= \left(\frac{2(\tau_1+\tau_3)}{\tau_1\tau_3 \mathrm{B}\left(\tau_1/2, \tau_3/2\right)} \right)^{2/(\tau_1+\tau_3)} \\ &= \left(\frac{\Gamma\left(\tau_1/2+\tau_3/2+1\right)}{\Gamma\left(\tau_1/2+1\right)\Gamma\left(\tau_3/2+1\right)} \right)^{2/(\tau_1+\tau_3)}, \end{aligned} \tag{6.96}$$

where we have used $\mathrm{B}(x,y) = \Gamma(x)\Gamma(y)/\Gamma(x+y)$ [72, p. 909, Eq. 8.384.1]. Substituting $x = \tau_1/2$ and $y = \tau_3/2$ in Corollary 6.2, we obtain

$$\frac{\Gamma\left(\tau_1/2+\tau_3/2+1\right)}{\Gamma\left(\tau_1/2+1\right)\Gamma\left(\tau_3/2+1\right)} \geq 1, \tag{6.97}$$

and consequently (6.37) is proved.

Chapter 7

Concluding Remarks

7.1 Summary of Contributions

In this dissertation, we have investigated and analyzed several diversity techniques for FSO communications. In Chapter 3, we analyzed the performance of receive diversity in coherent FSO systems considering both atmospheric turbulence-induced amplitude fluctuations and phase aberrations. Modal compensation technique is deployed at each receive aperture to mitigate the turbulence-induced wavefront phase distortion. We have derived closed form expressions for the diversity gain which quantifies the link reliability and the DMT which quantifies the compromise between the link reliability and the spectral efficiency (i.e., the multiplexing gain). For sufficiently large SNR, we demonstrate that the DMT converges to $N(1-r)$ where N and r respectively denote the number of receive apertures and the multiplexing gain. Asymptotical diversity gain (i.e., DMT evaluated at $r = 0$) is therefore determined by the number of receive apertures. Our results further demonstrate that for practical SNR values the diversity gain can be larger than N as a result of phase compensation deployed in the system. In other words, phase compensation acts as an additional diversity source besides the diversity gain offered by the multiple apertures.

In Chapter 4, we presented multi-hop relaying as a powerful fading mitigation tool in coherent FSO communications over atmospheric turbulence channels. Different from those employed in RF wireless systems, multi-hop FSO relaying takes advantage of the resulting shorter hops as a diversity source. This is a result of the distance-dependency characteris-

tics of the fading amplitude and phase variance in coherent FSO systems. We have derived the outage probability, finite SNR DMT, and finite SNR diversity gains taking into account the effects of both turbulence-induced amplitude fluctuation and phase aberration. Our results quantify the performance gains in terms of the diversity and multiplexing available through multi-hop relaying and yield impressive performance improvements over the conventional direct transmission.

In Chapter 5, we have presented an information-theoretic analysis of H-ARQ protocols in coherent FSO communications. Specifically, we have analyzed three H-ARQ protocols, namely ALO, RTD and INR protocols. For each protocol, we have derived the outage performance and then, based on the derived expressions, quantified the diversity and coding gains at high-SNR regime. Our results have demonstrated significant performance improvements available through the deployment of ARQ over atmospheric channels. These improvements are as a result of the temporal diversity gain inherent to ARQ. In the Gamma-Gamma atmospheric channel under consideration, we have shown that all three protocols achieve the same diversity gain given by $MN \min\{\alpha, \beta\}$ where α and β are the Gamma-Gamma channel parameters, N is the number of receive apertures, and M is the maximum number of ARQ rounds. We have further investigated and compared the throughput of ARQ protocols. Our results have demonstrated that INR protocol considerably brings more throughput advantages at large values of transmission rate compared to the other protocols.

In Chapter 6, we have analyzed parallel relaying in IM/DD FSO communications. Specifically, we have considered an FSO system with a line-of-sight link between the source and the destination and a single relay with either DF or AF relaying strategy. For each cooperation mode, we have derived the asymptotic outage performance and then, based on the derived expression, quantified the diversity and coding gains at high-SNR regime. Our results demonstrate that parallel relaying improves the performance of FSO systems by bringing diversity advantages. Moreover, between S-R and R-D channels, the channel with worse statistical characteristics dominates the outage performance (both diversity and coding gains) at high-SNR regime. Comparing two cooperation modes, we have shown that both modes achieve the same diversity gain given by the diversity gain of S-D channel plus the minimum of the diversity gains of S-R and R-D channels. However, their coding gains can be different depending on the channels' characteristics. In fact, when R-D channel is

statistically worse than S-R channel, both modes provide the same coding gain. On the other hand, when S-R channel is statistically worse than R-D channel, the AF mode brings higher coding gain than the DF mode and consequently outperforms the DF mode at high SNR regime. We have also investigated the DMT of direct transmission and cooperation modes. Our results demonstrate that both cooperation modes achieve the same optimal DMT. Furthermore, it has been shown that the optimal DMT of the direct transmission and the DF mode can be achieved by $\mathcal{M}$-PAM.

7.2 Future Research Directions

In Chapter 3, we have assumed that the receive apertures are placed sufficiently far apart, so that the turbulence-induced fading coefficients of diversity branches are statistically independent. This condition maximizes the receive diversity gain. However, for some scenarios in which the receive apertures cannot be located in enough distance from each other, the fading coefficients may be correlated. Therefore, performance analysis of coherent FSO systems with multiple receive apertures and correlated fading coefficients is of interest as a future research topic.

In Chapter 4, the performance analysis has been carried out for equal power allocation among different nodes. However, when the system has an asymmetrical configuration, the transmit-optical power of each node can be adjusted properly to optimize the outage performance of the system. Therefore, optimal transmit power allocation among relay nodes in the proposed multi-hop relay-assisted system can be investigated as a future work. Moreover, investigating the performance of multi-hop relaying in coherent FSO communications with AF relay nodes can be another topic for the future work.

The information theoretic analysis of H-ARQ protocols in coherent FSO communications, presented in Chapter 5, is based on the infinite-length Gaussian random codes. In practice, the complexity resulting from using such unstructured codebooks may be restrictive. Extending this analysis to practical finite-length codes can be considered as an interesting topic. In addition, our analysis has been based on heterodyne detection at the receiver side. Investigating the outage performance of H-ARQ protocols in IM/DD FSO systems can be also a potential future work.

In Chapter 6, we focused on a single-relay channel. Our analysis can be extended to multiple-relay scenario. Also, our analysis has been carried out for the DF and AF cooperation modes. Other modes of cooperation have been also proposed in the context of RF communications, e.g., compress-and-forward and compute-and-map [18, 79]. In compress-and-forward the relay compressed the received signal, which contains the source message and noise, into a new codeword and sends it to the destination. In compute-and-map the relay first quantizes the received signal at the noise level and then re-encodes and retransmits it to the destination. These cooperation modes can be also extended to the parallel FSO relaying.

References

[1] R. M. Gagliardi and S. Karp, *Optical Communications*. New York, USA: John Wiley & Sons, 1995. 1, 2, 9, 10, 11, 16, 20

[2] L. C. Andrews and R. L. Phillips, *Laser Beam Propagation Through Random Media*. Bellingham, Washington: SPIE Press, 2005. 1, 12, 14, 69

[3] D. Kedar and S. Arnon, "Urban optical wireless communication networks: The main challenges and possible solutions," *IEEE Communications Magazine*, vol. 42, pp. s2–s7, May 2004. 2

[4] V. W. Chan, "Free-space optical communications," *IEEE Journal of Lightwave Technology*, vol. 24, pp. 4750–4762, December 2006. 3

[5] X. Zhu and J. M. Kahn, "Free-space optical communication through atmospheric turbulence channels," *IEEE Transactions on Communications*, vol. 50, pp. 1293–1300, August 2002. 3, 11

[6] X. Zhu and J. M. Kahn, "Performance bounds for coded free-space optical communications," *IEEE Transactions on Communications*, vol. 51, pp. 1233–1239, August 2003. 3

[7] M. Uysal, J. T. Li, and M. Yu, "Error rate performance analysis of coded free-space optical links," *IEEE Transactions on Wireless Communications*, vol. 5, pp. 1229–1233, June 2006. 3

[8] X. Zhu and J. M. Kahn, "Markov chain model in maximum-likelihood sequence detection for free-space optical communication through atmospheric turbulence channels," *IEEE Transactions on Communications*, vol. 51, pp. 509–516, March 2003. 3

[9] X. Zhu, J. M. Kahn, and W. Jin, "Mitigation of turbulence-induced scintillation noise in free-space optical links using temporal-domain detection techniques," *IEEE Photonics Thechnology Letters*, vol. 15, pp. 623–625, April 2003. 3

[10] S. M. Haas, J. H. Shapiro, and V. Tarokh, "Space-time codes for wireless optical communications," *EURASIP Journal on Applied Signal Processing*, vol. 3, pp. 211–220, March 2002. 3, 4, 6

[11] E. Lee and V. W. Chan, "Part 1: Optical communication over the clear turbulent atmospheric," *IEEE Journal on Selected Areas in Communications*, vol. 22, pp. 1896–1906, November 2004. 3, 4, 73

[12] S. G. Wilson, M. Brandt-Pearce, Q. Cao, and J. H. Leveque, "Free-space optical MIMO transmission with Q-ary PPM," *IEEE Transactions on Communications*, vol. 53, pp. 1402–1412, August 2005. 3, 4

[13] S. M. Navidpour, M. Uysal, and M. Kavehrad, "BER performance of free-space optical transmission with spatial diversity," *IEEE Transactions on Wireless Communications*, vol. 6, pp. 2813–2819, August 2007. 3, 4

[14] E. Lee and V. W. Chan, "Diversity coherent receivers for optical communication over the clear turbulent atmosphere," in *IEEE International Conference on Communications*, (Glasgow), pp. 2485–2492, June 2007. 3, 4, 6

[15] E. Lee and V. w. Chan, "Diversity coherent and incoherent receivers for free-space optical communication in the presence and absence of interference," *IEEE/OSA Journal of Optical Communucations and Networking*, vol. 1, pp. 463–483, October 2009. 3, 4, 6

[16] E. Bayaki, R. Schober, and R. Mallik, "Performance analysis of MIMO free-space optical systems in Gamma-Gamma fading," *IEEE Transactions on Communications*, vol. 57, pp. 1119–1128, November 2009. 3, 4, 69

[17] N. Letzepis and A. G. Fàbregas, "Outage probability of the Gaussian MIMO free-space optical channel with PPM," *IEEE Transactions on Communications*, vol. 57, pp. 3682–3689, December 2009. 3, 4

[18] T. M. Cover and A. El Gamal, "Capacity theorems for the relay channel," *IEEE Transactions on Information Theory*, vol. 25, pp. 572–584, September 1979. 4, 99

[19] A. Sendonaris, E. Erkip, and B. Aazhang, "User cooperation diversity-part I: System description," *IEEE Transactions on Communications*, vol. 51, pp. 1927–1938, November 2003. 4

[20] N. Laneman, D. N. C. Tse, and G. W. Wornell, "Cooperative diversity in wireless networks: Efficient protocols and outage behavior," *IEEE Transactions on Information Theory*, vol. 50, pp. 3062–3080, December 2004. 4, 90

[21] A. S. Acampora and S. V. Krishnamurthy, "A broadband wireless access network based on mesh-connected free-space optical links," *IEEE Personal Communications*, vol. 6, no. 5, pp. 62–65, 1999. 4, 5, 6

[22] J. Akella, M. Yuksel, and S. Kalyanaraman, "Error analysis of multihop free-space optical communications," in *IEEE Internatioanl Conference on Communications*, (Seoul, Korea), pp. 1777–1781, May 2005. 4, 5, 6

[23] G. K. Karagiannidis, T. A. Tsiftsis, and H. G. Sandalidis, "Outage probability of relayed free space optical communication systems," *Electronics Letters*, vol. 42, pp. 994–995, August 2006. 4, 5, 6

[24] M. Safari and M. Uysal, "Relay-assisted free-space optical communication," *IEEE Transactions on Wireless Communications*, vol. 7, pp. 5441–5449, December 2008. 4, 5, 6, 42

[25] M. Karimi and M. Nasiri-Kenari, "Free-space optical communications via optical amplify-and-forward relaying," *IEEE/OSA Journal of Lightwave Technology*, vol. 29, pp. 242–248, January 2011. 4, 5

[26] N. D. Chatzidiamantis, D. S. Michalopoulos, E. E. Kriezis, G. K. Karagiannidis, and R. Schober, "Protocols for relay-assisted free-space optical systems," *Submitted to IEEE Transactions on Communications*, May 2011. Available on [arXiv:1105.3835v1]. 4, 5

[27] M. Safari and M. Uysal, "Diversity gain analysis of free-space optical communication systems," in *Canadian Conference on Electrical and Computer Engineering*, (Niagara Falls), pp. 1239–1244, May 2008. 5

[28] R. Comroe and D. Costello, "ARQ schemes for data transmission in mobile radio systems," *IEEE Journal on Selected Areas in Communications*, vol. 2, pp. 472–481, July 1984. 5

[29] S. Lin and D. J. Costello, *Error Control Coding: Fundamentals and Applications*. Englewood Cliffs, New Jersey: Pearson Prentice-Hall, 2004. 5

[30] D. Costello, J. Hagenauer, H. Imai, and S. Wicker, "Applications of error-control coding," *IEEE Transactions on Information Theory*, vol. 44, pp. 2531–2560, October 1998. 5

[31] C. Kose and T. R. Halford, "Incremental redundancy hybrid ARQ protocol design for FSO link," in *IEEE Military Communications Conference*, (Boston, MA), 2009. 5

[32] K. Kiasaleh, "Hybrid ARQ for FSO communications through turbulent atmosphere," *IEEE Communications Letters*, vol. 14, pp. 866–868, September 2010. 5

[33] A. R. Hammons and F. Davidson, "On the design of automatic repeat request protocols for turbulent free-space optical links," in *IEEE Military Communications Conference*, (San Jose, CA), pp. 808–813, 2010. 5, 6

[34] R. K. Tyson, *Principles of Adaptive Optics*. San Diego, USA: Academic Press, 1991. 6, 15, 19

[35] A. Belmonte and J. M. Kahn, "Performance of synchronous optical receivers using atmospheric compensation techniques," *Optics Express*, vol. 16, pp. 14151–14162, September 2008. 6, 16, 17, 18

[36] E. Biglieri, J. Proakis, and S. Shamai, "Fading channels: Information theoretic and communications aspects," *IEEE Transactions on Information Theory*, vol. 44, pp. 2619–2692, October 1998. 6, 24

[37] L. Zheng and D. N. C. Tse, "Diversity and multiplexing: A fundamental tradeoff in multiple antenna channels," *IEEE Transactions on Information Theory*, vol. 49, pp. 1073–1096, May 2003. 6, 23, 26, 39, 46, 76

[38] S. M. Aghajanzadeh and M. Uysal, "DMT analysis of coherent free-space optical systems over atmospheric turbulence channels," in *Canadian Conference on Electrical and Computer Engineering*, (Calgary, AB), pp. 1–4, May 2010. 6

[39] S. M. Aghajanzadeh and M. Uysal, "Diversity-multiplexing trade-off in coherent free-space optical systems with multiple receivers," *IEEE/OSA Journal of Optical Communications and Networking*, vol. 2, pp. 1087 – 1094, December 2010. 6

[40] S. M. Aghajanzadeh and M. Uysal, "DMT analysis of multi-hop coherent FSO communication over atmospheric channels," in *Canadian Workshop on Information Theory*, (Kelowna, BC), pp. 112–115, May 2011. 7

[41] S. M. Aghajanzadeh and M. Uysal, "Multi-hop coherent free-space optical communications over atmospheric turbulence channels," *IEEE Transactions on Communications*, vol. 59, pp. 1657–1663, June 2011. 7

[42] S. M. Aghajanzadeh and M. Uysal, "Outage analysis of hybrid-ARQ protocols in coherent free-space optical communications," in *IEEE International Symposium on Personal, Indoor and Mobile Radio Communications*, (Toronto, ON), September 2011. 7

[43] S. M. Aghajanzadeh and M. Uysal, "Information theoretic analysis of hybrid ARQ protocols in coherent free-space optical systems," *Submitted to IEEE Transactions on Communications*, June 2011. 7

[44] S. M. Haas, *Capacity of and Coding for Multiple-Aperture Wireless Optical Communications*. PhD thesis, Massachusetts Institute of Technology, 2003. 11

[45] G. R. Osche, *Optical Detection Theory for Laser Applications*. New York, USA: John Wiley & Sons, 2002. 12, 13, 15, 17

[46] M. Al-Habash, L. Andrews, and R. Phillips, "Mathematical model for the irradiance probability density function of a laser beam propagating through turbulent media," *Optical Engineering*, vol. 40, pp. 1554–1562, August 2001. 12, 13, 14

[47] R. J. Hill and R. G. Frehlich, "Probability distribution of irradiance for the onset of strong scintillation," *Journal of Optical Society of America A*, vol. 14, no. 7, pp. 1530–1540, 1997. 13

[48] G. Parry, "Measurements of atmospheric turbulence-induced intensity fluctuations in a laser beam," *Optica Acta*, vol. 28, no. 5, pp. 715–728, 1981. 13

[49] F. Bowman, *Introduction to Bessel Functions*. New York, USA: Dover, 1958. 14, 18, 25, 26

[50] D. L. Fried, "Optical heterodyne detection of an atmospherically distorted signal wave front," in *Proceedings of the IEEE*, vol. 55, pp. 57–67, January 1967. 15

[51] R. J. Noll, "Zernike polynomials and atmospheric turbulence," *Journal of Optical Society of America*, vol. 66, no. 3, pp. 207–211, 1976. 15, 16

[52] V. F. Canales and M. P. Cagigal, "Generalized Fried parameter after adaptive optics partial wave-front compensation," *Journal of Optical Society of America*, vol. 17, pp. 903–910, May 2000. 17

[53] J. W. Goodman, *Speckle Phenomena in Optics: Theory and Applications*. Greenwood Village, USA: Roberts and Company Publishers, 2007. 17

[54] E. F. Beckenbach and R.Bellman, *Inequalities*. Berlin, Germany: Springer, 1961. 22, 55, 56

[55] A. Goldsmith, *Wireless Communications*. New York, USA: Cambridge University Press, 2005. 22

[56] R. Narasimhan, "Finite-SNR diversity multiplexing tradeoff for correlated Rayleigh and Ricean MIMO channels," *IEEE Transactions on Information Theory*, pp. 3965–3979, September 2006. 23, 24, 28

[57] M. K. Simon and M.-S. Alouini, *Digital Communication over Fading Channels*. Hoboken, New Jersey: John Wiley & Sons, 2 ed., 2005. 24, 25, 26, 34, 42, 46, 47, 49, 72, 86, 89

[58] G. Boros and V. Moll, *Irresisitible Integrals: Symbolic, Analysis and Experiments in the Evaluation of Integrals*. Cambridge, England: Cambridge University Press, 2004. 25

[59] E. L. Bradley and H. F. Inman, "The overlapping coefficient as a measure of agreement between probability distributions and point estimation of the overlap of two normal densities," *Communications in Statistics - Theory and Methods*, vol. 18, no. 10, pp. 3851–3874, 1989. 27

[60] W. Y. Shin, S. Y. Chung, and Y. H. Lee, "Diversity-multiplexing tradeoff and outage performance for Rician MIMO channels," *IEEE Transactions on Information Theory*, vol. 54, pp. 1186–1196, March 2008. 28

[61] D. Gündüz, M. A. Khojastepour, A. Goldsmith, and H. V. Poor, "Multi-hop MIMO relay networks: Diversity-multiplexing trade-off analysis," *IEEE Transactions on Wireless Communications*, vol. 9, pp. 1738–1747, May 2010. 37

[62] F. S. Vetelino, L. C. A. C. Young, and J. Recolons, "Aperture averaging effects on the probability density of irradiance fluctuations in moderate-to-strong turbulence," *Applied Optics*, vol. 46, pp. 2099–2108, April 2007. 41

[63] L. C. Andrews, "Aperture-averaging factor for optical scintillations of plane and spherical waves in the atmosphere," *Optical Society of America*, vol. 9, pp. 597–600, April 1992. 42

[64] G. Caire and D. Tuninetti, "The throughput of hybrid-ARQ protocols for the Gaussian collision channel," *IEEE Transactions on Information Theory*, vol. 47, pp. 1971–1988, July 2001. 48, 49, 52, 53, 54, 57, 59, 60

[65] Z. Wang and G. Giannakis, "A simple and general parameterization quantifying performance in fading channels," *IEEE Transactions on Communications*, vol. 51, pp. 1389–1398, August 2003. 51

[66] N. D. Chatzidiamattis, G. K. Karagiannidis, and D. S. Michalopoulos, "On the distribution of the sum of Gamma-Gamma variates and application in RF and optical wireless communication," *IEEE Transactions on Communications*, vol. 59, pp. 1298 – 1308, May 2011. 51, 52

[67] A. Papoulis, *Probability, Random Variables, and Stochastic Processes*. McGraw-Hill, 4 ed., 2002. 51

[68] A. P. Prudnikov, Y. A. Brychkov, and O. I. Marichev, *Integrals and Series, Volume 3: More Special Functions*. New York, USA: Gordon and Breech Science, 1986. 52, 54, 68, 71, 75, 85

[69] A. M. Mathai, *A Handbook of Generalized Special Functions for Statistical and Physical Sciences*. Oxford, UK: Clarendon Press, 1993. 53, 69, 70, 71

[70] B. S. W. Schröder, *Mathematical Analysis: A Concise Introduction*. New Jersey, USA: John Wiley & Sons, 2008. 58, 71

[71] M. Schwartz, W. R. Bennett, and S. Stein, *Communication Systems and Techniques*. New York, USA: McGraw-Hill, 1966. 67

[72] I. S. Gradshteyn and I. M. Ryzhik, *Tables of Integrals, Series, and Products*. San Diego, CA: Academic Press, 7 ed., 2007. 68, 69, 70, 78, 86, 88, 89, 93, 95

[73] A. Lapidoth, S. M. Moser, and M. A. Wigger, "On the capacity of free-space optical intensity channels," *IEEE Transactions on Information Theory*, vol. 55, pp. 4449–4461, October 2009. 74

[74] A. A. Farid and S. Hranilovic, "Channel capacity and non-uniform signalling for free-space optical intensity channels," *IEEE Transactions on Information Theory*, vol. 27, pp. 1553–1563, December 2009. 74

[75] S. Hranilovic, *Wireless Optical Communication Systems*. New York, USA: Springer, 2004. 75

[76] J. G. Proakis, *Digital Communications*. Boston, MA: McGraw-Hill, 2001. 86

[77] I. B. Djordjevic, "Adaptive modulation and coding for free-space optical channels," *IEEE/OSA Journal of Optical Communications and Networking*, vol. 2, pp. 221–229, May 2010. 86

[78] P. Kumar, S. P. Singh, and S. S. Dragomir, "Some inequalities involving Beta and Gamma functions," *Nonlinear Analysis Forum*, vol. 6, no. 1, pp. 143–150, 2001. 94

[79] G. Kramer, M. Gastpar, and P. Gupta, "Cooperative strategies and capacity theorems for relay networks," *IEEE Transactions on Information Theory*, vol. 51, pp. 3037–3063, September 2005. 99